

UNIVERSITY OF HULL

The Use of Enzymes, Isomerisable Lipid Analogues and Small Molecules to  
Modulate the Structure and Dynamics of Lipid Bilayers

Being a Thesis submitted for the Degree of Doctor of Philosophy

In the University of Hull

By

Rebecca Batchelor, MChem (Hons)

September 2010

## **Abstract**

A series of experiments were carried out to assess the effects and interactions of isomerisable lipid analogues, small molecules, and enzyme catalysed substrates on the structure and dynamics of lipid bilayers.

### *Modulation of Enzyme Activity Using an Azobenzene-Containing Lipid Analogue*

– An azobenzene-containing phosphocholine lipid analogue (bis-Azo-PC) was synthesised and incorporated into 1,2-dioleoyl-*sn*-glycero-3-phosphocholine (DOPC) liposomes containing diacylglycerol kinase (DGK) in order to assess the effect of photoisomerisation of the azobenzene group on the activity of the protein. The increase in volume of bis-Azo-PC in the *cis* state should have a significant effect on protein activity as bilayer tension increases. Protein activity was measured using an enzyme activity assay. The difference in specific activity between the *trans* and *cis* states of the azobenzene was too small to discern a significant effect on protein activity.

*Lipid Phase Behaviour* – The phase behaviour of 1,2-dipalmitoyl-*sn*-glycerol-3-phosphocholine- $d_{62}$  ( $d_{62}$ -DPPC) samples containing cholesterol and the serotonin receptor agonist drugs quipazine and LY-165,135 was analysed using proton and deuterium NMR spectroscopy and differential scanning calorimetry (DSC). The effect of quipazine and LY-165,135 on  $d_{62}$ -DPPC was an elongation of the gel-to-fluid lamellar phase transition, lowering of the start of the phase transition, and disappearance of the ripple phase observed in  $d_{62}$ -DPPC alone. The effect of cholesterol on  $d_{62}$ -DPPC was a smoothing of the phase transition due to the presence of the liquid-ordered phase. Spectra of  $d_{62}$ -DPPC, cholesterol and quipazine also show the presence of the liquid-ordered phase. Spectra of  $d_{62}$ -DPPC and cholesterol with LY-165,135 show that the drug widens the temperature range over which the liquid-ordered phase exists. These results indicate that the presence of small molecules such as serotonin-receptor agonists can have a significant effect on the phase behaviour of the lipid bilayer.

### *Analysis of Drug Localisation and Orientation in a Model Membrane by NMR*

*Spectroscopic Methods* – NOESY cross-relaxation rates were used to generate location probabilities for serotonin-receptor agonist drugs in  $d_{62}$ -DPPC bilayers

with and without cholesterol. Both drugs were found to locate in the interface region of the bilayer, although they had different orientations relative to the bilayer normal; quipazine was oriented parallel to the  $d_{62}$ -DPPC molecules, while LY-165,135 was oriented perpendicular to the lipid. The presence of cholesterol was found to affect the drugs' positions in the bilayer. Quipazine was pushed further towards the centre of the bilayer (the acyl chain termini) when the sample was in the fluid lamellar phase. The effect on LY-165,135, conversely, was to push it towards the headgroup region as the fluid lamellar phase approached. The drug interactions with cholesterol during the mixed  $[l_o + l_d]$  phases indicate that these compounds may be partitioning into the liquid-ordered phase under these conditions.

*Use of an Enzyme Substrate to Investigate Bilayer Dynamics* – DROSS NMR,  $^{31}\text{P}$  NMR and fluorescence emission spectroscopy were used to analyse the effect of catalysing an enzyme substrate on a lipid bilayer. 1,2-Dioctanoyl-*sn*-glycerol (DOG) is a substrate of DGK. DGK phosphorylates DOG in the presence of adenosine triphosphate (ATP), producing phosphatidic acid (PA). DROSS was used to generate order parameters while fluorescence emission spectroscopy was used to give an indication of bilayer tension. Bilayer tension and order parameters were lower for the sample containing PA co-dissolved with DOPC relative to the sample containing catalysed PA. This is due to sequestration of the catalysed PA in the immediate vicinity of the protein rather than an even distribution throughout the bilayer (as observed for co-dissolved PA), which affects the physical properties of the bilayer.

## **Acknowledgements**

I would like to thank my supervisor Mark Lorch for all of his help, support and advice during the research.

I would also like to thank Steve Archibald, my second supervisor, and Georg Mehl for all of their help and support. I would also like to thank Georg for the use of his research lab for the duration of the PhD. Thanks also to Rob Lewis, Bob Knights and Kath Bulmer (Department of Biological Sciences) for additional support.

I would like to thank H. Schwalbe (Goethe University, Frankfurt) for the gift of azobenzene compounds; P. J. Booth (University of Bristol) for the gift of dibutyrylglycerol; C. Sanders (Vanderbilt University) for the gift of *E. coli* strain BL21; N. Goehring and O. Ces (Imperial College London) for the fluorescence emission measurements; and C. Windle (University of Hull) for NMR measurements.

Thanks to everyone in C302 for providing such a great working atmosphere; Lili, Chris, Alex, Ana, Rocket, Gabi, Ionuț, and Ana's chocolate fudge cake. I would also like to thank Elliot, Danielle, Matt and Jenny for their advice on various matters and their company at meal-times.

I would like to thank my family and friends; Dad, Ann, Joseph, Lizzie, Paul and Richard. Last of all I would like to thank Mum, whose encouragement, advice and support has proved invaluable throughout the PhD, and throughout my life.

## Abbreviations

|              |  |
|--------------|--|
| <b>5-HT</b>  | 5-Hydroxytryptamine  |
| <b>ADP</b>   | Adenosine diphosphate  |
| <b>AFM</b>   | Atomic force microscopy  |
| <b>APS</b>   | Ammonium persulphate   |
| <b>ar.</b>   | Aromatic (I.R. characterisation)                               |
| <b>ATP</b>   | Adenosine triphosphate   |
| <b>bR</b>    | Bacteriorhodopsin  |
| <b>brs</b>   | Broad singlet (NMR characterisation)                           |
| <b>COSY</b>  | Correlation spectroscopy                                       |
| <b>CP</b>    | Cross-polarisation   |
| <b>CTM</b>   | Central terminal methyl  |
| <b>DAG</b>   | Diacylglycerol   |
| <b>DBG</b>   | Dibutyrylglycerol  |
| <b>DBGP</b>  | Dibutyrylglycerol phosphate                                    |
| <b>dd</b>    | Double doublet (NMR characterisation)                          |
| <b>ddd</b>   | Double double doublet (NMR characterisation)                   |
| <b>DEPT</b>  | Distortionless enhancement by polarisation transfer            |
| <b>DGK</b>   | Diacylglycerol kinase  |
| <b>DM</b>    | n-Decyl- $\beta$ -D-maltopyranoside                            |
| <b>DOPC</b>  | 1,2-Dioleoyl- <i>sn</i> -glycero-3-phosphocholine              |
| <b>DPPC</b>  | 1,2-Dipalmitoyl- <i>sn</i> -glycero-3-phosphocholine           |
| <b>DRM</b>   | Detergent-resistant membrane                                   |
| <b>DROSS</b> | Dipolar recoupling on-axis with scaling and shape preservation |
| <b>DSC</b>   | Differential scanning calorimetry                              |
| <b>EDTA</b>  | Ethylenediaminetetraacetic acid                                |
| <b>FID</b>   | Free induction decay   |
| <b>FRET</b>  | Fluorescence energy resonance transfer                         |
| <b>FTIR</b>  | Fourier transform infrared spectroscopy                        |
| <b>GPCR</b>  | G-coupled protein receptor                                     |
| <b>GPI</b>   | Glycophosphatidylinositol                                      |
| <b>HSQC</b>  | Heteronuclear single-quantum coherence                         |

|                                |   |
|--------------------------------|---|
| <b>IMP</b>                     | Integral membrane protein                     |
| <b>IPTG</b>                    | Isopropyl- $\beta$ -D-thiogalactopyranoside   |
| <b>L<math>_{\alpha}</math></b> | Fluid lamellar phase                          |
| <b>L<math>_{\beta}</math></b>  | Gel phase                                     |
| <b>l<math>_d</math></b>        | Liquid-disordered phase                       |
| <b>l<math>_o</math></b>        | Liquid-ordered phase                          |
| <b>LB</b>                      | Luria-Burtani                                 |
| <b>LDH</b>                     | Lactate dehydrogenase                         |
| <b>LGCI</b>                    | Ligand-gated ion channel                      |
| <b>LY</b>                      | LY-165,135                                    |
| <b>M<math>_1</math></b>        | First spectral moment ( $^2\text{H-NMR}$ )    |
| <b>M<math>_2</math></b>        | Second spectral moment ( $^2\text{H-NMR}$ )   |
| <b>m</b>                       | Medium (I.R. characterisation)                |
| <b>m</b>                       | Multiplet (NMR characterisation)              |
| <b>MAS</b>                     | Magic-angle spinning                          |
| <b>m. p.</b>                   | Melting point                                 |
| <b>MscL</b>                    | Mechanosensitive channel of large conductance |
| <b>NADH</b>                    | Nicotinamide adenine dinucleotide             |
| <b>NMR</b>                     | Nuclear magnetic resonance                    |
| <b>NOE</b>                     | Nuclear Overhauser effect                     |
| <b>NOESY</b>                   | Nuclear Overhauser effect spectroscopy        |
| <b>NTA</b>                     | Nitrilotriacetic acid                         |
| <b>OG</b>                      | n-Octyl- $\beta$ -D-glucopyranoside           |
| <b>P<math>_{\beta}</math>'</b> | Ripple phase                                  |
| <b>PC</b>                      | Phosphocholine                                |
| <b>PE</b>                      | Phosphoethanolamine                           |
| <b>PEP</b>                     | Phosphoenolpyruvate                           |
| <b>PG</b>                      | Phosphoglycerol                               |
| <b>PI</b>                      | Phosphoinositol                               |
| <b>PIPES</b>                   | 1,4-Piperazine-bis(ethanesulphonic acid)      |
| <b>PK</b>                      | Pyruvate kinase                               |
| <b>PMSF</b>                    | Phenylmethanesulphonyl fluoride               |
| <b>PS</b>                      | Phosphoserine                                 |
| <b>Q</b>                       | Quipazine                                     |

|                      |  |
|----------------------|--|
| <b>RF</b>            | Radiofrequency                               |
| <b>R<sub>f</sub></b> | Retention factor (TLC)                       |
| <b>s</b>             | Strong (I.R. characterisation)               |
| <b>SCEE</b>          | Stored curvature elastic energy              |
| <b>SDS</b>           | Sodium dodecyl sulphate                      |
| <b>SDS-PAGE</b>      | SDS-polyacrylamide gel electrophoresis       |
| <b>str.</b>          | Stretch (I.R. characterisation)              |
| <b>t</b>             | Triplet (NMR characterisation)               |
| <b>TEMED</b>         | <i>N,N,N',N'</i> -Tetramethylethylenediamine |
| <b>TLC</b>           | Thin layer chromatography                    |
| <b>TMS</b>           | Tetramethylsilane                            |
| <b>TPPM</b>          | Two pulse phase modulation                   |
| <b>TRIS</b>          | Tris(hydroxymethyl)aminomethane              |
| <b>UV</b>            | Ultraviolet                                  |
| <b>w</b>             | Weak (I.R. characterisation)                 |

## Contents

|   | Page Number |
|---|-------------|
| <b>Chapter 1. Introduction</b>  |             |
| Part 1. The Cell Membrane   | 6           |
| <i>Definition</i>   | 6           |
| <i>Composition</i>  | 7           |
| Part 2. Membrane Lipids   | 7           |
| <i>Lipid Structure</i>  | 7           |
| <i>Lipid Behaviour</i>  | 10          |
| <i>Bilayer Properties</i>   | 13          |
| Part 3. Introduction to Lipid Domains   | 15          |
| <i>Interactions between Lipids and Drug Molecules</i>                         | 16          |
| Part 4. Membrane Proteins   | 17          |
| <i>Introduction</i>   | 17          |
| <i>Roles of Membrane Proteins</i>   | 18          |
| <i>Membrane Protein/Lipid Interactions</i>                                    | 18          |
| <i>Previous Analysis of Membrane Proteins</i>                                 | 20          |
| Part 5. NMR Spectroscopy  | 21          |
| <i>Introduction</i>   | 21          |
| <i>Background</i>   | 22          |
| <i>Signal Generation</i>  | 24          |
| <i>The NMR Spectrum</i>   | 24          |
| <i>NMR Experiments</i>  | 26          |
| <i>2D NMR</i>   | 26          |
| <i>Solid-State NMR Spectroscopy</i>   | 27          |
| <i>Dipolar Recoupling On-Axis with Scaling and Shape</i>                      |             |
| <i>Preservation</i>   | 28          |
| <i>Deuterium (<sup>2</sup>H) NMR</i>  | 29          |
| Part 6. Use of Isomerisable Lipid Analogues to Modulate<br>Membrane Behaviour | 30          |
| <i>Azobenzenes</i>  | 30          |
| Part 7. References  | 33          |

## Chapter 2. Modulation of Enzyme Activity Using an Azobenzene-Containing Lipid Analogue

|  |    |
|--|----|
| Part 1. Introduction   | 40 |
| <i>Diacylglycerol Kinase</i>   | 41 |
| Part 2. Aims   | 41 |
| Part 3. Experimental   | 43 |
| <i>Materials</i>   | 43 |
| <i>Synthesis of bis-Azo-PC</i>   | 43 |
| <i>Synthesis of 4-((4-Butylphenyl)diazenyl)phenol</i>  | 44 |
| <i>Characterisation of 4-((4-Butylphenyl)diazenyl)phenol</i>   | 44 |
| <i>Synthesis of 6-(4-((4-Butylphenyl)diazenyl)phenoxy)hexanoic acid</i>  | 45 |
| <i>Characterisation of 6-(4-((4-Butylphenyl)diazenyl)phenoxy)hexanoic acid</i>   | 45 |
| <i>Synthesis of 6-(4-((4-Butylphenyl)diazenyl)phenoxy)hexanoic pivalic anhydride</i>   | 46 |
| <i>Synthesis of 1,3-bis(6-(4-((E))-4-Butylphenyl)diazenyl)phenoxy)hexanoyloxy)propan-2-yl 2-(trimethylammonio)ethyl phosphate (bis-Azo-PC)</i> | 47 |
| <i>Characterisation of bis-Azo-PC</i>  | 48 |
| <i>Protein Synthesis</i>   | 48 |
| <i>SDS-PAGE</i>  | 49 |
| <i>Extraction of DGK</i>   | 49 |
| <i>Preparation of Liposomes</i>  | 50 |
| <i>UV Spectroscopy</i>   | 50 |
| <i>Enzyme Assay</i>  | 51 |
| <i>Calculation of Enzyme Activity</i>  | 52 |
| Part 4. Results and Discussion   | 54 |
| <i>Protein Synthesis</i>   | 54 |
| <i>Changing the Conformation of Azobenzene-Containing Compounds in Solvents</i>  | 54 |

|  |    |
|--|----|
| <i>Changing the Conformation of<br/>Azobenzene-Containing Compounds in Liposomes</i> | 56 |
| <i>The Enzyme Assay Experiment</i>   | 58 |
| <i>Problems with the Methodology</i>   | 65 |
| Part 5. Conclusion   | 66 |
| Part 6. References   | 67 |

### **Chapter 3. Phase Behaviour**

|   |     |
|---|-----|
| Part 1. Introduction  | 70  |
| <i>Analysis of Lipid Phase Behaviour</i>  | 70  |
| <i>Serotonin Receptor Agonists</i>  | 70  |
| <i>Analysis of the Phase Behaviour of DPPC Samples using<br/><sup>2</sup>H-NMR Spectroscopy</i> | 72  |
| <i>Characteristics of <sup>2</sup>H-NMR Spectra of Lipid Bilayers</i>                           | 72  |
| <i>Moments Analysis</i>   | 74  |
| <i>Central Terminal Methyl Splitting</i>  | 75  |
| Part 2. Aims  | 75  |
| Part 3. Experimental  | 75  |
| <i>Materials</i>  | 75  |
| <i>Sample Preparation</i>   | 76  |
| <i>NMR Measurements</i>   | 76  |
| Part 4. Results and Discussion  | 77  |
| <i>NMR Assignments</i>  | 77  |
| <i>Phase Behaviour</i>  | 78  |
| <i>Visual Analysis</i>  | 79  |
| <i>M<sub>1</sub> Data</i>   | 83  |
| <i>Δ<sub>2</sub> Data</i>   | 90  |
| <i>Central Terminal Methyl Splitting Data</i>   | 94  |
| <i>Order Parameter Data</i>   | 97  |
| <i>Differential Scanning Calorimetry Data</i>   | 98  |
| Part 5. Conclusion  | 100 |
| Part 6. References  | 103 |

**Chapter 4. Analysis of Drug Localisation and Orientation in a Model Membrane by NMR Spectroscopic Methods**

|  |     |
|--|-----|
| Part 1. Introduction   | 107 |
| Part 2. Aims   | 109 |
| Part 3. Experimental   | 109 |
| <i>Materials</i>   | 109 |
| <i>Sample Preparation</i>  | 109 |
| <i>NMR Measurements</i>  | 109 |
| <i>NOESY Cross-Relaxation Rates and Location Probability Determination</i>   | 110 |
| Part 4. Results and Discussion   | 111 |
| <i>NMR Assignments</i>   | 111 |
| <i>NOESY Location Probabilities for the DPPC/Agonist Samples</i>             | 116 |
| <i>NOESY Location Probabilities for the DPPC/Cholesterol/Agonist Samples</i> | 119 |
| <i>The Effect of Agonist Molecules on the Bilayer</i>                        | 124 |
| Part 5. Conclusion   | 125 |
| Part 6. References   | 126 |

**Chapter 5. Use of an Enzyme Substrate to Investigate Bilayer Dynamics**

|   |     |
|---|-----|
| Part 1. Introduction  | 128 |
| <i>Dipolar Recoupling On-Axis with Scaling and Shape Preservation</i> | 128 |
| <i>Fluorescence Emission Spectroscopy of Lipid Bilayers</i>           | 129 |
| Part 2. Aims  | 130 |
| Part 3. Experimental  | 132 |
| <i>Materials</i>  | 132 |
| <i>Sample Preparation</i>   | 132 |

|   | <b>Page Number</b> |
|---|--------------------|
| <i>NMR Measurements</i>   | 132                |
| <i>Fluorescence Emission Spectroscopy</i>                                     | 133                |
| Part 4. Results and Discussion  | 133                |
| <i>DROSS Results</i>  | 133                |
| <i><sup>31</sup>P NMR Results</i>   | 137                |
| <i>Fluorescence Results</i>   | 138                |
| <i>Differences between Doped and Enzyme-Catalysed PA<br/>in DOPC Bilayers</i> | 139                |
| Part 5. Conclusion  | 141                |
| Part 6. References  | 141                |
| <b>Conclusion</b>   | 143                |

## **Chapter 1: Introduction**

### **Part 1. The Cell Membrane**

*Definition* - Cell membranes are biological assemblies which compartmentalise all living cells. They were once thought to be a passive bystander of the activities occurring in the cell's interior; however now it is known that the cell membrane itself is as dynamic an environment as the cytoplasm.

As well as the various lipid dynamics and phase formations, there are also a variety of protein-mediated processes taking place. The main role of cell membranes is to encapsulate and separate the cell from its external environment; additionally, membranes within the eukaryotic cytoplasm compartmentalise organelles. The membrane is selectively permeable to a variety of molecules, mediated by the membrane proteins in the form of ion channels and gates. Membranes are host to a range of extremely important protein-mediated reactions; for example, the energy-conversion processes of photosynthesis and oxidative phosphorylation are both membrane-based. Membrane proteins account for thirty to forty percent of a proteome and are also thought to account for up to seventy percent of drug targets<sup>1-3</sup>.

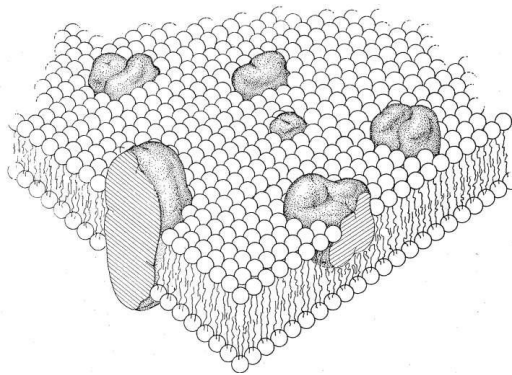


*Figure 1.1. The classic Singer-Nicholson model of the cell membrane, showing integral membrane proteins in a lipid matrix<sup>4</sup>*

The classic Singer-Nicholson model describes the cell membrane as a semi-permeable “fluid mosaic” in which membrane proteins are surrounded by a membrane lipid matrix<sup>4</sup> (Figure 1.1). The lipid matrix is formed of two back-to-

back lipid monolayers (six to ten nanometres in width), primarily phospholipid, with the hydrophilic headgroups facing out to the aqueous environments of the cytoplasm and the extracellular space, and the hydrophobic hydrocarbon chains facing into the centre of the bilayer<sup>4,5</sup>.

*Composition* - Cell membranes are heterogeneous, composed of thousands of different lipid species, membrane proteins, and other biological molecules such as carbohydrates<sup>6</sup>. The lipid species include phospholipids, sterols, glycolipids and sphingolipids. The lipid composition of cell membranes varies with species, with cell type within the same species, and in response to various external and internal stimuli. The cell composition is also observed to vary with certain disease states; for example, increased amounts of cholesterol were observed in erythrocyte plasma membranes of patients with various types of liver disease<sup>7</sup>. Cell membranes also contain a large variety of proteins, including receptors, transporters and structural proteins.

## Part 2. Membrane Lipids

*Lipid Structure* - The majority of the lipid content in most eukaryotic and prokaryotic cells are phospholipids. The general structure of the amphiphilic phospholipid molecule can be divided into three regions: the headgroup, the glycerol, and the chain or tail regions (Figure 1.2).

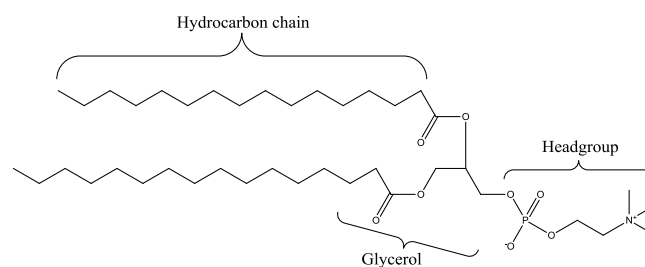


*Figure 1.2. Structure of 1,2-dipalmitoyl-sn-glycero-3-phosphocholine (DPPC) demonstrating the three regions: the hydrocarbon chain, the glycerol, and the headgroup regions*

The tail region usually contains two hydrocarbon chains, which vary between fourteen and twenty-four carbon atoms in length, the most common lengths being sixteen or eighteen carbon atoms<sup>8, 9</sup>. There are also varying degrees of saturation, with saturated, mono-unsaturated, and poly-unsaturated chains. These hydrocarbon chains are usually linked to the headgroup region by an interfacial glycerol group. The headgroup also varies in chemical composition. The most common headgroups include phosphocholine (PC), phosphoethanolamine (PE), phosphoserine (PS), and phosphoglycerol (PG) (Figure 1.3).

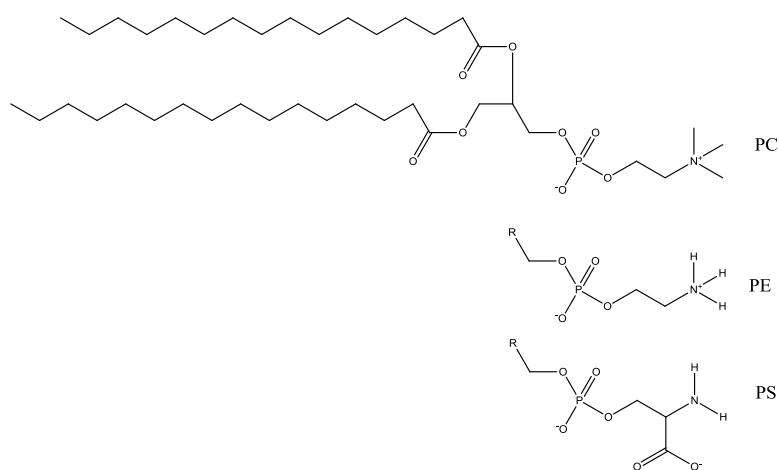


*Figure 1.3. Structures of phosphocholine (PC), phosphoethanolamine (PE) and phosphoserine (PS) headgroups, where R is the glycerol and chain region as shown in the structure of phosphocholine*

The identity of the phospholipid is therefore determined by the composition of the headgroup (e.g. PC, PE, PS, phosphoinositol (PI), etc.) and the length and saturation of the hydrocarbon tail. The headgroups in general are polar and charged, and the charge density varies with the identity of the headgroup; for example, the charge density of PS is greater than that of PC. The length of the hydrocarbon chain and the degree of saturation also affects the tail region of the membrane.

Sphingolipids are a type of phospholipid which contains an amide linkage between the hydrocarbon chain and the headgroup in place of the glycerol linkage. The hydrocarbon chain is normally eighteen or twenty carbon atoms in

length, varying in saturation. The identity of the sphingolipid depends on the chemical nature of the headgroup and also includes PC, PE and PS headgroups (Figure 1.4).

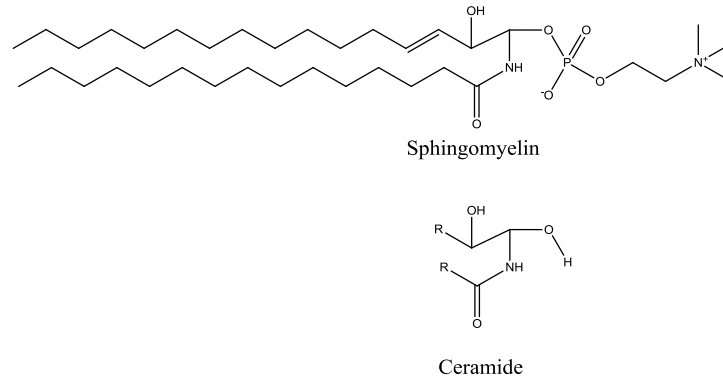


*Figure 1.4. Structures of sphingomyelin and ceramide headgroups, where R represents the hydrocarbon chains as shown in the structure of sphingomyelin*

Other membrane lipids include sterols and glycolipids. Cholesterol is the most common sterol in the eukaryotic cell membrane, with the exception of fungi, bacteria and plants. All sterols have the general structure of three cyclohexane rings and one cyclopentane ring with additional side-chains (Figure 1.5).

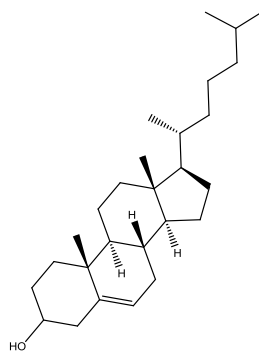


*Figure 1.5. The structure of cholesterol, the most abundant sterol in the cell membrane, showing the three cyclohexane rings joined to a cyclopentane ring*

Glycolipids are lipids (including phospholipids and sphingolipids) with a carbohydrate headgroup; they are concentrated in the exofacial leaflet of the cell membrane.

*Lipid Behaviour* - In aqueous environments amphiphilic lipid molecules may self-organise into a number of forms, depending on the structure and concentration of the lipids present. These forms include the lamellar, micellar and inverse hexagonal phases (Figure 1.6).

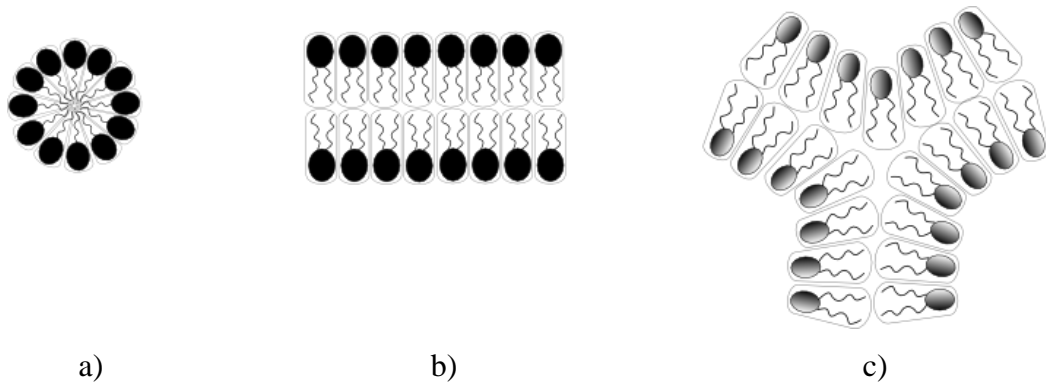


*Figure 1.6. Diagram showing some of the possible lipid phases in an aqueous environment, depending on lipid structure and concentration. The micellar phase formed by lyso-lipids is depicted in a), the lamellar bilayer adopted by cylindrical lipids such as PCs is shown in b), and the inverse hexagonal phase formed by cone-shaped lipids such as PEs is shown in c)*

The form adopted by lipids in an aqueous environment is highly dependent on their structure, as demonstrated in Figure 1.6. Lysolipids, containing a single hydrocarbon chain, and short chain lipids tend to spontaneously form micelles due to their tapering cone shape. Cylindrical lipids, in which the headgroup occupies approximately the same cross sectional area as the hydrocarbon chain, spontaneously form lamellar bilayers, as observed in the cell membrane. Examples of lamellar-forming lipids include phosphocholines. Cone-shaped lipids, in which the headgroup occupies a smaller volume than the hydrocarbon chain, tend to form the inverse hexagonal phase. Cone-shaped lipids include phosphoethanolamines<sup>6, 10, 11</sup>.

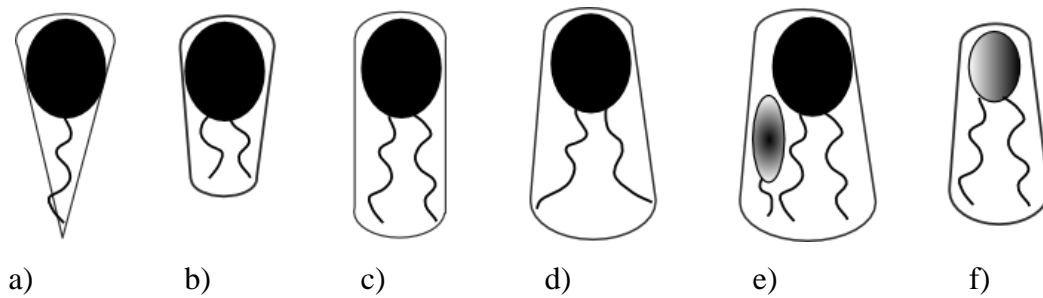


*Figure 1.7a - f. Diagram showing approximate lipid shapes. The shape that lipids adopt in the bilayer depends on the nature of the headgroup and hydrocarbon chains. Lipids such as lyso-lipids, with a large headgroup relative to the volume of the hydrocarbon chain, adopt a tapering cone shape (a) and tend to form micelles; short-chain lipids (b) adopt a stunted cylindrical shape; lipids with a cylindrical shape (c), such as PC lipids, tend to form lamellar bilayers; and lipids with a cone shape, such as PE lipids (d) and interdigitated lipids (e), tend to form the inverse hexagonal. Lipids with smaller headgroups (f) take up smaller volumes of space*

The shapes of various lipids are also influenced by saturation. The presence of double bonds leads to kinks in hydrocarbon chains, increasing the volume that the hydrocarbon chain region occupies, as observed for cone-shaped lipids; lack of saturation enables closer lipid packing.

In a eukaryotic cell membrane environment, the bulk of the phospholipids are phosphocholines, leading to the lamellar lipid bilayer form observed. This is the only form viable for biological life, as it provides encapsulation and compartmentalisation.

Lipids in the lamellar phase may adopt several sub-phases depending on several factors, including temperature. At low temperatures lipids adopt the  $L_{\beta}$  or gel phase, in which there is minimal lateral or transbilayer diffusion of individual lipid molecules, minimal rotation of the lipid about the long axis, and relatively close packing. The phase displays a high order parameter (a measure of the rigidity of the lipid molecule at various sections along its length, giving an indication of the freedom of movement in a particular region of the bilayer). As

temperature increases the lipids enter the  $L_{\alpha}$  or liquid-disordered ( $l_d$ ) phase. In this phase there are increased lateral and transbilayer diffusions, increased rotations about the long axis, and increased chain isomerisations together with looser packing of molecules and a corresponding decrease in order parameter. Other sub-phases include the  $L_{\beta}'$  or ripple phase, and the liquid-ordered ( $l_o$ ) phase, which is of particular interest. The  $l_o$  phase is intermediate between the gel and  $l_d$  phases in its properties, and has been shown to coexist with both the gel and  $l_d$  phases in model membranes by techniques such as NMR spectroscopy and fluorescence microscopy<sup>6, 12-14</sup>. In cell membranes it may coexist with the  $l_d$  phase. The formation of the  $l_o$  phase is induced by the presence of intercalation of relatively bulky sterols or sphingomyelin with the phospholipid molecules, reducing the freedom of movement of the phospholipids and increasing the bilayer pressure in the region. The  $l_o$  phase has a relatively high order parameter in comparison with the  $l_d$  phase, but with fast lipid dynamics (Figure 1.8)<sup>6, 15</sup>.

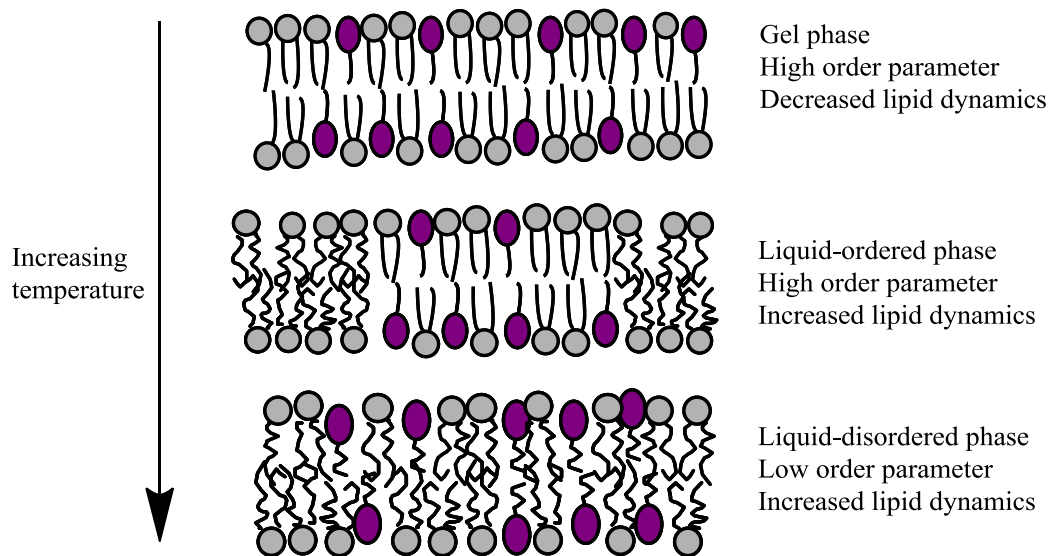


*Figure 1.8. Simplified diagram showing lipid phases. At the lowest temperature, lipids adopt the gel phase. As temperature increases lipids adopt the intermediate liquid-ordered phase, finally followed by the liquid-disordered phase*

*Bilayer Properties* - The lipid bilayer can be considered as three separate regions, following the division of the general phospholipid molecule: the headgroup, glycerol, and hydrocarbon chain regions. The headgroup region is highly hydrated. Interactions between individual headgroup moieties depend on their charges and sizes, and attractive interactions may arise due to hydrogen bonding. Headgroup moieties are relatively flexible and disordered<sup>11</sup>. The glycerol region, which acts as an interface between the headgroup and the hydrocarbon chain, is less hydrated than the headgroup region, and is more rigid than either of the neighbouring regions<sup>11</sup>. Interactions in this region are due to hydrogen bond formation from the carbonyl groups. The degree of hydration is lowest in the hydrocarbon chain region due to the hydrophobic character of the acyl chains. Interactions between neighbouring chains or protein residues are due to van der Waals' forces.

The degree of saturation present (one or more double bonds) affects the volume and the packing of lipid molecules in this region; fully saturated chains pack more closely together than unsaturated chains, giving rise to less free volume. The presence of double bonds leads to the existence of areas of lower pressure or free volume in the bilayer, as well as conferring an amount of rigidity on the acyl chain. This region has a high degree of disorder relative to the glycerol region, due to the flexibility of the acyl chains<sup>11</sup>.

The physical properties of the bilayer include lipid packing; lipid phase; surface tension; bilayer lateral pressure; curvature stress and the associated stored curvature elastic energy (SCEE); and individual lipid dynamics. There is an amount of surface tension present in lipid bilayers, which is due to competition between the attractive force between surface molecules and their immediately neighbouring molecules, and between surface molecules and the bulk of the molecules below the surface<sup>11</sup>. The attraction to the bulk is stronger than the attraction to the neighbouring surface molecules, so the molecule always experiences a downward-pulling force, setting up the tension.

Lipid movements in the bilayer give rise to an internal pressure which may be as high as 400 atm in certain regions<sup>15</sup>. The effect of bilayer lateral pressure can be observed in a pressure profile of the three regions (Figure 1.9)<sup>15</sup>.

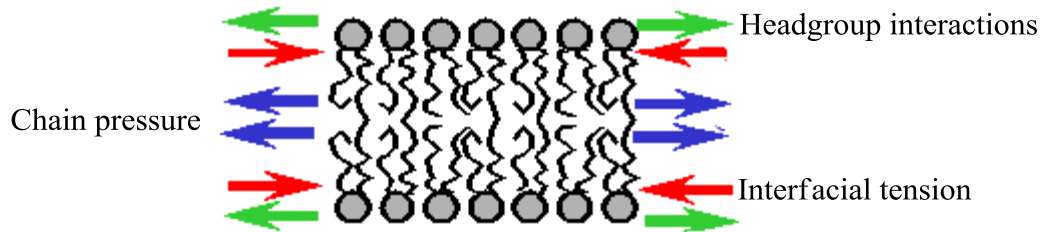


*Figure 1.9. Bilayer lateral pressure profile, indicating regions of headgroup interactions (green arrows), chain pressures (blue arrows), and interfacial tension*

In the headgroup region there are both repulsive and attractive forces between the molecules. Steric hindrance between molecules is a repelling force; electrostatic and hydrogen bonding forces are attractive. The net pressure in this region is a positive (i.e. acting “outwards”), repelling lateral pressure, leading to bilayer expansion in this region. In the glycerol region there is an attractive tension arising from the interactions between the tops of the acyl chains and water molecules; that is, the hydrophobic tops of the chains tend to pull together to avoid contact with water. This produces a net negative (i.e. acting “inwards”), attractive lateral pressure, causing bilayer contraction in this region. In the acyl chain region there are both repulsive forces (thermal motions) and attractive forces (van der Waals’ interactions) in play; overall there is a net positive, repelling lateral pressure in this region, leading to bilayer expansion. In general, the bilayer expands in the headgroup and acyl chain regions, pushing other bilayer molecules “outwards”, and contracts in the glycerol region, pulling molecules “inwards”<sup>10, 15 - 17</sup>. The pressure profile in the acyl chain region is also dependent on chemical structure to an extent, and can be increased by the presence of double bonds<sup>10</sup>.

### Part 3. Introduction to Lipid Domains

The lipid heterogeneity of the classical Singer-Nicholson fluid mosaic model raises questions; a passive lipid matrix has no need for the variety of lipid structures and physical properties encountered in cell membranes. The cell membrane is particularly enriched in cholesterol and sphingomyelin, both structurally rigid lipids involved in the formation of the  $l_o$  phase. It was hypothesised that the presence of cholesterol and sphingomyelin could lead to the formation of areas or ‘rafts’ or  $l_o$  phase lipids within the  $l_d$  phase bulk<sup>18</sup>. Extraction of whole cells using cold, non-ionic detergents produces detergent-resistant membranes (DRMs) enriched in cholesterol and sphingomyelin, and sometimes associated with certain proteins e.g. acylated proteins, glycosphosphatidylinositol (GPI)-anchored proteins, and some receptor proteins. DRMs are a product of cold detergent extraction. It is thought that the association of certain proteins with DRMs indicates a higher probability of association of these proteins with rafts in a cell membrane, making them useful indicators of possible “raftophilic” proteins<sup>19, 20</sup>. Detergent extraction is not an ideal method; it relies on using detergents at low temperatures, which can produce an artificially high fraction of  $l_o$  and gel phase lipids. The use of alternative, room-temperature detergents may not solubilise all  $l_d$  phase lipids. However it can be a useful technique when used in conjunction with other methods of extraction, which include the use of sodium carbonate gradients (which rely on pH) and immunoisolation<sup>20</sup>.

Several roles for rafts have been proposed, based on the protein associations that have been discovered. These include roles as platforms for protein-mediated events such as signal transduction, membrane fusion, organisation of the cytoskeleton, lipid sorting and protein trafficking<sup>20</sup>. It is also thought that they may play a role in facilitating viral invasions and plaque formation during Alzheimer’s disease. Research has shown the co-localisation of psychotropic drugs with their receptors in rafts, implying that lipid rafts may play a role in co-localising receptor proteins with their substrate molecules to facilitate and enhance signal transduction<sup>21-23</sup>. Observing rafts in cell membranes poses more challenges than the analysis of microdomains in models, mainly due to their

small size (10 - 200 nm in diameter) and transient lifetimes. One method is tracking the distribution of the fluorescent probe LAURDAN (6-dodecanoyl-2-dimethylaminonaphthalene) in a membrane using two-photon microscopy<sup>24</sup>.

Areas of  $l_o/l_d$  phase coexistence, termed lipid microdomains, may be observed in model membranes with the correct composition. These are thought to be analogous to the biological rafts which form in the cholesterol- and sphingolipid-enriched environment of the cell membrane. Fluorescence quenching experiments have been used to show preferential partitioning of fluorophore molecules and quenching molecules into  $l_o$  and  $l_d$  phases, respectively, producing intense fluorescence for detection<sup>12, 13, 25, 26</sup>. Microdomains can also be visualised indirectly using solid-state deuterium and proton NMR methods to show phase transitions and phase coexistence<sup>14, 27-29</sup>. X-ray diffraction can be used to determine the thickness of bilayers, as microdomains are expected to be thicker than the surrounding liquid-disordered matrix<sup>20</sup>.

*Interactions between Lipids and Drug Molecules* - Drug molecules must interact with a number of membranes on the way to their target receptor proteins. If taken orally they must first cross from the digestive system to the blood vessels, and must then cross into the cell membrane to interact with membrane-situated receptors. In addition, certain drugs must also cross the blood-brain barrier. The majority of drug molecules then interact with a membrane protein, although lipid-soluble molecules may pass through the membrane without first interacting with a membrane protein or receptor. Sargent and Schwyzer proposed the membrane catalysis mechanism of ligand/receptor binding, based on their observation of the interactions of the polypeptide hormones (adrenocorticotropin-(1-24)-tetracosapeptide, ACTH<sub>1-24</sub>, and dynorphin-(1-13)-tridecapeptide, dynorphin<sub>1-13</sub>) with model membranes<sup>30</sup>. In this mechanism, the final ligand/receptor binding step is preceded by accumulation of ligands in the membrane and interactions of ligands with membrane lipids. Therefore, interaction of drug molecules with cell membranes is important to pharmacological activity. Once in the cell membrane the drug molecule binds with the active site of its target protein. In the case of agonist drugs the binding activates a cascade of signalling events within the cell, the results of which are

responsible for the drug's activity. Therefore it is important for the interaction between the drug molecule and the receptor protein to be optimised. The observation of certain receptor proteins isolated in detergent-resistant membranes has led to the hypothesis that signal transduction may be amplified by the co-localisation of drug molecules with their receptor proteins<sup>21, 31</sup>. Research has been carried out into the localisation of psychotropic drugs in detergent-resistant membranes<sup>21,31</sup>.

#### **Part 4. Membrane Proteins**

*Introduction* - Membrane proteins are a family of proteins that are defined by their relationship to biological membranes; they are not soluble in the aqueous environment of the cytoplasm and can only fold to the correct configuration when provided with a hydrophobic environment such as a biological membrane, artificial lipid bilayer or some detergent micelles. Analysis of genome sequence data has predicted that membrane proteins may account for thirty to forty percent of the total protein complement of the cell<sup>1, 15, 32-34</sup>. Despite this, information about their three-dimensional structures, folding behaviours, and interactions with the membrane is relatively scarce compared to the knowledge amassed regarding soluble proteins<sup>1, 33, 34</sup>. For example, known three-dimensional structures of water-soluble proteins number in their thousands, but less than one percent of the final structures in the Protein Data Bank are membrane proteins<sup>1, 32, 35-39</sup>.

Membrane proteins have a range of three-dimensional configurations and molecular weights. They are categorised according to the level of their interaction with the membrane. Peripheral membrane proteins are relatively loosely bound to either side of the cell membrane, facing out into either the cytoplasm or the exoplasm. Integral membrane proteins (IMPs) may be amphipathic in nature, containing a hydrophobic, transmembranous domain and hydrophilic, extramembranous domains, which enables them to pass through the bilayer and extend on either side of the membrane. IMPs are proteins that may only be extracted by disruption of the bilayer using detergents or organic solvents, while peripheral proteins are more readily extracted<sup>8</sup>.

The final three-dimensional structure of a membrane protein depends on the sequence of amino acids (the primary structure). Chemical interactions between the amino acid side chains produce structures such as  $\alpha$ -helices and  $\beta$ -pleated sheets. Interactions between the  $\alpha$ -helices and  $\beta$ -sheets of the same protein produce the final three-dimensional structure. For enzymes, the final structure contains the active site. The shape of the final folded enzyme is essential to its activity, because activity is conferred through the use of binding sites specifically suited to substrate molecules. In addition proteins may incorporate intrinsic metal atoms as part of their three-dimensional structure, such as haemoglobin<sup>40</sup>.

*Roles of Membrane Proteins* - The roles of membrane proteins include control of cell permeability, via channels, gates, pumps, and transporters; signal transduction across the membrane; energy generation; mediation of biosynthetic pathways; and catalysis. They are also potential targets for pharmaceutical agents; in particular, for example G-coupled protein receptors (GPCRs), act as targets for the majority of drug molecules<sup>1, 5, 35, 40, 41</sup>.

*Membrane Protein/Lipid Interactions* - The effects of lipids on membrane proteins are divided into specific and non-specific effects, and include both physical and chemical effects. While the majority of the lipids in the membrane have a non-specific effect on proteins, it must also be considered that proteins themselves exert an effect on their neighbouring lipids; thus there are a number of mutual lipid-protein interactions governing the behaviour of membrane proteins<sup>10</sup>.

The non-specific effects of lipids on membrane proteins arise from the molecular structures of phospholipids. The effect of the interactions may be negligible, or may influence the folding and activity of the protein. The effect of lipid dynamics, such as exchange, on membrane protein activity or folding is negligible. Exchange from the lipids immediately surrounding the protein (the annular lipids) to the bulk does not alter the protein's lipid environment; these motions are sufficiently rapid relative to the timescale of protein motion that the protein experiences an average of the lipid motions. Exchange of co-factor lipids occurs but is rare due to the strength of their interactions with the protein. Other

physical properties, such as hydrocarbon chain length, have more of an effect on the protein<sup>10</sup>.

Protein activity occurs at active sites, the structures of which are determined by the three-dimensional folding of the protein. Hence proper function of the protein is highly dependent on its folded structure; misfolding of certain membrane proteins is known to contribute to several serious diseases, such as cystic fibrosis, Alzheimer's disease, and Creutzfeldt-Jakob disease<sup>42, 43</sup>. The folded state is determined by the confines of the surrounding environment – the cell membrane. Parameters such as lateral pressure and curvature stress would be expected to have a significant effect on insertion, folding and activity of membrane proteins.

Protein transmembrane domains are subject to a range of forces in the bilayer. They exist under great pressure – the pressure in the bilayer has been calculated to reach several hundred atm in the acyl chain region<sup>16</sup> – and under varying amounts of curvature frustration, depending on the composition of the membrane. Both of these bulk physical properties have an effect on the insertion, folding and activity of membrane proteins<sup>44-46</sup>. The effects can be studied by manipulating the degree of curvature frustration in a model membrane; a greater amount of PE lipids will increase the stored curvature elastic energy (SCEE), while a greater amount of single-chain or saturated PC lipids in an unsaturated PC lipid bilayer will decrease SCEE. Research has shown that both increasing and decreasing SCEE can affect the protein. For example, the folding yield of the membrane protein bacteriorhodopsin (bR) decreases when SCEE is increased by introducing greater amounts of PE lipids into a PC bilayer, and increases when SCEE is reduced by introducing single-chain or short-chain PC lipids<sup>47</sup>. It can be seen from these studies that there must be an optimum level of SCEE (and hence curvature frustration) for the insertion, folding and activity of membrane proteins, which may be controlled homeostatically by the cell itself<sup>47</sup>. Since pressure in the bilayer is closely linked to membrane composition and curvature frustration, it may be expected that a similar feedback mechanism is utilised to provide the optimum pressure conditions for membrane proteins. Protein activity is also affected by the acyl

chain length, with the optimum activity taking place in bilayers containing acyl chains eighteen carbon atoms in length; protein activity decreases when this length is exceeded or reduced<sup>8</sup>. The acyl chain length is closely connected to hydrophobic mismatch. The energetic cost of allowing either the hydrophobic acyl chains or the hydrophobic amino acid residues into contact with water is high, so the bilayer is expected to distort to match the span of the protein. In fact the bilayer is not seen to distort as much as expected; instead there is a mutual deformation of the lipids surrounding the protein (by distortion of the acyl chains) together with the transmembrane domains (by changing the tilt angles or packing of the  $\alpha$ -helices) (Figure 1.10)<sup>11</sup>.

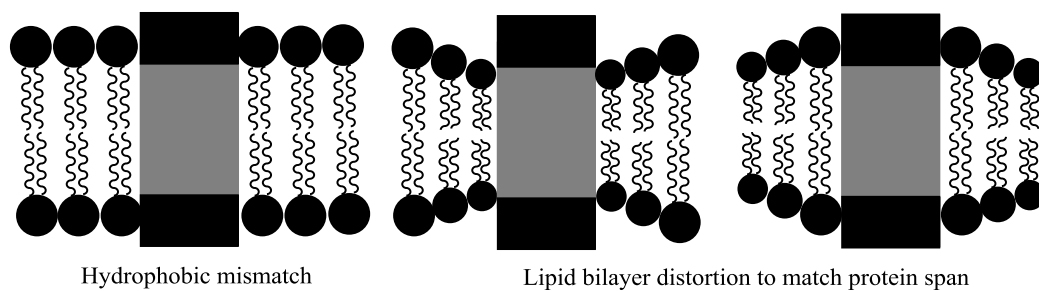


*Figure 1.10. Diagram showing hydrophobic mismatch, and subsequent deformations of the lipid bilayer to reduce exposure of hydrophobic protein domains to the aqueous environment*

There are also specific, molecular interactions between lipid molecules and membrane protein domains. The crystallisation of membrane proteins for x-ray crystallographic analysis has shown the presence of lipids bound to sites on the membrane protein. These are known as non-annular lipids, and are thought to play a role in the activity of the protein<sup>11, 16, 45</sup>. The interactions between the lipid molecule and the protein are strong enough to resist detergent solubilisation.

*Previous Analysis of Membrane Proteins* - The most common method of obtaining high-resolution structural data from isolated water-soluble proteins is by x-ray diffraction of crystals, because these types of proteins are amenable to crystallisation; however this method has not been so extensively used to analyse membrane proteins. The x-ray diffraction method first relies on the synthesis

and purification of relatively large amounts of protein, which is more difficult for membrane proteins. While there are a large number of water-soluble proteins which can be first over-expressed and then purified from microbial hosts, the number of membrane proteins amenable to over-expression is limited. In addition, they must also be provided with a suitable membrane-like environment in which to fold, which must not degrade over time. Membrane proteins may be switched between a number of membrane model systems during a single purification route.

Other methods of protein structural analysis include electron microscopy and NMR spectroscopy. In previous years, NMR spectroscopy was hindered by the insolubility of membrane proteins in aqueous environments; however, the development of solid-state NMR spectroscopy, in combination with advances in NMR hardware and software, have led to this becoming an important method for structural and dynamical investigations of membrane proteins<sup>48, 49</sup>. The production of membrane protein suffers from a number of problems. Only relatively small proteins can be analysed, because protein over-expression can lead to aggregation within the host due to the lack of insertion machinery in prokaryotes; in addition, the protein can only be purified by partitioning into detergent micelles, which destabilises and degenerates the protein over time. Because of the reasons above, only a very small percentage of the fully elucidated protein structures available in the Protein Data Bank belong to membrane proteins; at the time of writing, only four hundred structures (seventy-one of which were produced using NMR spectroscopic methods) out of a total of over seventy-two thousand belonged to membrane proteins<sup>37</sup>. It is an important field which merits a great deal of research to overcome these experimental hurdles.

## **Part 5. NMR Spectroscopy**

*Introduction* - Nuclear magnetic resonance (NMR) spectroscopy is a useful, versatile technique for the detection of molecular structure and composition that relies on measuring the interactions of nuclear magnetic fields with an applied magnetic field. It can be used with liquid, solid or gas samples, with compounds

of various masses and compositions, and can be used to detect a wide range of nuclides depending on instrumentation. It has been used in a diverse range of research areas, including organic, inorganic, and physical chemistry, medicine, biochemistry, protein science, and the food industry<sup>50</sup>.

*Background* - All nuclei possess an intrinsic property known as spin, a form of intrinsic angular momentum, which may have an integral or non-integral value<sup>50-52</sup>. Nuclei also have an intrinsic magnetic moment,  $\mu$ , which is linked to spin by Equation 1<sup>51</sup>:

$$\mu = \gamma \hbar I$$

*Equation 1. Equation for the calculation of magnetic moment; where  $\gamma$  is the*

$$\text{magnetogyric ratio; } I \text{ is spin; and } \hbar \text{ is } \frac{h}{2\pi} \text{ where } h \text{ is Planck's constant}^{51}$$

The magnetogyric ratio varies between different species of nuclei; for example, the magnetogyric ratio of protons,  $\gamma_{1H} = 26.7522 \times 10^7 \text{ rad s}^{-1} \text{ T}^{-1}$ , is the largest magnetogyric ratio among commonly examined nuclei<sup>51, 52</sup>. It determines the resonant frequency,  $\nu$ , of a nucleus in a particular magnetic field strength<sup>51</sup>.

In simple terms, a spin- $\frac{1}{2}$  nucleus (for example, the proton) may be regarded as a bar magnet with north and south poles. In the absence of an external applied magnetic field, the spins may align in any possible direction, and all orientations are equally represented; the sample is in equilibrium<sup>50</sup>. All of these possible orientations are degenerate<sup>52</sup>. The application of a magnetic field,  $B_0$ , breaks the degeneracy, and the spins align into  $(2I + 1)$  possible orientations. For a spin- $\frac{1}{2}$  nucleus, therefore, there are two possible orientations: aligned parallel to the  $B_0$  field, or aligned antiparallel to the  $B_0$  field<sup>51, 52</sup>. The energy of the two possible energy states is quantised. The allowed energies are given by the magnetic quantum number,  $m_I$ , with values of  $-I, -I + 1, -I + 2 \dots I - 1$ , etc. Therefore, for a spin- $\frac{1}{2}$  nucleus the possible values of  $m_I$  are  $-\frac{1}{2}$  and  $+\frac{1}{2}$ . The energy levels correspond to the parallel (lower energy) and antiparallel (higher energy)

orientations of the spins. The difference between the energy levels is  $\Delta E$ , where  $E$  is energy<sup>32</sup>. The energy gap depends on the magnitude of the nuclear magnetic moment,  $\mu$  (and hence on the magnetogyric ratio, from Equation 1) and on the strength of the external applied magnetic field,  $B_0$ <sup>32, 33</sup>. Since the energy of the interaction of the spins with the field is proportional to  $\mu$  and  $B_0$ , then<sup>32</sup>:

$$E = -\gamma\hbar m_l B_0$$

*Equation 2. Equation for the calculation of energy of the interaction between the spins and the magnetic field*

The energy difference,  $\Delta E$ , between the two energy levels is then<sup>51</sup>:

$$\Delta E = \gamma\hbar B_0$$

*Equation 3. Equation for the calculation of the energy difference between two energy levels when  $m_l$  is 1; the minus sign has been dropped due to formality*

Using Planck's law,  $\Delta E = h\nu$ , the difference in energy between the two orientations can be calculated in terms of frequency<sup>51, 52</sup>:

$$\nu = \frac{\gamma B_0}{2\pi}$$

*Equation 4. Equation for the calculation of energy difference in terms of frequency; where  $\nu$  is the frequency of nuclear precession about the  $B_0$  axis (in Hz)*

This frequency,  $\nu$ , is known as the Larmor frequency. The application of electromagnetic radiation of this frequency (using radiofrequency (RF) radiation) allows the spins to flip from one energy level to the other<sup>52</sup>. However, the exact resonance frequency of a nucleus is a characteristic of its chemical environment, because the magnetic field experienced by the nucleus varies due to the shielding

and deshielding effects of neighbouring electrons and nuclei. This is known as the chemical shift<sup>52</sup>.

The populations of the energy levels are determined by the Boltzmann population distribution<sup>51, 52</sup>:

$$\frac{N_{upper}}{N_{lower}} = \exp \frac{-\Delta E}{kT}$$

*Equation 5. The Boltzmann distribution for the population of energy levels; where  $N_{upper, lower}$  is the populations of the spins in the upper and lower energy levels;  $k$  is the Boltzmann constant; and  $T$  is temperature*

As there is only a small difference in populations between the upper and lower energy levels, NMR spectroscopy is an inherently insensitive technique. This sensitivity becomes worse for protons analysed using weak fields or for nuclei with lower magnetogyric ratios<sup>52</sup>.

*Signal Generation* - The NMR spectrum is obtained by generating a pulsed RF field from a coil which is placed in a suitable arrangement around the sample. An oscillating current is passed through the coil, which generates an oscillating magnetic field of the correct frequency to excite the sample nuclei. The excited nuclei then precess about the  $B_0$  axis at their individual resonance frequencies, producing an oscillating magnetic field. This field induces an alternating current in a nearby receiver coil<sup>52</sup>. The radiofrequency signals generated by the precessing nuclear magnetic moments are then processed by the computer software into the free induction decay (FID). The FID, which is a time-domain spectrum, is transformed into the frequency-domain NMR spectrum using Fourier transformation.

*The NMR Spectrum* - The resonance frequency,  $\nu$ , of a particular nucleus is affected by its position in a molecule and by its neighbouring nuclei. This is displayed on the NMR spectrum as the chemical shift<sup>51</sup>:

$$\delta = \frac{\nu - \nu_0}{\nu_0} \times 10^6$$

*Equation 6. Equation for the calculation of chemical shift,  $\delta$ , in parts per million (ppm); where  $\nu_0$  is the Larmor frequency and  $\nu$  is the resonant frequency of the particular nucleus*

The difference between the nucleus's resonant frequency and the Larmor frequency arises because of the electron cloud surround the nucleus<sup>51, 52</sup>. The electron cloud induces its own magnetic field (electrons are also spin-1/2 particles) which opposes the  $B_0$  field. The magnetic field experienced by the nucleus then becomes<sup>51</sup>:

$$B_{eff} = B_0(1 - \sigma)$$

*Equation 7. Equation for the calculation of the effective magnetic field ( $B_{eff}$ ) experienced by the nucleus; where  $\sigma$  is the shielding constant*

The electron-generated field is proportional to  $B_0$ ; the stronger the external applied field, the greater the opposing electron-generated field. Nuclei may also be affected by the electron clouds of neighbouring nuclei, which may have shielding (opposed to the  $B_0$  field), or deshielding (augmenting the  $B_0$  field) effects<sup>52</sup>.

The NMR resonance of a particular atom is also affected by scalar coupling, which determines the splitting pattern. Scalar coupling only takes place through directly bonded atoms (over a distance of no more than three chemical bonds) and is generated by the interactions of the electron clouds of bonded atoms<sup>50</sup>. Since it is not a through-space interaction, it can give information about the chemical bonds present in a compound. For spin-1/2 nuclei, the number of splittings for each signal is equal to  $n + 1$ . The number of splittings therefore indicates the number of protons in an adjacent group. The distance (the coupling constant) between the splittings may also provide useful information about

aromatic protons<sup>52</sup>. Coupling constants for protons separated by three bonds are used to determine the conformations of protein secondary structures (such as  $\alpha$ -helices and  $\beta$  sheets) by calculating characteristic dihedral angles between the amide and carboxylic acid groups of the peptide backbone. The dihedral angle is calculated from the measured coupling constants using the Karplus equation<sup>52</sup>:

$${}^3J = A + B \cos \theta + C \cos^2 \theta$$

*Equation 8. Equation for the calculation of dihedral angles from measured coupling constants; where  ${}^3J$  is the three-bond spin-spin coupling constant; A, B, C are coefficients with the values 2 Hz, -1 Hz and 10 Hz, respectively; and  $\theta$  is the dihedral angle<sup>52</sup>*

*NMR Experiments* - There is a wide range of available NMR experiments, depending on what information is required about the sample and what instrumentation is present. The most commonly used, and simplest, NMR experiments are the 1D proton 90° experiments routinely used in organic synthetic laboratories to quickly produce confirmation of structures of novel compounds. 1D carbon experiments such as DEPT experiments are also used to give structural information about the presence of primary, secondary, tertiary and quaternary carbon atoms. Further structural detail can be obtained by using more advanced 2D experiments such as NOESY, COSY or HSQC.

NMR is not limited to the measurement of carbon and hydrogen; technically any spin>0 element may be analysed, although in practice limitations with the available instrumentation may limit the possibilities. Some other commonly measured nuclides include  ${}^{31}\text{P}$ ,  ${}^{19}\text{F}$ ,  ${}^{15}\text{N}$  and  ${}^{29}\text{Si}$ . More complex spectra are generated by analysing quadrupolar nuclides such as  ${}^2\text{H}$  (or D) and  ${}^{14}\text{N}$ .

*2D NMR* - In a simple 1D experiment, there is a single 90° RF pulse followed by an acquisition period, during which the FID is collected. This process is expanded for 2D NMR. The primary 90° pulse is followed by a delay ( $t_1$ ), before a secondary 90° pulse is applied and the FID acquired. The program is then

repeated for a series of  $t_1$  values. The data set is deconvoluted as normal using Fourier transformation to produce a 2D spectrum<sup>50</sup>. 2D NMR experiments, such as COSY (correlation spectroscopy) and NOESY (nuclear Overhauser effect spectroscopy) show hetero- and homonuclear spin-spin couplings as cross-peaks along a diagonal axis and enable structural elucidation of complex compounds that may not be possible using 1D NMR methods.

The 2D-NOESY experiment relies on the nuclear Overhauser effect (nOe), which is the transfer of magnetisation from one spin to another in a hetero/homonuclear dipole. The nOe is a distance-dependent, through-space interaction which can give information on structure and on interactions between different moieties in the same sample.

*Solid-State NMR Spectroscopy* - The main difference between solution-state and solid-state NMR is the effect of anisotropic interactions, such as homo- and heteronuclear dipolar interactions, which are no longer averaged out due to the random molecular motions occurring in a liquid. This random tumbling can be replicated by spinning the sample at an angle of  $54.74^\circ$  to the  $B_0$  axis, which is the average of the  $x$ ,  $y$  and  $z$  axes.

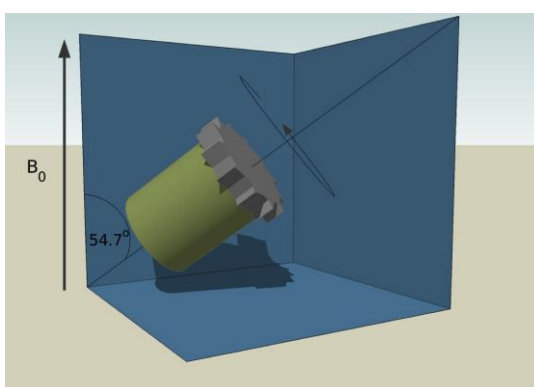


*Figure 1.11 Diagram showing the position of a sample rotor with finned cap at  $54.7^\circ$  to the  $B_0$  axis*

Samples are loaded into rotors and fitted with finned caps, as shown in Figure 1.11. The caps are designed so that the rotor can be spun using currents of air. Spinning speeds are normally between 2.5 and 12 kHz.

Since its invention, magic-angle spinning (MAS) has been used with a wide range of compounds, including catalysts, polymers and biomolecules<sup>35</sup>. MAS-NMR is well-suited to the analysis of native and model membranes, membrane proteins, and lipid/protein interactions<sup>59-62</sup>. MAS produces resonance peaks with linewidths comparable to those of solution spectra, and allows the analysis of proteins in complex environments<sup>57</sup>. Unlike solution-state spectroscopy, there is no upper limit to the molecular mass of proteins that may be analysed. Despite the advantages of the ability to analyse a wide variety of compounds in various states, there are some drawbacks to the MAS technique. The spectral resolution is worse than that found for solution-state NMR, and it requires greater amounts of sample due to the decrease in sensitivity<sup>60</sup>. This problem may be overcome to a certain extent with the use of rotor inserts which help to position a small amount of sample at the correct position in the NMR coils to achieve results with maximum efficiency. There may also be problems associated with localised heating of the sample due to high spinning speeds, and with non-uniform distribution of the sample due to high centrifugal forces. There is also a loss of information on lipid conformations and dynamics in the bilayer due to the averaging out of anisotropic interactions. The signal-to-noise ratio found with MAS may be improved using the cross-polarisation (CP) technique, which allows the transfer of polarisation from abundant spins (such as protons) to rare spins (<sup>13</sup>C or <sup>15</sup>N, for example), thus improving detection of these rare nuclei<sup>60</sup>. The MAS experiment may be further improved by using high-power decoupling, which simplifies the spectrum by decoupling protons from rare nuclei.

*Dipolar Recoupling On-Axis with Scaling and Shape Preservation* – DROSS is a NMR technique which measures <sup>13</sup>C-<sup>1</sup>H dipolar couplings in solids. The widths of the dipolar couplings are used to produce order parameter measurements using Equation 9<sup>53</sup>:

$$S_{CH} = \frac{(W_{CH} \div \chi)}{20200} \text{ MHz}$$

*Equation 9. Equation for the calculation of order parameter using DROSS, where  $S_{CH}$  is the  $^{13}\text{C}$ - $^1\text{H}$  order parameter,  $W_{CH}$  is the width of the  $^{13}\text{C}$ - $^1\text{H}$  dipolar splitting, and  $\chi$  is the scaling factor (equal to 0.393). The  $W_{CH}$  term is divided by 20200 MHz in the case of methylene protons, and 20800 MHz in the case of vinylic protons<sup>54</sup>*

Equation 9 is derived from the equation used to calculate order parameter from deuterium NMR measurements<sup>55</sup>:

$$\Delta\nu_Q = \left(\frac{3}{4}\right) \left(\frac{e^2qQ}{h}\right) S_{CD}$$

*Equation 10. Equation for the calculation of order parameter using deuterium NMR, where  $\Delta\nu_Q$  is doublet spacing (equivalent to  $W_{CH}$ ),  $(e^2qQ/h)$  is the static quadrupole splitting constant (equal to 20200 MHz for methylene  $^{13}\text{C}$ - $^1\text{H}$  dipolar splittings, and 20800 MHz for vinylic  $^{13}\text{C}$ - $^1\text{H}$  dipolar splittings), and  $S_{CD}$  is the  $^{13}\text{C}$ -D order parameter<sup>55</sup>*

There are a number of advantages to the use of DROSS over other methods. There is no need for isotopic enrichment of samples; it has greater sensitivity and resolution than deuterium NMR; and it can be used to analyse natural abundance membranes, which is not possible for deuterium NMR<sup>53, 56-58</sup>. However, the precision in the order parameter values calculated for deuterium NMR is higher than the values calculated for DROSS because the  $^{13}\text{C}$ - $^1\text{H}$  dipolar couplings are about an order of magnitude smaller than the deuterium quadrupolar coupling<sup>58</sup>.

*Deuterium ( $^2\text{H}$ ) NMR* – Deuterium NMR is commonly used in the analysis of lipid membranes, films and liquid crystals<sup>63</sup>. Deuterium is a spin-1 nucleus and has an electric quadrupole moment in addition to the nuclear magnetic moment.

The quadrupole moment interacts with the electric field gradients generated by the nucleus. The nuclear electric field gradients are anisotropic and produce characteristic static powder patterns for non-crystalline samples known as Pake patterns. Deuterium NMR is not usually carried out under MAS conditions. The spectra may be de-Paked using various software programs to display the quadrupolar splittings for each resonance<sup>48, 63</sup>. The main disadvantage of using deuterium NMR is the use of deuterated molecules, which may be expensive and difficult to synthesise; however, this technique can provide a wealth of structural and physical information.

## **Part 6. Use of Isomerisable Lipid Analogues to Modulate Membrane Behaviour**

The modulation of membranes by inclusion of a non-perturbing molecule into a bilayer has potentially useful applications, such as drug release from liposomes enabling targeted drug delivery<sup>64</sup>. Lipid analogues containing azobenzene moieties are suitable candidates for research, as their structure can be tailored to avoid bilayer perturbation by matching acyl chain lengths.

*Azobenzenes* - The term 'azobenzene' encompasses a class of molecules containing the following functional group (Figure 1.12):

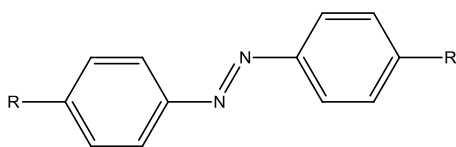


*Figure 1.12. The azobenzene moiety in the trans configuration*

Where groups R and R' may be identical or non-identical. The extended aromatic structure produces a strong optical absorption; for this reason, azobenzene-containing molecules are used in many dyestuffs and colourants<sup>65</sup>. The optical properties are due to an intense  $\pi$ - $\pi^*$  absorption band in the near-UV region, with a  $\lambda_{\text{max}}$  of 318 nm and an extinction coefficient,  $\epsilon$ , of 21000 M<sup>-1</sup> cm<sup>-1</sup>, and a weaker, symmetry-forbidden n- $\pi^*$  absorption band in the visible region,

with a  $\lambda_{\text{max}}$  of 433 nm and  $\epsilon$  of  $490 \text{ M}^{-1} \text{ cm}^{-1}$  for the azobenzene moiety in the trans configuration<sup>66, 67</sup>. In the cis configuration, the stronger  $\pi\text{-}\pi^*$  absorption band shifts to 254 nm, with  $\epsilon$  of  $7 - 10 \times 10^3 \text{ M}^{-1} \text{ cm}^{-1}$ , while the extinction coefficient of the  $n\text{-}\pi^*$  absorption band at 433 nm increases to  $1500 \text{ M}^{-1} \text{ cm}^{-1}$ <sup>66, 69</sup>. The absorption bands are shown in Figure 1.13:

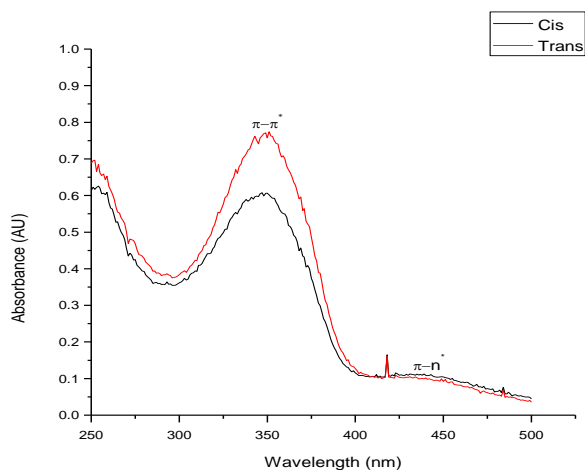


*Figure 1.13. The absorption bands of an azobenzene-containing compound in methanol, showing the allowed  $\pi\text{-}\pi^*$  and forbidden  $\pi\text{-}n^*$  transitions, and the difference between the cis and trans spectra*

Azobenzene moieties are shown (Figure 1.14) in the trans and cis configurations:

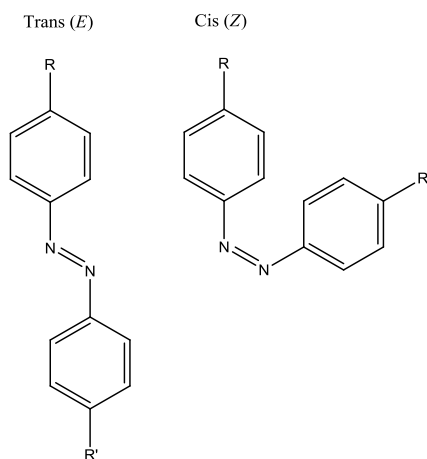


*Figure 1.14. The trans (E) and cis (Z) configurations of the azobenzene moiety*

The planar trans state of the azobenzene molecule is shown on the left-hand side of Figure 1.14, while the non-planar cis state is shown on the right<sup>64</sup>. Azobenzenes undergo trans-to-cis isomerisation on irradiation with 360 nm-wavelength light (in the UV region), and undergo cis-to-trans isomerisation on irradiation with 420 nm-wavelength light (in the visible region) or by thermal excitation<sup>66, 70, 71</sup>. Trans-to-cis isomerisation results in a structural rearrangement as the distance between the *p*-carbon atoms decreases from 9 Å to 5.5 Å, and the dipole moment increases from 0 D to 3.0 D<sup>65-67</sup>. The trans isomer is thermally stable while the cis isomer is metastable<sup>67</sup>.

Azobenzene-containing molecules have many applications, including their use in photoresponsive molecular and supramolecular systems in the form of films, polymers or dyes<sup>66, 67, 69, 71</sup>, fluorescence probes<sup>72</sup>, optical storage media<sup>65, 66</sup>, and in the modification of oligonucleotides<sup>73</sup>. They have also been used to control biological systems and mechanisms, such as membrane permeability to drugs<sup>70-79</sup>. The advantages of using azobenzene molecules include a high quantum efficiency of photoisomerisation which is easy and reversible, and no fluorescence or phosphorescence<sup>65, 66, 77</sup>. Balasubramanian *et al.* observed that it was possible to alter the properties of model membrane containing embedded azobenzene molecules by illumination under the appropriate wavelength of light, and then found that this change altered the activity of an enzyme ( $\alpha$ -chymotrypsin) in the membrane<sup>74</sup>. Further studies using specifically-synthesised lipid analogues containing azobenzene moieties showed that it was possible for them to form liposomes with lipid molecules such as DOPC or DPPC, which were then used to analyse ion leakage from the bilayer and the photoisomerisable control of bilayer permeability to trapped fluorescent molecules, and to investigate the possibility of using azobenzene-doped liposomes to release drug molecules to targets<sup>64, 68, 71, 77</sup>. Folgering *et al.* used the photoisomerisation of azobenzene-containing lipid analogues in liposomes to affect the activity of the membrane protein MscL (mechanosensitive channel of large conductance)<sup>80</sup>. The use of azobenzenes allows a range of parameters, such as wavelength and intensity, to be adjusted during the course of an experiment without physical disruption<sup>70, 77</sup>. Disadvantages include the possibility of packing or aggregation effects such as J-aggregation, in which the azobenzene molecules aggregate in a

'head-to-tail' arrangement, or H-aggregation, where the azobenzene molecules form a parallel arrangement<sup>65, 76</sup>. J-aggregation has the effect of shifting the absorption maximum to a longer wavelength (red-shift) while H-aggregation shifts the absorption maximum to a shorter wavelength (blue-shift)<sup>76</sup>.

## Part 7. References

1. Seddon, A. M.; Curnow, P.; Booth, P. J., Membrane proteins, lipids and detergents: not just a soap opera. *Biochim. Biophys. Acta* **2004**, 1666, (1-2), 105-117.
2. Lopez, J. J.; Lorch, M., Location and orientation of serotonin receptor 1a agonists in model and complex lipid membranes. *J. Biol. Chem.* **2008**, 283, (12), 7813-7822.
3. Scheidt, H. A.; Huster, D., The interaction of small molecules with phospholipid membranes studied by <sup>1</sup>H NOESY NMR under magic-angle spinning. *Acta Pharmacol. Sin.* **2008**, 29, (1), 35-49.
4. Singer, S. J.; Nicolson, G. L., Fluid mosaic model of structure of cell-membranes. *Science* **1972**, 175, (4023), 720-730.
5. Turner, T. C. M., A. G.; Bates, A. D.; White, M. R. H., In *Instant Notes: Molecular Biology*, 2 ed.; BIOS Scientific Publishers: Abingdon, 2000; p 13.
6. Van Meer, G.; Voelker, D. R.; Feigenson, G., Membrane lipids: where they are and how they behave. *Nat. Rev.: Mol. Cell Biol.* **2008**, 9, (2), 112-124.
7. Owen, J. S.; Bruckdorfer, K. R.; Day, R. C.; McIntyre, N., Decreased erythrocyte membrane fluidity and altered lipid composition in human liver disease. *J. Lipid Res.*, **1982**, 23, 124-132.
8. Alberts, B. B., D.; Lewis, J.; Raff, M.; Roberts, K.; Watson, J. D., In *Molecular Biology of the Cell*, 2 ed.; Garland Publishing, Inc.: New York, 1989; pp 275-287.
9. Stryer, L., In *Biochemistry*, 4 ed.; W. H. Freeman and Company: New York, 1995; pp 263-280.
10. Lee, A. G., Lipid-protein interactions in biological membranes: A structural perspective. *Biochim. Biophys. Acta* **2003**, 1612, 1-40.
11. Lee, A. G., How lipids affect the activities of integral membrane proteins. *Biochim. Biophys. Acta* **2004**, 1666, (1-2), 62-87.

12. Veatch, S. L.; Polozov, I. V.; Gawrisch, K.; Keller, S. L., Liquid domains in vesicles investigated by NMR and fluorescence microscopy. *Biophys. J.* **2004**, *86*, (5), 2910-2922.
13. Veatch, S.; Keller, S. L., Seeing spots: Complex phase behavior in simple membranes. *Biochim. Biophys. Acta* **2005**, *1746*, 172-185.
14. Polozov, I. V.; Gawrisch, K., Characterization of the liquid-ordered state by proton MAS NMR. *Biophys. J.* **2006**, *90*, (6), 2051-2061.
15. Booth, P. J. T., R. H.; Meijberg, W.; Allen, S. J.; Curran, A. R.; Lorch, M., In *Critical Reviews in Biochemistry and Molecular Biology*, Fasman, G. D., Ed. CRC Press LLC: Boca Raton, 2001; Vol. 36, pp 505-573.
16. Bezrukov, S. M., Functional consequences of lipid packing stress. *Curr. Op. Coll. Interface Sci.* **2000**, *5*, 247-243.
17. Booth, P. J.; Curnow, P., Folding scene investigation: Membrane proteins. *Curr. Op. Struct. Biol.* **2009**, *19*, 8-13.
18. Simons, K.; Ikonen, E., Functional rafts in cell membranes. *Nature* **1997**, *387*, 569-572.
19. Brown, D. A., Lipid rafts, detergent-resistant membranes, and raft targeting signals. *Physiol.* **2006**, *21*, 430-439.
20. McIntosh, T. J., *Lipid Rafts*. Humana Press: Totowa, NJ, 2007; p 1-40, 85, 107-128.
21. Allen, J. A.; Halverson-Tamboli, R. A.; Rasenick, M. M., Lipid raft microdomains and neurotransmitter signalling. *Nat. Rev.: Neurosci.* **2007**, *8*, (2), 128-140.
22. Pike, L. J., Lipid rafts: Bringing order to chaos. *J. Lipid Res.* **2003**, *44*, (4), 655-667.
23. Simons, K.; Toomre, D., Lipid rafts and signal transduction. *Nat. Rev.: Mol. Cell Biol.* **2000**, *1*, (1), 31-39.
24. Gaus, K.; Gratton, E.; Kable, E. P. W.; Jones, A. S.; Gelissen, I.; Kritharides, L.; Jessup, W., Visualizing lipid structure and raft domains in living cells with two-photon microscopy. *Proc. Natl. Acad. Sci.* **2003**, *100*, (26), 15554-15559.
25. Veatch, S.; Keller, S. L., Separation of lipid phases in giant vesicles of ternary mixtures of phospholipids and cholesterol. *Biophys. J.* **2003**, *85*, 3074-3083.

26. Heberle, F. A.; Buboltz, J. T.; Stringer, D.; Feigenson, G., Fluorescence methods to detect phase boundaries in lipid bilayer mixtures. *Biochim. Biophys. Acta* **2005**, 1746, 186-192.
27. Scheidt, H. A.; Huster, D.; Gawrisch, K., Diffusion of cholesterol and its precursors in lipid membranes studied by  $^1\text{H}$  PFG MAS NMR. *Biophys. J.* **2005**, 89, 2504-2512.
28. Huang, T.-H.; Lee, C. W. B.; Das Gupta, S. K.; Blume, A.; Griffin, R. G., A  $^{13}\text{C}$  and  $^2\text{H}$  nuclear magnetic resonance study of phosphatidylcholine/cholesterol interactions: Characterization of liquid-gel phases. *Biochem.* **1993**, 32, 13277-13287.
29. Polozov, I. V.; Gawrisch, K., Domains in binary SOPC/POPE lipid mixtures studied by pulsed field gradient H-1 MAS NMR. *Biophys. J.* **2004**, 87, (3), 1741-1751.
30. Sargent, D. F.; Schwyzer, R., Membrane lipid phase as catalyst for peptide-receptor interactions. *Proc. Natl. Acad. Sci.* **1986**, 83, 5774-5778
31. Eisensamer, B.; Uhr, M.; Meyr, S.; Gimpl, G.; Deiml, T.; Rammes, G.; Lambert, J. J.; Zieglansberger, W.; Holsboer, F.; Rupprecht, R., Antidepressants and antipsychotic drugs colocalize with 5-HT<sub>3</sub> receptors in raft-like domains. *J. Neurosci.* **2005**, 25, (44), 10198-10206.
32. Curran, A. R.; Templer, R. H.; Booth, P. J., Modulation of folding and assembly of the membrane protein bacteriorhodopsin by intermolecular forces within the lipid bilayer. *Biochem.* **1999**, 38, (29), 9328-9336.
33. Hong, R. I.; Sansom, M. S. P., In *Membrane Transport*, Baldwin, S. A., Ed. Oxford University Press: Oxford, 2000; p 209.
34. Wallin, E.; von Heijne, G., Genome-wide analysis of integral membrane proteins from eubacterial, archaean, and eukaryotic organisms. *Prot. Sci.* **1998**, 7, (4), 1029-1038.
35. Laws, D. D.; Bitter, H. M. L.; Jerschow, A., Solid-state NMR spectroscopic methods in chemistry. *Angew. Chem. Int. Ed.* **2002**, 41, (17), 3096-3129.
36. Ward, A. S., N. M.; O'Reilly, J.; Rutherford, N. G.; Poolman, B.; Henderson, P. J. F., In *Membrane Transport*, Baldwin, S. A., Ed. Oxford University Press: Oxford, 2000; p 141.
37. Protein Data Bank: [www.pdb.org/pdb/home/home.do](http://www.pdb.org/pdb/home/home.do)

Date of last access: 13.04.11

38. Membrane Proteins of Known Structure Determined by NMR:  
[www.drorlist.com/nmr/MPNMR.html](http://www.drorlist.com/nmr/MPNMR.html)

Date of last access: 18.08.10

39. Stephen White Laboratory, U. I., Membrane Proteins of Known 3D Structure: [http://blanco.biomol.uci.edu/Membrane\\_Proteins\\_xtal.html](http://blanco.biomol.uci.edu/Membrane_Proteins_xtal.html)

Date of last access: 18.08.10

40. Branden, C.; Tooze, J., *Introduction to Protein Structure*. 2nd ed.; Garland Publishing, Inc.: New York, NY, 1999; p 410.

41. Postma, D. S.; Koppelman, G. H., Confirmation of GPRA - A putative drug target for asthma. *Am. J. Resp. Crit. Care Med.* **2005**, 171, (12), 1323-1324.

42. Sanders, C. R.; Nagy, J. K., Misfolding of membrane proteins in health and disease: The lady or the tiger? *Curr. Op. Struct. Biol.* **2000**, 10, (4), 438-442.

43. Selkoe, D. J., Folding proteins in fatal ways. *Nature* **2003**, 426, 900-904.

44. Booth, P. J., Sane in the membrane: Designing systems to modulate membrane proteins. *Curr. Op. Struct. Biol.* **2005**, 15, 435-440.

45. Charalambous, K.; Miller, D.; Curnow, P.; Booth, P. J., Lipid bilayer composition influences small multidrug transporters. *BMC Biochem.* **2008**, 9, 31-43.

46. Meijberg, W.; Booth, P. J., The activation energy for insertion of transmembrane  $\alpha$  helices is dependent on membrane composition. *J. Mol. Biol.* **2002**, 319, 839-853.

47. Allen, S. J.; Curran, A. R.; Templer, R. H.; Meijberg, W.; Booth, P. J., Controlling the folding efficiency of an integral membrane protein. *J. Mol. Biol.* **2004**, 342, 1293-1304.

48. Brown, M. F.; Lope-Piedrafita, S.; Martinez, G. V.; Petrache, H. I., Solid-state deuterium NMR spectroscopy of membranes. In *Modern Magnetic Resonance*, Webb, G. A., Ed. Springer: 2008; pp 249-260.

49. Warschawski, D. E.; Traikia, M.; Devaux, P. F.; Bodenhausen, G., Solid-state NMR for the study of membrane systems: The use of anisotropic interactions. *Biochim.* **1998**, 80, (5-6), 437-450.

50. Levitt, M. H., In *Spin Dynamics: Basics of Nuclear Magnetic Resonance*, John Wiley and Sons, Ltd.: Chichester, 2001; pp 7-8.

51. Evans, J. N. S., In *Biomolecular NMR Spectroscopy*, Oxford University Press: New York, 1995; pp 5-415.
52. Hore, P. J., In *Nuclear Magnetic Resonance*, Oxford Science Publications: New York, 1995; pp 1-9.
53. Gross, J. D.; Warschawski, D. E.; Griffin, R. G., Dipolar recoupling in MAS NMR: A probe for segmental order in lipid bilayers. *J. Am. Chem. Soc.* **1997**, 119, (4), 796-802.
54. Warschawski, D. E.; Devaux, P. F.,  $^1\text{H}$ - $^{13}\text{C}$  polarization transfer in membranes: A tool for probing lipid dynamics and the effect of cholesterol. *J. Magn. Reson.* **2005**, 177, 166-171.
55. Seelig, J., Deuterium magnetic-resonance - Theory and application to lipid-membranes. *Quart. Rev. Biophys.* **1977**, 10, (3), 353-418.
56. Dvinskikh, S. V.; Castro, V.; Sandstrom, D., Efficient solid-state NMR methods for measuring heteronuclear dipolar couplings in unoriented lipid membrane systems. *Phys. Chem. Chem. Phys.* **2005**, 7, (4), 607-613.
57. Gawrisch, K.; Eldho, N. V.; Polozov, I. V., Novel NMR tools to study structure and dynamics of biomembranes. *Chem. Phys. Lipids* **2002**, 116, (1-2), 135-151.
58. Warschawski, D. E.; Devaux, P. F., Order parameters of unsaturated phospholipids in membranes and the effect of cholesterol: a  $^1\text{H}$ - $^{13}\text{C}$  solid-state NMR study at natural abundance. *Eur. Biophys. J. Biophys. Lett.* **2005**, 34, (8), 987-996.
59. De Groot, H. J. M., Solid-state NMR spectroscopy applied to membrane proteins. *Curr. Op. Struct. Biol.* **2000**, 10, (5), 593-600.
60. Krushelnitsky, A.; Reichert, D., Solid-state NMR and protein dynamics. *Prog. Nuc. Magn. Reson. Spect.* **2005**, 47, (1-2), 1-25.
61. Urbina, J. A.; Moreno, B.; Arnold, W.; Taron, C. H.; Orlean, P.; Oldfield, E., A carbon-13 nuclear magnetic resonance spectroscopic study of inter-proton pair order parameters: A new approach to study order and dynamics in phospholipid membrane systems. *Biophys. J.* **1998**, 75, (3), 1372-1383.
62. Watts, A.; Burnett, I. J.; Glaubitz, C.; Grobner, G.; Middleton, D. A.; Spooner, P. J. R.; Watts, J. A.; Williamson, P. T. F., Membrane protein structure determination by solid state NMR. *Nat. Prod. Rep.* **1999**, 16, (4), 419-423.

63. Brown, M. F.; Nevzorov, A. A.,  $^2\text{H}$ -NMR in liquid crystals and membranes. *Coll. Surf. A: Physicochem. Eng. Aspects* **1999**, 158, 281-298.
64. Bisby, R. H.; Mead, C.; Morgan, C. C., Wavelength-programmed solute release from photosensitive liposomes. *Biochem. Biophys. Res. Commun.* **2000**, 276, (1), 169-173.
65. Yager, K. G.; Barrett, C. J., Novel photo-switching using azobenzene functional materials. *J. Photochem. Photobiol. A - Chem.* **2006**, 182, (3), 250-261.
66. Archut, A.; Vogtle, F.; De Cola, L.; Azzellini, G. C.; Balzani, V.; Ramanujam, P. S.; Berg, R. H., Azobenzene-functionalized cascade molecules: Photoswitchable supramolecular systems. *Chem. Eur. J.* **1998**, 4, (4), 699-706.
67. Tsuda, K.; Dol, G. C.; Gensch, T.; Hofkens, J.; Latterini, L.; Weener, J. W.; Meijer, E. W.; De Schryver, F. C., Fluorescence from azobenzene functionalized poly(propylene imine) dendrimers in self-assembled supramolecular structures. *J. Am. Chem. Soc.* **2000**, 122, (14), 3445-3452.
68. Song, X. D.; Perlstein, J.; Whitten, D. G., Supramolecular aggregates of azobenzene phospholipids and related compounds in bilayer assemblies and other microheterogeneous media: Structure, properties, and photoreactivity. *J. Am. Chem. Soc.* **1997**, 119, (39), 9144-9159.
69. Tamai, N.; Miyasaka, H., Ultrafast dynamics of photochromic systems. *Chem. Rev.* **2000**, 100, (5), 1875-1890.
70. Liu, X. M. Y., B.; Wang, Y. L.; Wang, J. Y., Photoisomerisable cholesterol derivatives as photo-trigger of liposomes: Effect of lipid polarity, temperature, incorporation ratio, and cholesterol. *Biochim. Biophys. Acta* **2005**, 1270, (1-2), 28-34.
71. Sandhu, S. S.; Yianni, Y. P.; Morgan, C. G.; Taylor, D. M.; Zaba, B., The formation and Langmuir-Blodgett deposition of monolayers of novel photochromic azobenzene-containing phospholipid molecules. *Biochim. Biophys. Acta* **1986**, 860, (2), 253-262.
72. Zacharias, P. S.; Ameerunisha, S.; Korupoju, S. R., Photoinduced fluorescence changes on *E-Z* isomerisation in azobenzene derivatives. *J. Chem. Soc. Perkin Trans.* **1998**, (9), 2055-2059.

73. Asanuma, H.; Yoshida, T.; Ito, T.; Komiyama, M., Photo-responsive oligonucleotides carrying azobenzene at the 2'-position of uridine. *Tetrahedron Lett.* **1999**, 40, (45), 7995-7998.
74. Balasubramanian, D.; Subramani, S.; Kumar, C., Modification of a model membrane structure by embedded photochrome. *Nature* **1975**, 254, (5497), 252-254.
75. Harvey, J. H.; Butler, B. K.; Trauner, D., Functionalized azobenzenes through cross-coupling with organotrifluoroborates. *Tetrahedron Lett.* **2007**, 48, (9), 1661-1664.
76. Kuiper, J. M.; Engberts, J. B. F. N., H-aggregation of azobenzene-substituted amphiphiles in vesicular membranes. *Langmuir* **2004**, 20, (4), 1152-1160.
77. Morgan, C. G.; Thomas, E. W.; Yianni, Y. P.; Sandhu, S. S., Incorporation of a novel photochromic phospholipid molecule into vesicles of dipalmitoylphosphatidylcholine. *Biochim. Biophys. Acta* **1985**, 820, (1), 107-114.
78. Patnaik, S.; Kumar, P.; Garg, B. S.; Gandhi, R. P.; Gupta, K. C., Photomodulation of PS-modified oligonucleotides containing azobenzene substituent at pre-selected positions in phosphate backbone. *Bioorg. Med. Chem.* **2007**, 15, (24), 7840-7849.
79. Yamana, K.; Kan, K.; Nakano, H., Synthesis of oligonucleotides containing a new azobenzene fragment with efficient photoisomerizability. *Bioorg. Med. Chem.* **1999**, 7, (12), 2977-2983.
80. Folgering, J. H. A.; Kuiper, J. M.; de Vries, A. H.; Engberts, J.; Poolman, B., Lipid-mediated light activation of a mechanosensitive channel of large conductance. *Langmuir* **2004**, 20, (17), 6985-6987.

## Chapter 2: Modulation of Enzyme Activity Using an Azobenzene-Containing Lipid Analogue

### **Part 1. Introduction**

The research of Kaufman *et al.* and Bieth *et al.* showed that the photoisomerisation of an azobenzene-containing photochromic compound could effect a change in the activity of the enzymes chymotrypsin and acetylcholinesterase<sup>1, 2</sup>. The research was expanded by Balasubramanian *et al.* with the addition of a model membrane into which  $\alpha$ -chymotrypsin was incorporated<sup>3</sup>. The photoisomerisation of an azobenzene compound in the model membrane was found to induce differences in electrical resistance and to alter the activity of chymotrypsin. Both effects were theorised to be caused by the perturbation of the model membrane which took place when the azobenzene compound was switched from one isomer to the other<sup>3</sup>. These results gave rise to the concept of control over certain biological processes, such as enzyme catalysis, by using photochromic compounds. Sandhu *et al.* synthesised and characterised azobenzene-containing phospholipid analogues, which had one or both acyl chains replaced by an azobenzene-containing chain<sup>4</sup>. The research demonstrated that the azobenzene phospholipids were able to form stable vesicles in isolation, and in combination with another phospholipid of comparable length (DPPC). At low concentrations ( $\leq 5$  % w/w) in a DPPC bilayer there were no signs of aggregation (although a previous study had shown some evidence of phase separation of azobenzene phospholipids at a concentration of 10 % w/w in a DPPC bilayer)<sup>4, 5</sup>. Photoisomerisation of the monolayers induced large changes in molecular surface area<sup>4</sup>.

Further research utilising the photochromic properties of azobenzene lipids involved the investigation into controlling solute leakage from liposomes and controlling the activity of a protein channel<sup>6, 7</sup>. Azobenzene-containing lipids were investigated as a possible release mechanism for liposomes containing substances, which might provide a possible method for site-specific delivery of certain drugs<sup>6</sup>. Photoisomerisation of azobenzene compounds in lipid bilayers

containing the MscL (mechanosensitive channel of large conductance) protein resulted in changes in protein activity<sup>7</sup>.

Although azobenzene provide a relatively simple, non-invasive method of modifying both lipid bilayer properties and protein activity, the main disadvantage of their use is that of aggregation. Both H- (parallel) and J-aggregation ('head-to-tail') lead to changes in the UV spectrum of the compound, and to phase separation of the azobenzene containing lipids from the phospholipid matrix<sup>8,9</sup>.

*Diacylglycerol Kinase* – Prokaryotic diacylglycerol kinase (DGK) is a membrane-based enzyme with a molecular mass of 13 kDa<sup>10, 11</sup>. In *E. coli*, it is situated in the cytoplasmic membrane<sup>12, 13</sup>. It contains 121 amino acid residues, making it a relatively small membrane protein<sup>10, 14-16</sup>. It catalyses the reversible phosphorylation of diacylglycerol (DAG) to phosphatidic acid (PA) via the transfer of a phosphate group from MgATP to leave MgADP<sup>10-12, 14-16</sup>. DGK is associated with the synthesis of carbohydrates and the synthesis of lipids used in the maintenance of the bacterial cell wall<sup>13</sup>.

DGK consists of two cytoplasmic  $\alpha$ -helices (amino acid residues 1 – 34, and 69 – 95) and three transmembrane (TM) domains (amino acid residues 35 – 48, 52 – 68, and 96 – 117)<sup>10, 11</sup>. The functional form is homotrimeric with three active sites<sup>11</sup>. It is an ideal candidate for analysis because it is relatively small for an integral membrane protein; it is tolerant to amino acid sequence mutations; and it is stable to expression and refolding into membrane mimetics such as liposomes<sup>10, 13</sup>. It is naturally present in *E. coli*, which makes it amenable to overexpression. These properties meant that it was one of the first integral membrane proteins to be purified and characterised.

## **Part 2. Aims**

The aim was to synthesise a photoisomerisable lipid analogue according to the synthetic route by Song *et al.*, which could then be incorporated into lipid vesicles<sup>17</sup>.

The target compound was designed to have an effective length matching those of DOPC molecules, so that it could be incorporated into DOPC liposomes without leading to hydrophobic mismatch. It was also designed to mimic the typical structure of a phospholipid molecule in order to attribute any observable changes in the behaviour of the lipid bilayer solely to the photoisomerisation of the azobenzene moieties, rather than to the presence of structurally incompatible molecules. The target compound therefore contains a phosphocholine headgroup (chemically identical to the DOPC headgroup), a glycerol backbone, and two hydrocarbon tails; the most significant difference between the target compound and DOPC is the presence of the photoisomerisable azobenzene moieties. The cis and trans states of the azobenzene lipid analogue are shown (Figure 2.1).

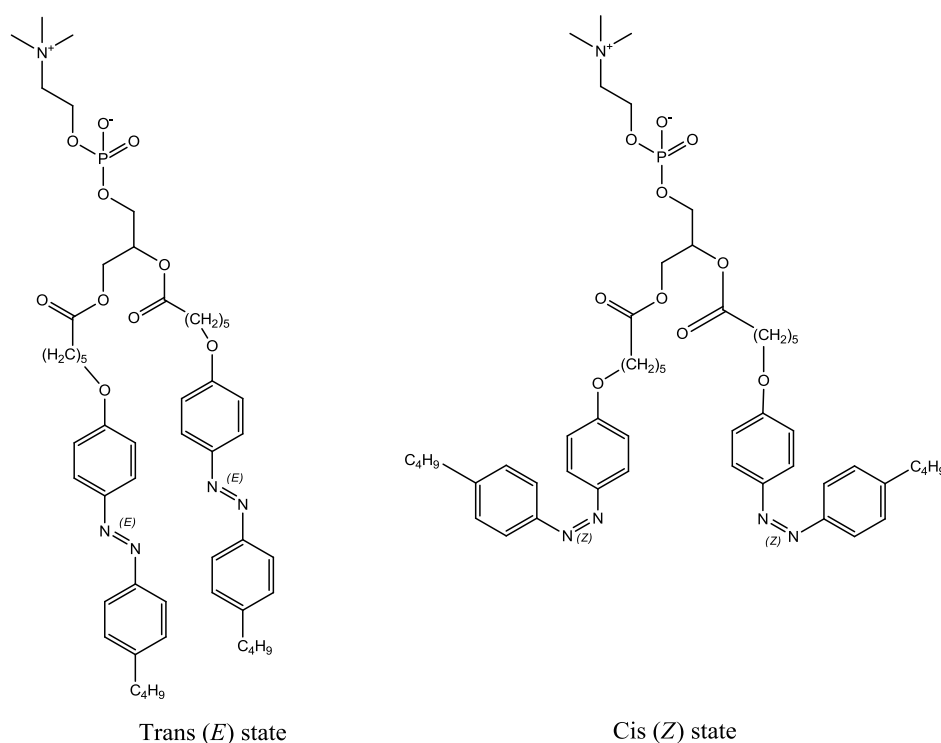


*Figure 2.1. The trans (E) and cis (Z) states of a photoisomerisable azobenzene-containing phospholipid analogue*

Enzyme activity assay experiments on liposomes containing an azobenzene lipid analogue were carried out with the aim of assessing the difference between the activity of DGK when the photoisomerisable lipid is in the trans state compared

to when it is in the cis state. It is hypothesised that the cis state isomers will affect the activity of the enzyme due to compression of the lipid bilayer, since the cis state isomers occupy more space in the bilayer than those in the trans state. Therefore a series of enzyme activity assays should demonstrate a difference in activity depending on the state of the photoisomerisable lipid analogues.

In order to accomplish the enzyme activity assay experiments, a photoisomerisable azobenzene-containing lipid analogue was first synthesised.

### **Part 3. Experimental**

*Materials* - 1,2-Dioleoyl-*sn*-glycero-3-phosphocholine (DOPC) was purchased from Avanti Polar Lipids (Alabaster, AL). 4-(4-Heptylphenylazo)phenol and 6-[4-(4-Heptylphenylazo)phenoxy]hexanoic acid (referred to in the text as azobenzene compounds **1** and **2**, respectively) were gifts from H. Schwalbe of Goethe University, Frankfurt. DBG was a gift from P. J. Booth of the University of Bristol.

1,3-Bis(6-4-((*E*)-(4-butylphenyl)diazenyl)phenoxy)hexanoyloxy)propan-2-yl-2-(trimethylammonio)ethyl phosphate (referred to in the text as bis-Azo-PC) was synthesised as described. Lactate dehydrogenase-pyruvate kinase was purchased from Roche. All other chemicals were purchased from Sigma.

*Synthesis of bis-Azo-PC* - Two possible synthetic routes were considered. The synthetic route by Song *et al.* was chosen in favour of that of Morgan *et al.* due to the lack of the necessary apparatus<sup>4, 5, 17</sup>. There are two significant differences between the routes. The steps prior to the synthesis of the crude anhydride is different in each route (a diazotisation followed by a Williamson etherification in the case of Song *et al.*, and an acid oxidation and catalytic hydrogenation followed by diazotisation in the case of Morgan *et al.*), which leads to a slightly different final structure of the azobenzene phospholipid compound; the phospholipid compounds produced by following the route of Song *et al.* contain an additional ether oxygen atom<sup>4, 5, 17</sup>. However both routes produce

azobenzene-containing phospholipid analogues to a length which may be dictated by the choice of starting materials.

*Synthesis of 4-((4-Butylphenyl)diazenyl)phenol* – The reaction scheme is shown in Figure 2.2.

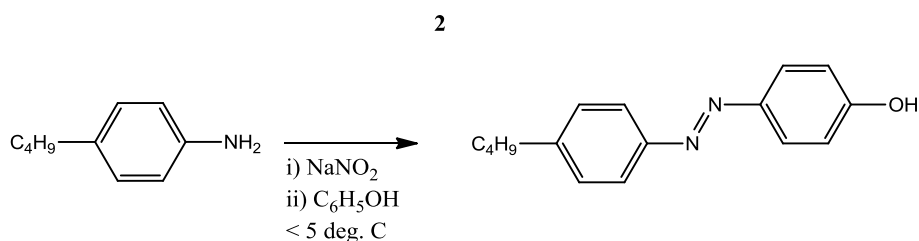


*Figure 2.2. Diazotisation of butylaniline 1*

HCl (10 mL, 36% w/w, 0.12 mol) was added slowly to a stirred solution of 4-n-butylaniline **1** (5.96 g, 0.040 mol) in acetone:water (1:1, 100 mL). After cooling to 0°C, a cooled solution of sodium nitrite (2.9 g, 0.042 mol) in water (50 mL) was added. The resulting solution was stirred for 15 min. The solution was then added to a cooled, stirred solution of phenol (4 g, 0.043 mol), sodium hydroxide (1.7 g, 0.043 mol) and sodium carbonate (7 g, 0.066 mol) in water (100 mL). On addition a bright yellow solid was formed, which was then filtered off. The product was purified by recrystallisation from minimum amounts of toluene:hexane (1:1, x 3) to give 4-((4-butylphenyl)diazenyl)phenol **2** (3.22 g, 32%) as orange crystals.

*Characterisation Data* -  $R_f$  [chloroform:methanol (9:1)] 0.53;  $\nu_{\max}$  (CHCl<sub>3</sub>) cm<sup>-1</sup> 3018 (OH, s), 1525 (trans ar. N=N str., w), 1477 (cis ar. N=N str., w-m) and 1424 (cis ar. N=N str., w-m);  $\delta_H$  (400 MHz; CDCl<sub>3</sub>) 7.86 (2H, ddd, J 8.98, 3.12 and 2.10, 2 x CHCN; ArOH), 7.79 (2H, ddd, J 8.43, 2.20 and 2.02, 2 x CHCN; Ar), 7.30 (2H, ddd, J 8.43, 2.20 and 2.02, 2 x CH; Ar), 6.94 (2H, ddd, J 8.98, 3.12 and 2.10, 2 x CHCO; ArOH), 5.30 (1H, brs, OH), 2.68 (2H, dd, J 7.70 and 7.70, CH<sub>2</sub>CH<sub>2</sub>CH<sub>2</sub>CH<sub>3</sub>), 1.68 – 1.59 (2H, m, CH<sub>2</sub>CH<sub>2</sub>CH<sub>2</sub>CH<sub>3</sub>), 1.38 (2H, sextuplet, J 7.51, CH<sub>2</sub>CH<sub>2</sub>CH<sub>2</sub>CH<sub>3</sub>) and 0.94 (3H, t, J 7.33, CH<sub>2</sub>CH<sub>2</sub>CH<sub>2</sub>CH<sub>3</sub>);  $\delta_C$  (100 MHz; CDCl<sub>3</sub>) 158.2 (COH; ArOH), 150.9 (CN; Ar), 147.2 (CN; ArOH),

145.9 (C-CH<sub>2</sub>CH<sub>2</sub>CH<sub>2</sub>CH<sub>3</sub>; Ar), 129.0 (2 x CH; Ar), 124.8 (2 x CHCN; ArOH), 122.6 (2 x CHCN; Ar), 115.7 (2 x CHCO; ArOH), 35.5 (CH<sub>2</sub>CH<sub>2</sub>CH<sub>2</sub>CH<sub>3</sub>), 33.4 (CH<sub>2</sub>CH<sub>2</sub>CH<sub>2</sub>CH<sub>3</sub>), 22.3 (CH<sub>2</sub>CH<sub>2</sub>CH<sub>2</sub>CH<sub>3</sub>) and 13.9 (CH<sub>2</sub>CH<sub>2</sub>CH<sub>2</sub>CH<sub>3</sub>); found M<sup>+</sup>, 254.2; C<sub>16</sub>H<sub>18</sub>N<sub>2</sub>O requires 254.3; m/z 254.2 (40%, M<sup>+</sup>), 133.2 (55, CH<sub>3</sub>CH<sub>2</sub>CH<sub>2</sub>CH<sub>2</sub>C<sub>6</sub>H<sub>4</sub><sup>+</sup>), 121.1 (60, N=NC<sub>6</sub>H<sub>4</sub>OH<sup>+</sup>) and 93.1 (100, C<sub>6</sub>H<sub>4</sub>OH<sup>+</sup>); m. p. 81.8 °C

*Synthesis of 6-(4-((4-Butylphenyl)diazenyl)phenoxy)hexanoic acid* – The reaction scheme is shown in Figure 2.3.

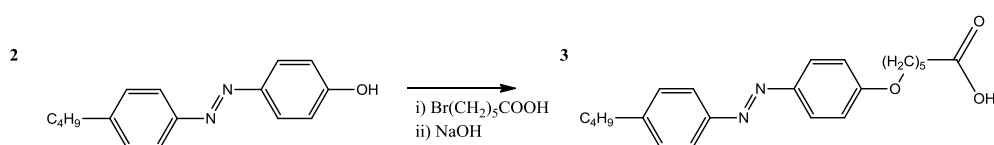


*Figure 2.3. Etherification of 4-((4-butylphenyl)diazenyl)phenol 2*

A solution of 4-((4-butylphenyl)diazenyl)phenol **2** (4.50 g, 0.02 mol), 6-bromohexanoic acid (4.0 g, 0.02 mol) and sodium hydroxide (1.6 g, 0.04 mol) in ethanol (120 mL) was refluxed for 8 hr. The resulting precipitate was filtered off under vacuum. The precipitate was suspended in water (150 mL) and acidified with dilute HCl. The resulting solution was separated into diethyl ether (100 mL; x 3) and the solvent removed. The product was dried using a vacuum pump to give 6-(4-((4-butylphenyl)diazenyl)phenoxy)hexanoic acid **3** (1.18 g, 36%) as a yellow solid.

*Characterisation Data* - R<sub>f</sub> [methanol] 0.73; ν<sub>max</sub> (CHCl<sub>3</sub>) cm<sup>-1</sup> 3020 (OH, s), 1524 (trans ar. N=N str., w), 1476 (cis ar. N=N str., w-m) and 1426 (cis ar. N=N str., w-m); δ<sub>H</sub> (400 MHz; CDCl<sub>3</sub>) 7.89 (2H, ddd, J 8.98, 3.12 and 2.02, 2 x CHCN; ArO), 7.79 (2H, ddd, J 8.25, 1.65 and 2.02, 2 x CHCN; Ar), 7.30 (2H, ddd, J 8.25, 1.65 and 2.02, 2 x CH; Ar), 6.94 (2H, ddd, J 8.98, 3.12 and 2.02, 2 x CHCO; ArO), 4.05 (2H, t, J 6.42, HOOCCH<sub>2</sub>(CH<sub>2</sub>)<sub>3</sub>CH<sub>2</sub>O), 2.68 (2H, dd, J 7.70 and 7.70, CH<sub>2</sub>CH<sub>2</sub>CH<sub>2</sub>CH<sub>3</sub>), 2.42 (2H, t, J 7.33, HOOCCH<sub>2</sub>(CH<sub>2</sub>)<sub>3</sub>CH<sub>2</sub>O), 1.86 (2H, quintuplet, J 7.15, -CH<sub>2</sub>-), 1.75 (2H, quintuplet, J 7.88, -CH<sub>2</sub>-), 1.68 – 1.53

(4H, m, -CH<sub>2</sub>-), 1.38 (2H, sextuplet, J 7.51, CH<sub>2</sub>CH<sub>2</sub>CH<sub>2</sub>CH<sub>3</sub>) and 0.94 (3H, t, J 7.42, CH<sub>2</sub>CH<sub>2</sub>CH<sub>2</sub>CH<sub>3</sub>); δ<sub>C</sub> (100 MHz; CDCl<sub>3</sub>) 177.0 (HOOC), 161.3 (COH; ArO), 151.0 (CN; Ar), 145.9 (CN; ArO), 145.8 (C-CH<sub>2</sub>CH<sub>2</sub>CH<sub>2</sub>CH<sub>3</sub>; Ar), 129.1 (2 x CH; Ar), 124.6 (2 x CHCN; ArO), 122.6 (2 x CHCN; Ar), 114.7 (2 x CHCO; ArO), 67.9 (HOOCCH<sub>2</sub>(CH<sub>2</sub>)<sub>3</sub>CH<sub>2</sub>O), 35.6 (CH<sub>2</sub>CH<sub>2</sub>CH<sub>2</sub>CH<sub>3</sub>), 28.9 (HOOCCH<sub>2</sub>(CH<sub>2</sub>)<sub>3</sub>CH<sub>2</sub>O), 25.6 (HOOCCH<sub>2</sub>(CH<sub>2</sub>)<sub>3</sub>CH<sub>2</sub>O), 24.4 (HOOCCH<sub>2</sub>(CH<sub>2</sub>)<sub>3</sub>CH<sub>2</sub>O), 22.3 (CH<sub>2</sub>CH<sub>2</sub>CH<sub>2</sub>CH<sub>3</sub>) and 13.9 (CH<sub>2</sub>CH<sub>2</sub>CH<sub>2</sub>CH<sub>3</sub>); found M<sup>+</sup>, 368; C<sub>22</sub>H<sub>28</sub>N<sub>2</sub>O<sub>3</sub> requires 368.3; m/z 368 (3%, M<sup>+</sup>), 194 (13, C<sub>6</sub>H<sub>4</sub>-N=N-C<sub>6</sub>H<sub>4</sub>O<sup>+</sup>), 180 (3, C<sub>6</sub>H<sub>4</sub>-N=N-C<sub>6</sub>H<sub>4</sub><sup>+</sup>), 148 (3, CH<sub>3</sub>CH<sub>2</sub>CH<sub>2</sub>CH<sub>2</sub>-C<sub>6</sub>H<sub>4</sub>-NH<sup>+</sup>), 133 (3, CH<sub>3</sub>CH<sub>2</sub>CH<sub>2</sub>CH<sub>2</sub>-C<sub>6</sub>H<sub>4</sub><sup>+</sup>), 91 (44, N-C<sub>6</sub>H<sub>4</sub><sup>+</sup>) and 44 (100, COO<sup>+</sup>); m. p. 147.5°C; crystalline, 147.5°C [nematic phase, 136.0°C] isotropic

*Synthesis of 6-(4-((4-Butylphenyl)diazenyl)phenoxy)hexanoic pivalic anhydride –*

The reaction scheme is shown in Figure 2.4.

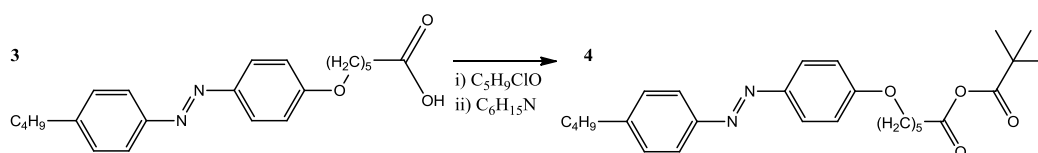


*Figure 2.4. Synthesis of the crude anhydride 4*

A solution of 6-(4-((4-butylphenyl)diazenyl)phenoxy) hexanoic acid **3** (0.46 g, 1.26 x 10<sup>-3</sup> mol) in dichloromethane (20 mL) was stirred for 30 mins under nitrogen to remove moisture. Following this pivaloyl chloride (1.2 mL, 9.76 x 10<sup>-3</sup> mol) and triethylamine (0.4 mL, 2.87 x 10<sup>-3</sup> mol) were added, and the reaction mixture was left to stir for 20 h. The solvent was removed and the product was dried on a vacuum pump to give the crude anhydride **4** (0.92 g) as a yellow solid.

The crude anhydride was used in the acylation step with no further work-up; for this reason, there is no available characterisation data.

*Synthesis of 1,3-bis(6-4-((E)-(4-Butylphenyl)diazenyl)phenoxy)hexanoyloxy)propan-2-yl 2-(trimethylammonio)ethyl phosphate (bis-AzoPC) – The reaction scheme is shown in Figure 2.5.*

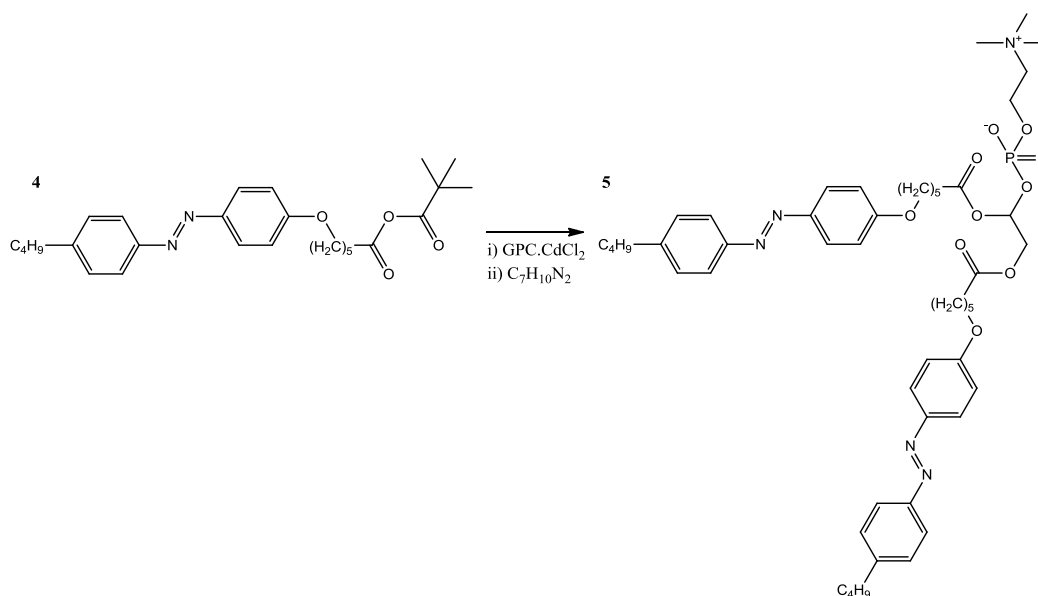


*Figure 2.5. Acylation of crude anhydride **4** to produce the azobenzene-containing lipid analogue **5***

A solution of crude anhydride **4** (0.92 g) in dichloromethane (20 mL) was added to a suspension of glycerophosphorylcholine as the cadmium chloride complex (0.26 g,  $6 \times 10^{-4}$  mol) and dimethylaminopyridine (0.14 g,  $1 \times 10^{-3}$  mol) in dichloromethane (20 mL) after both solutions were stirred under nitrogen to remove excess moisture. The reaction mixture was left to stir for 24 h. It was filtered through a sinter to remove solid residue. The solvent was removed and the solid redissolved in solvent A (chloroform:methanol:water, 65:25:4) and passed through an Amberlite column to remove any remaining impurities. The solvent was removed and the solid was redissolved in a minimum amount of dichloromethane and tetrahydrofuran to encourage crystallisation. The yellow precipitate **5** was filtered off (120 mg).

*Characterisation Data* -  $\delta_{\text{H}}$  (400 MHz;  $\text{CDCl}_3$ ) 7.86 (4H, ddd, J 8.98, 2.93 and 2.02, 2 x CHCN; ArO), 7.78 (4H, ddd, J 8.25, 1.65 and 2.02, 2 x CHCN; Ar), 7.28 (4H, ddd, J 8.25, 1.65 and 2.02, 2 x CH; Ar), 6.94 (4H, ddd, J 8.98, 2.93 and 2.02, 2 x CHCO; ArO), 5.27 – 5.22 (1H, m,  $(\text{CH}_3)_3\text{N}^+\text{CH}_2\text{CH}_2\text{OPO}_2^- \text{OCH}(\text{CH}_2\text{O})_2$ ), 4.45 – 4.34 (2H, m,  $(\text{CH}_3)_3\text{N}^+\text{CH}_2\text{CH}_2\text{OPO}_2^- \text{OCH}(\text{CH}_2\text{O})_2$ ), 4.18 – 4.13 (1H, m,  $(\text{CH}_3)_3\text{N}^+\text{CH}_2\text{CH}_2$ ), 4.00 (6H, quintuplet, J 6.23,  $\text{CH}_2\text{O}(\text{CH}_2)_3\text{CH}_2\text{COO}$ ), 3.77 (2H, br. s.,  $(\text{CH}_3)_3\text{N}^+\text{CH}_2\text{CH}_2$ ), 3.31 (8H, s,  $(\text{CH}_3)_3\text{N}^+\text{CH}_2\text{CH}_2$ ), 2.66 (4H, t, J 7.70,  $\text{CH}_2\text{CH}_2\text{CH}_2\text{CH}_3$ ), 2.37 – 2.27 (5H, m,  $\text{CH}_2\text{O}(\text{CH}_2)_3\text{CH}_2\text{COO}$ ), 1.85 – 1.75 (4H, m,  $\text{CH}_2\text{O}(\text{CH}_2\text{CH}_2\text{CH}_2)\text{CH}_2\text{COO}$ ), 1.71 – 1.59 (9H, m,  $\text{CH}_2\text{CH}_2\text{CH}_2\text{CH}_3$ ), 1.54 – 1.43 (5H, m,  $\text{CH}_2\text{O}(\text{CH}_2\text{CH}_2\text{CH}_2)\text{CH}_2\text{COO}$ ), 1.37 (4H, sextuplet, J 7.51,  $\text{CH}_2\text{CH}_2\text{CH}_2\text{CH}_3$ ) and 0.94 (7H, t, J 7.33,  $\text{CH}_2\text{CH}_2\text{CH}_2\text{CH}_3$ );  $\delta_{\text{C}}$  (100 MHz;  $\text{CDCl}_3$ ) 173.3 ( $\text{CH}_2\text{O}(\text{CH}_2)_3\text{CH}_2\text{COO}$ ), 161.3 (CO: ArO), 151.0 (CN; Ar), 147.0 (C- $\text{CH}_2\text{CH}_2\text{CH}_2\text{CH}_3$ ; Ar), 145.8 (CN; ArO), 129.1 (2 x CH; Ar), 124.6 (2x CHCN; ArO), 122.5 (2 x CHCN; Ar), 114.6 (2 x CH; ArO), 70.7 ( $(\text{CH}_3)_3\text{N}^+\text{CH}_2\text{CH}_2\text{OPO}_2^- \text{OCH}(\text{CH}_2\text{O})_2$ ), 68.0 ( $\text{CH}_2\text{O}(\text{CH}_2)_3\text{CH}_2\text{COO}$ ), 66.6 ( $(\text{CH}_3)_3\text{N}^+\text{CH}_2\text{CH}_2$ ), 63.5 ( $(\text{CH}_3)_3\text{N}^+\text{CH}_2\text{CH}_2\text{OPO}_2^- \text{OCH}(\text{CH}_2\text{O})_2$ ), 59.3 ( $(\text{CH}_3)_3\text{N}^+\text{CH}_2\text{CH}_2\text{OPO}_2^- \text{OCH}(\text{CH}_2\text{O})_2$ ), 54.6 ( $(\text{CH}_3)_3\text{N}^+\text{CH}_2\text{CH}_2$ ), 35.6 ( $\text{CH}_2\text{CH}_2\text{CH}_2\text{CH}_3$ ), 34.0 ( $\text{CH}_2\text{O}(\text{CH}_2)_3\text{CH}_2\text{COO}$ ), 33.5 ( $\text{CH}_2\text{CH}_2\text{CH}_2\text{CH}_3$ ), 28.9 ( $\text{CH}_2\text{O}(\text{CH}_2\text{CH}_2\text{CH}_2)\text{CH}_2\text{COO}$ ), 25.6 ( $\text{CH}_2\text{O}(\text{CH}_2\text{CH}_2\text{CH}_2)\text{CH}_2\text{COO}$ ), 25.0 ( $\text{CH}_2\text{O}(\text{CH}_2\text{CH}_2\text{CH}_2)\text{CH}_2\text{COO}$ ), 22.4 ( $\text{CH}_2\text{CH}_2\text{CH}_2\text{CH}_3$ ) and 13.9 ( $\text{CH}_2\text{CH}_2\text{CH}_2\text{CH}_3$ ); found  $\text{M}^+$ , 958.4;  $\text{C}_{52}\text{H}_{72}\text{N}_5\text{O}_{10}\text{P}$  requires 958.1;  $m/z$  958.4 (100%,  $\text{M}^+$ ), 959.4 (55,  $\text{M} + [\text{H}]^+$ ) and 980.2 (30,  $\text{M} + [\text{Na}]^+$ ); m. p. 168 °C; crystalline, 168.0 °C [Smectic C, 185.0 °C] [Smectic A, 197.2 °C] isotropic.

*Protein Synthesis* – The procedure for the synthesis of DGK was followed from Lau and Bowie<sup>17</sup>. Plates prepared with agar, LB growth medium (prepared using 10  $\text{g L}^{-1}$  tryptone, 5  $\text{g L}^{-1}$  yeast extract and 10  $\text{g L}^{-1}$  sodium chloride in distilled water, pH adjusted to 7.5) and 0.1  $\mu\text{g L}^{-1}$  ampicillin were streaked with *E. coli* from a previously prepared strain (strain BL21, containing the pSD004 plasmid, a gift from C. Sanders at Vanderbilt University) and incubated at 37 °C overnight. Sample bottles of 5 mL LB growth medium containing ampicillin

were then inoculated with colonies picked from the agar plates and incubated overnight at 37 °C with shaking. The samples were then transferred to 0.5 L of LB growth medium in 2 L flasks, with ampicillin and were incubated at 37 °C with shaking. The growth of the bacteria was monitored using UV/vis spectrophotometry at  $A_{600}$ . Isopropyl- $\beta$ -D-thiogalactopyranoside (IPTG) was added when the absorbance of the bacteria suspension reached 0.8 AU in order to activate the correct promoter section of the gene (the *lac* operon) on the plasmid and induce DGK expression. Samples were harvested at stages (30 min, 60 min, 120 min and 180 min) to monitor the progress of DGK expression using polyacrylamide gel electrophoresis (PAGE) and then incubated at 37 °C overnight.

*SDS-PAGE* – The harvested samples were pelleted and resuspended in gel loading buffer (sodium dodecyl sulphate (SDS) in 2-mercaptoethanol). The SDS-PAGE apparatus was set up and loaded with the separating gel, which resolves the protein (prepared using 4 mL glycerol, 3 mL 30% acrylamide, 2 mL distilled water, 20  $\mu$ L ammonium persulphate (APS) and 75  $\mu$ L *N,N,N',N'*-tetramethylethylenediamine (TEMED) in 10 mL TRIS base (2 M tris(hydroxymethyl)aminomethane (TRIS base) in distilled water, pH adjusted to 6.8) and the stacking gel (prepared using 1 mL acrylamide, 3.4 mL distilled water, 20  $\mu$ L APS, 75  $\mu$ L TEMED and 1.2 mL TRIS base, prepared as described previously). The tank was loaded with the anode and cathode buffers (anode buffer, prepared using 2 M tris(hydroxymethyl)aminomethane (TRIS base) in distilled water, pH adjusted to 8.9; and cathode buffer, prepared using 0.1 M TRIS base, 0.1 M tricine, and 0.1 % w/v SDS in distilled water). The gels were then loaded with samples in addition to a lysozyme marker and the PAGE was run. Following the completion of the separation, the gels were recovered, stained with a triphenylmethane dye, Coomassie Brilliant Blue R-250 ( $C_{45}H_{44}N_3NaO_7S_2$ ), and destained with a solution of 45 % methanol, 45 % distilled water, and 10 % glacial acetic acid.

*Extraction of DGK* – Cells were pelleted from the flasks by high speed, low temperature ultracentrifugation for 15 mins at 4°C, at a speed of 5000 rpm (6440 x g) using a Sorvall RC-5B Superspeed centrifuge. The cell paste was then

resuspended in buffer A (prepared using 50 mM sodium phosphate and 300 mM sodium chloride in distilled water, pH adjusted to 7.5). 1 mM phenylmethylsulphonyl fluoride (PMSF) solution was added to protect the target protein DGK from attack by other proteins from the lysed bacteria. The detergent n-octyl- $\beta$ -D-glucopyranoside (OG) was also added to a concentration of 3 % w/v, and the suspension stirred at 4 °C.

The suspension was then pelleted by centrifugation at a speed 5000 rpm and a temperature of 4 °C, giving a typical yield of pelleted material. The protein was suspended in 40 mL buffer A plus 1.5% OG and loaded onto a nickel-NTA-agarose resin column washed with buffer A. The protein was eluted off the column using buffer A containing 0.02 M imidazole and 0.5% n-decyl- $\beta$ -D-maltopyranoside (DM). The presence of protein in each fraction was confirmed using SDS-PAGE. The results of the SDS-PAGE procedure can be found in the Results and Discussion section. The protein was stored as a detergent solution at -80 °C until use.

*Preparation of Liposomes* - Samples of DOPC/azobenzene compound were prepared at molar ratios of 9:1. The typical amount of DOPC used in each experiment was approx. 80 mg. The lipids were co-dissolved in chloroform/methanol (1:1 v/v). The solvents were evaporated under vacuum, and the resulting lipid cake was suspended in 1 mL of doubly distilled water, frozen in liquid nitrogen, and then lyophilised overnight under high vacuum. Samples were then rehydrated with either distilled water (for UV spectroscopy) or PIPES buffer (prepared using 75 mM 1,4-piperazine-bis(ethanesulphonic acid) (PIPES), 50 mM lithium chloride, 0.1 mM ethylenediaminetetraacetic acid (EDTA) and 15 mM magnesium chloride in distilled water, pH adjusted to 6.8; used for enzyme assay experiments), and extruded to produce 0.2  $\mu$ m unilamellar liposomes.

*UV Spectroscopy* – Samples were made up in 1 mL quartz cuvettes with an appropriate solvent. The cis state was induced by irradiation at 350 nm, while the trans state was induced by irradiation at 440 nm using a mercury arc lamp at 250 W. Samples were typically irradiated for 15 mins. Experiments were

carried out at 10 °C. The blanks used matched the solvents used during each experiment.

*Enzyme Assay* - The basic scheme of the enzyme activity assay is shown in Figure 2.6<sup>19</sup>.

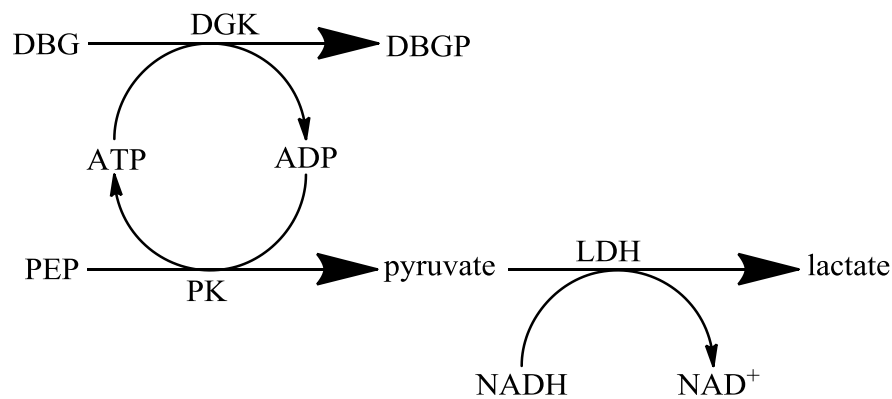


*Figure 2.6. Enzyme activity assay schematic. Abbreviations used are as follows: DBG (dibutyryl glycerol); DGK (diacylglycerol kinase); DBGP (phosphorylated DBG); ATP (adenosine triphosphate); ADP (adenosine diphosphate); PEP (phosphoenolpyruvate); PK (pyruvate kinase); LDH (lactate dehydrogenase) NADH (nicotinamide adenine dinucleotide); NAD<sup>+</sup> (oxidised NADH)*

The enzyme DGK, synthesised by *E. coli*, phosphorylates diacylglycerols (DAG) using adenosine triphosphate (ATP). In this assay dibutyryl glycerol (DBG) is used, as it is water-soluble and so the concentration can be easily controlled. In the first step, DGK phosphorylates DBG to DBGP using ATP, producing adenosine diphosphate (ADP). ADP from this step is then used in the catalysis of phosphoenolpyruvate (PEP) by the enzyme pyruvate kinase (PK), producing pyruvate and ATP. Pyruvate then acts as a substrate for the action of the enzyme lactate dehydrogenase (LDH), which produces lactate using nicotinamide adenine dinucleotide (NADH). NADH is transformed into NAD<sup>+</sup> during the reaction. NADH absorbs at a wavelength of 340 nm, while NAD<sup>+</sup> does not absorb in the UV/visible region. Therefore the entire reaction can be followed using UV-visible spectroscopy. The conversion of NADH to NAD<sup>+</sup> results in a

negative slope as NADH is turned over, with the gradient providing a measure of the enzyme activity<sup>19</sup>.

Samples for enzyme assay were typically made up in 270  $\mu\text{L}$  volume quartz cuvettes with a 1 cm pathlength as follows: 250  $\mu\text{L}$  of assay mix (0.5 nM NADH, 3 mM ATP, 3 mM DBG and 1 mM PEP in PIPES buffer), 10  $\mu\text{L}$  of enzymes and 10  $\mu\text{L}$  of liposomes (synthesised as described above), either DOPC or azobenzene-containing DOPC, followed by the addition of DGK immediately prior to the experiment. Experiments were typically carried out at 30 °C.

*Calculation of Enzyme Activity* – The enzyme activity is derived from the gradient of the slope, which is an indicator of the rate of change of absorption per minute. First of all the concentration of NADH, which has an extinction coefficient of  $6440 \text{ mol L}^{-1}$ , is calculated from the gradient using the Beer-Lambert equation (Equations 11 and 12). The volume of the reaction mixture is then calculated in order to express the amount of NADH in moles in the cuvette (in units of  $\mu\text{mol}$ ), followed by the amount of protein in mg. When the rate of NADH turnover is divided by the amount of protein present, the resulting figure is a measure of specific enzyme activity, in units of  $\mu\text{mol min}^{-1} \text{ mg}^{-1}$ . This figure is expected to change in relation to the conditions in the bilayer.

A number of azobenzene compounds were analysed during the series of experiments. These are referenced as shown in Table 2.1.

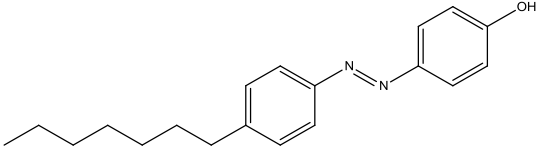
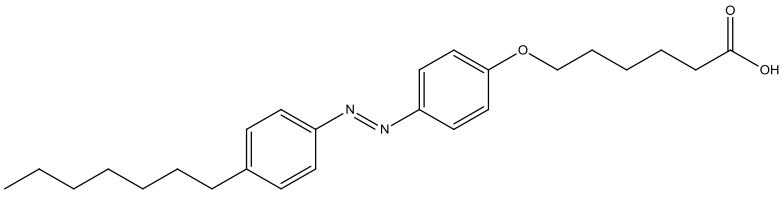
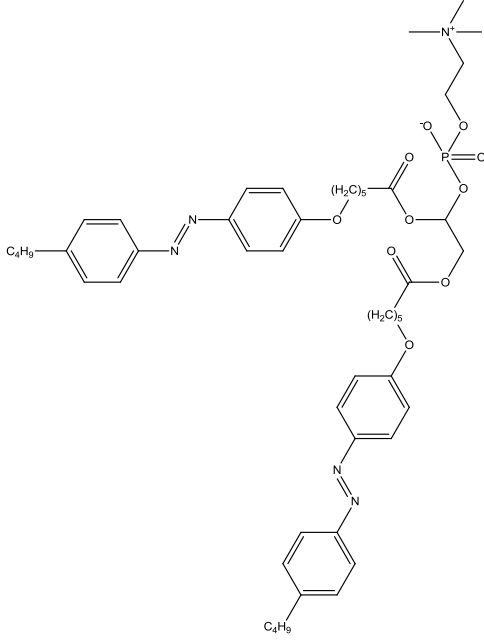
| Reference Name | Chemical Structure and Name  |
|----------------|--|
| Azo compound 1 |  <p data-bbox="769 654 1157 689">4-(4-Heptylphenylazo)phenol</p>   |
| Azo compound 2 |  <p data-bbox="646 922 1284 958">6-[4-(4-Heptylphenylazo)phenoxy]hexanoic acid</p>   |
| Bis-Azo-PC     |  <p data-bbox="694 1691 1236 1836">1,3-Bis(6-4-((<i>E</i>)-(4-butylphenyl)diazenyl)phenoxy)hexanoyloxypropan-2-yl 2-(trimethylammonio)ethyl phosphate</p> |

Table 2.1. Table showing the azobenzene compounds analysed

## Part 4. Results and Discussion

*Protein Synthesis* – Fractions eluted from the nickel-NTA-agarose column were analysed using SDS-PAGE to determine the final concentration of DGK. After destaining, two fractions (4 and 5) out of fourteen in total were observed to contain protein. UV/vis spectrophotometry at  $A_{280}$  was used to analyse the concentrations of protein in both fractions. The solution from fraction 4 was diluted 100-fold to produce an absorption of 0.13 AU. The Beer-Lambert law was used to calculate the concentration of this fraction (Equation 11):

$$A = \varepsilon c \ell$$

*Equation 11. Beer-Lambert law for the calculation of concentration from absorbance, where  $A$  is absorbance (AU),  $\varepsilon$  is the extinction coefficient ( $\text{mg mL}^{-1} \text{cm}^{-1}$ ),  $c$  is concentration ( $\text{mg mL}^{-1}$ ), and  $\ell$  is the pathlength of the cuvette (cm)*

The use of a cuvette with a 1 cm pathlength leaves a rearranged equation for concentration (Equation 12):

$$c = \frac{A}{\varepsilon}$$

*Equation 12. Rearranged Beer-Lambert law for the calculation of concentration*

The extinction coefficient of DGK is  $1.8 \text{ mg mL}^{-1} \text{cm}^{-1}$ . Using the rearranged Beer-Lambert equation (Equation 12), the total concentration of the fractions was  $7.39 \text{ mg mL}^{-1}$ .

*Changing the conformation of azobenzene-containing compounds in solvents* – The first step in the experiment was carried out in order to demonstrate that bis-Azo-PC could change conformations while dissolved in a suitable solvent. The experiments were first carried out on azobenzene compounds **1** and **2**.

Azobenzene **2** was dissolved in methanol and analysed (Figure 2.7).

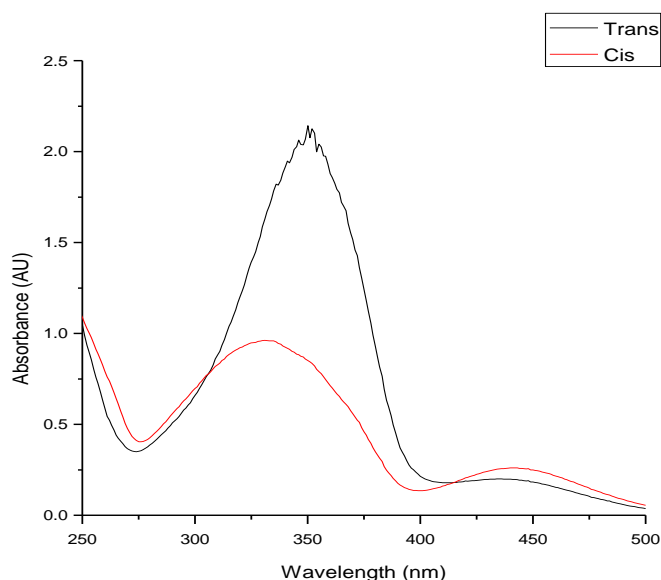
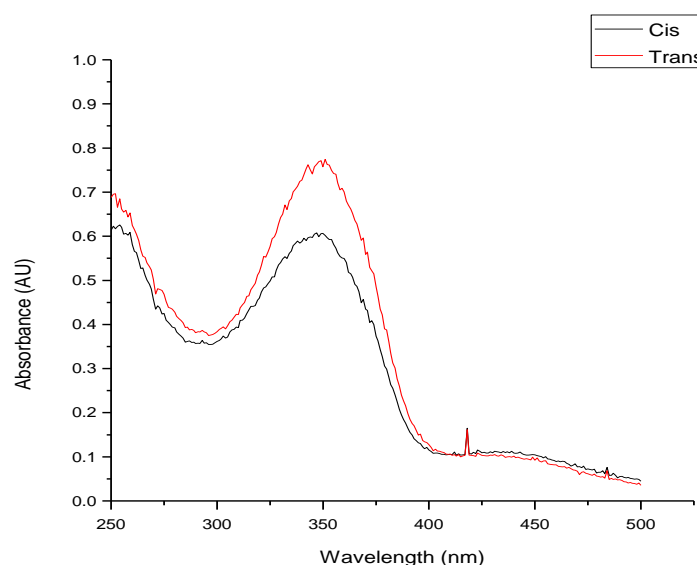


Figure 2.7. *Trans state (black) vs cis state (red) of azobenzene compound 2 in methanol*

Figure 2.7 shows the cis and trans spectra for the sample of azobenzene compound **2** in methanol. The plot gives a  $\pi$ - $\pi^*$  transition of 350 nm for the trans state (345 nm for the cis state) and an n- $\pi^*$  transition of  $\sim$  440 nm for both states. The absorbance of the ground state at  $\lambda_{\text{max}}$  is higher than for the cis state, while the opposite is noted for the n- $\pi^*$  transition. The isosbestic point occurs at approx. 420 nm. These changes in the spectra show the difference between an induced cis state and the trans state.

The analysis was also carried out on a sample of azobenzene **1** in methanol, but attempts to change the conformation failed, possibly due to tautomerism of the sample in solution. Tautomerism of hydroxyl moieties was also discussed in a study carried out by Liu *et al.* on azobenzene-containing cholesterol compounds in liposomes. The study found that a cholesterol compound terminating in a hydroxyl group was difficult to photoisomerise<sup>20</sup>.

The analysis was then carried out on a sample of bis-Azo-PC. Figure 2.8 shows the cis and trans spectra of bis-Azo-PC in methanol.



*Figure 2.8. Trans state (red) vs. cis state (black) of bis-Azo-PC in methanol*

The plot gives a  $\pi$ - $\pi^*$  transition of 349.04 nm for the trans state (342.97 nm for the cis state), and an  $n$ - $\pi^*$  transition of approx. 438 nm ( $\sim$  440 nm for the cis state). The absorbance at  $\lambda_{\max}$  is much higher for the trans state than for the cis state, while the opposite is noted for the  $n$ - $\pi^*$  transition. The isosbestic point occurs at approx. 410 nm.

The  $\pi$ - $\pi^*$  and  $n$ - $\pi^*$  transitions typically found for the spectra agree with the wavelengths found for typical azobenzene compounds in literature: approx. 350 nm for the  $\pi$ - $\pi^*$  transition and approx. 450 nm for the  $n$ - $\pi^*$  transition<sup>17</sup>.

*Changing the conformation of azobenzene-containing compounds in liposomes –* After demonstrating that bis-Azo-PC was amenable to photoisomerisation in solvents, the next step was to incorporate it into DOPC liposomes to establish if it could be photoisomerised as part of a liposome. A sample of DOPC/bis-Azo-PC liposomes in distilled water was analysed (Figure 2.9).

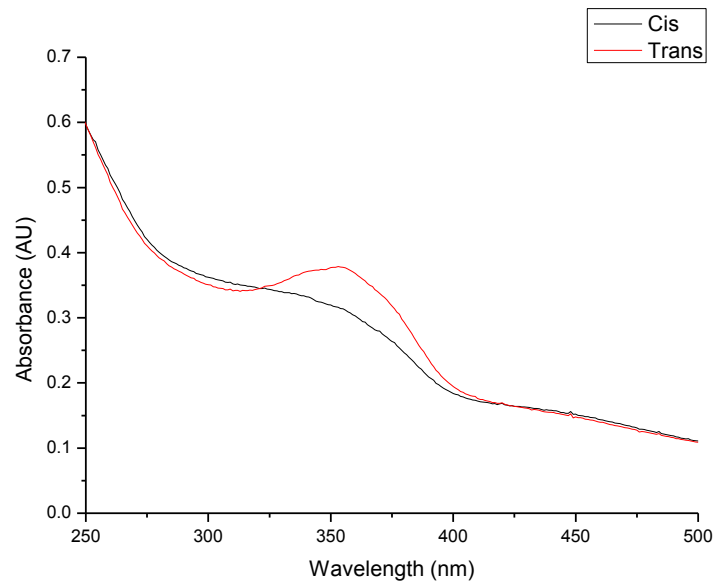


*Figure 2.9. Plot showing the trans state (red) vs. the cis state (black) of DOPC liposomes containing bis-Azo-PC*

The plot shows a considerable difference between the absorption spectra of bis-Azo-PC in methanol and those of DOPC/bis-Azo-PC liposomes. Figure 2.10, a comparison of the cis state spectra for each compound, shows that the  $\pi$ - $\pi^*$  transition has shifted from  $\sim 350$  nm for the pure azobenzene compound to  $\sim 320$  nm for the liposomes. The overall profile of the spectrum has also changed, with the presence of a slope followed by the loss of a visible n- $\pi^*$  transition peak. Figure 2.9 shows the presence of two isosbestic points (at  $\sim 340$  nm and  $\sim 390$  nm), in comparison to the single isosbestic point observed for pure azobenzene.

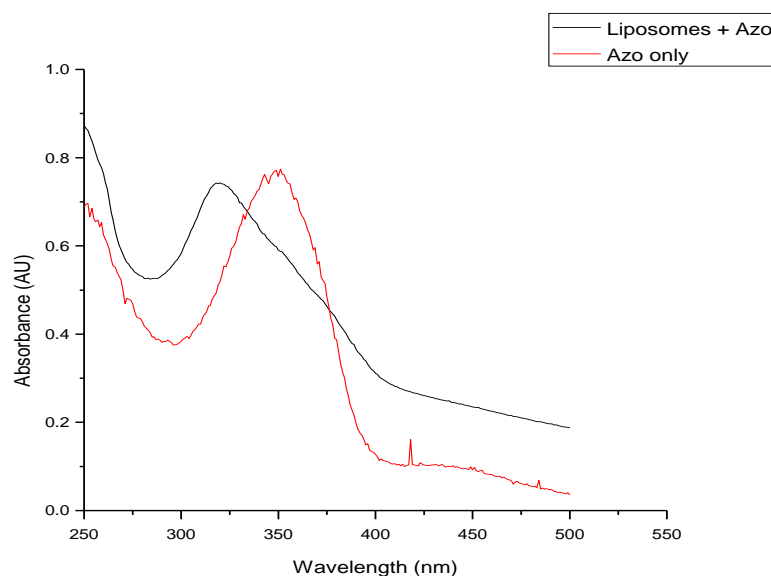


*Figure 2.10. Plot showing the difference between the cis states of bis-Azo-PC in methanol (red) and bis-Azo-PC incorporated into DOPC liposomes (black), measured in H<sub>2</sub>O*

The comparison of the spectra of the pure azobenzene compound against the DOPC/bis-Azo-PC liposomes shows that the presence of liposomes hinders the ability to visually separate the two states, as the difference between the trans and cis states is not as clear as it is between the states of the pure azobenzene compound. There may also be negative effects from the turbidity of the samples, as observed by the much higher absorbances of the liposomes.

Research into the aggregation behaviour of azobenzene-containing lipid analogues in liposomes by Kuiper and Engberts suggests that the blue-shift observed to occur in the liposomes is as result of a degree of H-aggregation of the azobenzene compounds<sup>9</sup>. A  $\pi$ - $\pi^*$  absorption band appearing between 320 and 350 nm may be attributed to the formation of clusters of azobenzene molecules within the bilayer<sup>9</sup>.

*The enzyme assay experiment* - The enzyme assay experiment was first tested on DOPC liposomes without bis-Azo-PC in order to check the validity and

repeatability of the method. Figure 2.11 shows a typical enzyme assay profile for DOPC liposomes containing DGK.

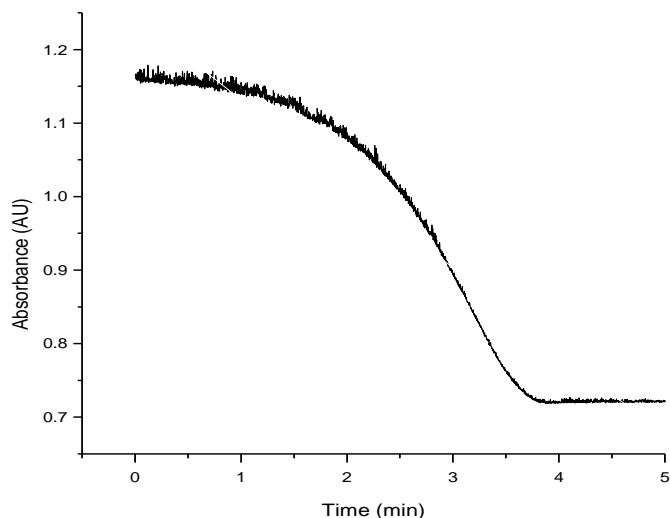


*Figure 2.11. A plot showing a typical enzyme assay profile for DOPC liposomes containing DGK*

The experiment was repeated a number of times using DOPC-only liposomes in order to ensure repeatability of the method and reagents used. The conditions for the experiments were as follows: 10  $\mu\text{L}$  DGK stock solution at a concentration of  $0.739 \mu\text{g } \mu\text{L}^{-1}$  was refolded into 100  $\mu\text{L}$  of DOPC liposomes. 20  $\mu\text{L}$  of this sample was then diluted into 100  $\mu\text{L}$  PIPES buffer. The DGK/liposome solution was then added to a cuvette containing 250  $\mu\text{L}$  of assay mix with 3 mM DBG and 10  $\mu\text{L}$  linking enzymes and mixed thoroughly. The enzyme assay measurements were then started. The experiments were carried out at 20  $^{\circ}\text{C}$ . The results for the experiments are shown in Figure 2.12.

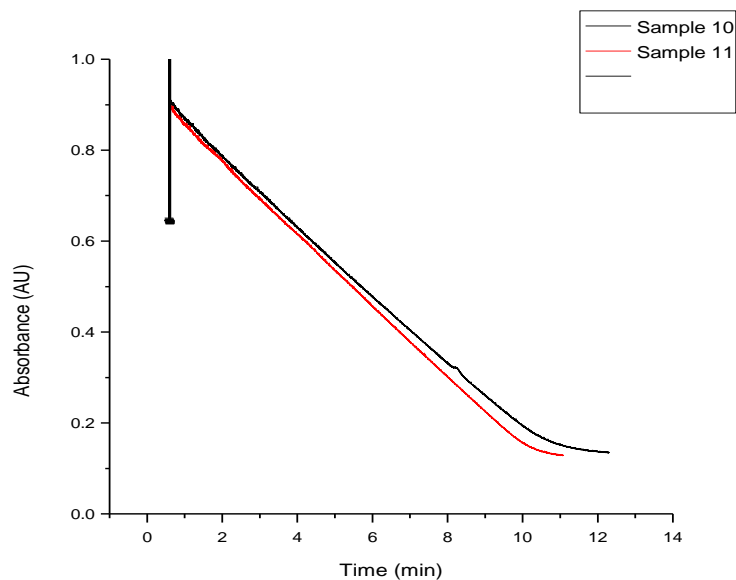


Figure 2.12. Plots for the enzyme assay analysis of two samples of DOPC liposomes containing DGK (samples 10 (black) and 11 (red))

Linear fitting analysis carried out on the plots gave slopes of  $-0.07036$  AU for sample 10, and  $-0.07671$  AU for sample 11, which shows a reasonably close correlation between the two experiments carried out under the same conditions. The specific enzyme activities for these samples are  $0.415 \mu\text{mol min}^{-1} \text{mg}^{-1}$  for sample 10 and  $0.452 \mu\text{mol min}^{-1} \text{mg}^{-1}$  for sample 11.

The experiment was then repeated with DOPC liposomes containing azobenzenes **1** and **2**. In the presence of these azobenzenes, there was no change in the absorbance, indicating there was an inhibiting factor present. It is possible that the azobenzene compounds, which terminate in a carboxylic acid group and a hydroxyl group respectively, were reacting with an active reagent of the assay mixture used in competition with the enzyme. In addition, Balasubramanian *et al.* discovered that an enzyme assay carried out using  $\alpha$ -chymotrypsin could be inhibited in the presence of an azobenzene carboxylic ester compound<sup>3</sup>.

The experiment was then repeated using liposomes containing bis-Azo-PC. The conditions for the experiment were as follows:  $10 \mu\text{L}$  of DGK stock solution was refolded into  $100 \mu\text{L}$  of bis-Azo-PC/DOPC liposomes.  $10 \mu\text{L}$  of this sample was then diluted into  $100 \mu\text{L}$  PIPES buffer. The DGK/liposomes solution was then

added to a cuvette containing 250  $\mu\text{L}$  of assay mix with 3 mM DBG and 10  $\mu\text{L}$  linking enzymes and mixed thoroughly. The enzyme assay measurements were then started. The experiment was carried out at 20  $^{\circ}\text{C}$ . The result for the experiment is shown in Figure 2.13.

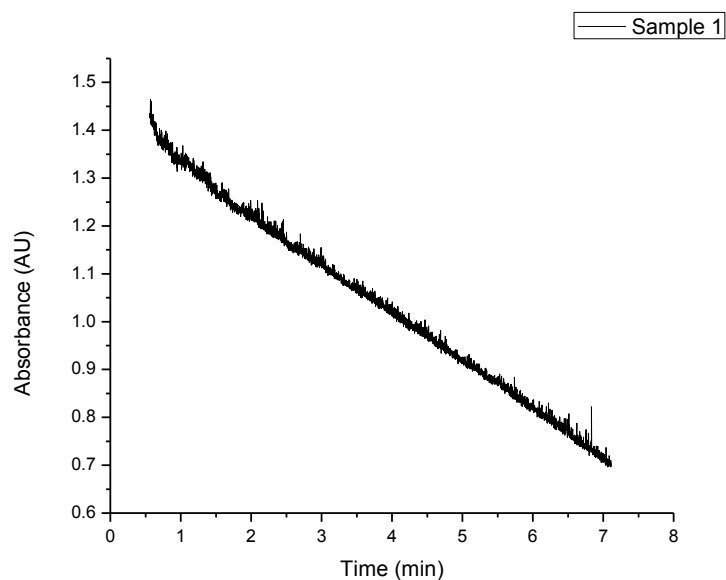


*Figure 2.13. Plot for the enzyme assay analysis of a sample of DOPC/bis-Azo-PC liposomes containing DGK (sample 1)*

Linear fitting analysis carried out on the graph gave a slope of  $-0.1027 \text{ AU}$ , and a specific activity of  $0.605 \mu\text{mol min}^{-1} \text{ mg}^{-1}$ , which is significantly higher than the slopes obtained for DOPC-only liposomes previously. This is not due to the presence of bis-Azo-PC, which is not expected to have an enhancing effect on the activity of the protein, but instead is probably due to the problems with repeatability of results encountered during this research.

In order to test the effect of photoswitching of bis-Azo-PC in DOPC liposomes on the activity of the protein, the liposomes were irradiated at 350 nm for 15 minutes in order to switch the azobenzene compound into the cis state. The sample was then incubated with DGK for a further 15 minutes (10  $\mu\text{L}$  of DGK stock solution refolded into 100  $\mu\text{L}$  of the liposomes, followed by a further dilution of 20  $\mu\text{L}$  of this sample into 100  $\mu\text{L}$  PIPES buffer). Following the incubation period, the reaction was initiated by adding the liposomes to the assay

mix. The samples were kept in the dark to avoid back-conversion into the ground state (an equilibrium mixture of trans and cis states). The experiment was repeated by photoswitching the samples into either the cis (350 nm) or trans (440 nm) states. The results of the repeated experiments are shown in Figures 2.14 and 2.15.

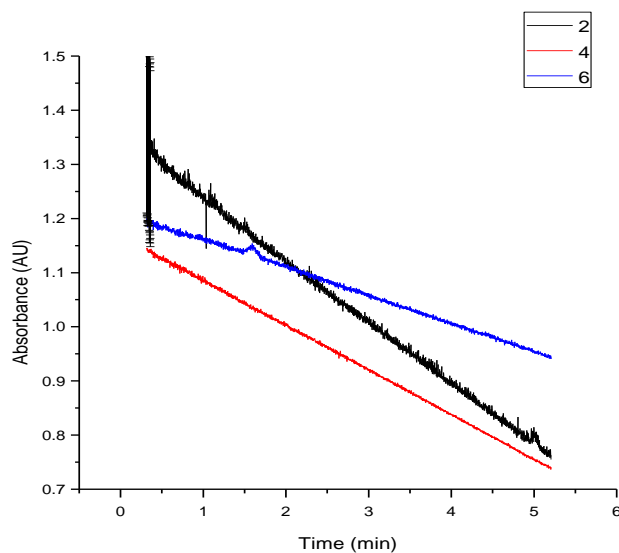


Figure 2.14. Plots for the enzyme assay analysis of samples of DOPC/bis-Azo-PC liposomes containing DGK after photoswitching samples 2 (black), 4 (red) and 6 (blue) to the cis state

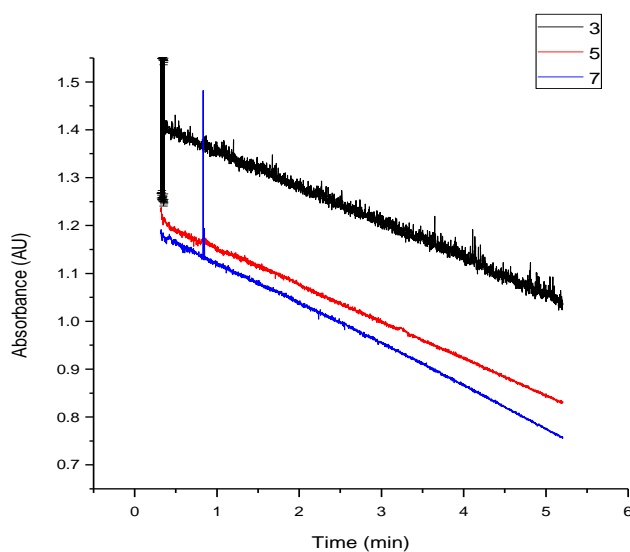


Figure 2.15. Plots for the enzyme assay analysis of samples of DOPC/bis-Azo-PC liposomes containing DGK after photoswitching samples 3 (black), 5 (red) and 7 (blue) to the trans state

Linear fitting analysis was carried out on each graph to produce a slope and the specific activity of the protein. These are shown in Table 2.2.

| Sample | State | Slope (AU)                    | Specific Activity<br>( $\mu\text{mol min}^{-1} \text{mg}^{-1}$ ) |
|--------|-------|-------------------------------|--|
| 2      | Cis   | -0.1142                       | 6.73   |
| 3      | Trans | -0.0731                       | 4.31   |
| 4      | Cis   | -0.0836                       | 4.93   |
| 5      | Trans | -0.0778                       | 4.59   |
| 6      | Cis   | -0.0515                       | 3.04   |
| 7      | Trans | -0.0898                       | 5.29   |
|        |       | <b>Standard<br/>Deviation</b> | 1.21   |

*Table 2.2. Table of specific activities for the enzyme assay of DOPC/bis-Azo-PC liposomes containing DGK*

From the calculated slopes and specific activities it can be seen that there is no reproducibility to these results; therefore they could not be used to give an indication of the effect of photoswitching the azobenzene on the activity of the protein.

The experiment was repeated on DOPC liposomes to try to produce an accurate, repeatable method of analysing each sample with as little variation as possible. The conditions were as follows: 10  $\mu\text{L}$  of DGK stock solution was refolded into 100  $\mu\text{L}$  of DOPC liposomes. 20  $\mu\text{L}$  of this sample was diluted into 100  $\mu\text{L}$  PIPES buffer. The DGK/liposome solution was then added to a cuvette containing 250  $\mu\text{L}$  of assay mix, with 3 mM DBG and 10  $\mu\text{L}$  linking enzymes, and mixed thoroughly. The enzyme assay measurement was then started. The experiments were carried out at 20 °C. The results for the experiments are shown in Figure 2.15.

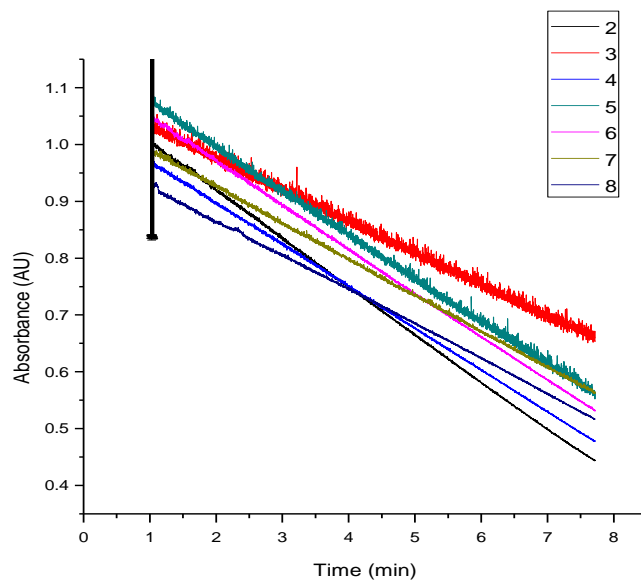


Figure 2.15. Plots for the enzyme assay analysis of samples of DOPC liposomes containing DGK (samples 2 (black), 3 (red), 4 (blue), 5 (green), 6 (pink), 7 (mustard) and 8 (dark blue))

Linear fitting analysis was carried out on each graph to produce a slope and specific activity. These are shown in Table 2.3.

| Sample | Slope (AU)                | Specific Activity ( $\mu\text{mol min}^{-1} \text{mg}^{-1}$ ) |
|--------|---------------------------|---|
| 2      | -0.0893                   | 5.26  |
| 3      | -0.0548                   | 3.23  |
| 4      | -0.0731                   | 4.31  |
| 5      | -0.0675                   | 3.98  |
| 6      | -0.0682                   | 4.02  |
| 7      | -0.063                    | 3.71  |
| 8      | -0.0607                   | 3.58  |
|        | <b>Standard Deviation</b> | 0.65  |

Table 2.3. Table of specific activities for the enzyme assay of DOPC liposomes containing DGK

These results show the amount of variation between samples using the same conditions, reagents and methods. At this point it was decided to discontinue this series of experiments due to the fact that, with such variation observed among identical samples, the difference between the slopes of the cis-state and trans-state bis-Azo-PC/DOPC liposomes would be too small to be able to form any firm conclusions about the effect of photoswitching on the enzyme activity.

*Problems with the methodology* – The results obtained for both the DOPC-only and the DOPC/bis-Azo-PC liposomes were not reproducible, which indicated that any experiments to switch the states of the azobenzene-containing compound between cis and trans in order to effect a change in the activity of the protein would not produce results with a sufficiently significant difference to be able to distinguish between the activities of the two states. This is probably due to the fact that the inherent difference in activity between the two photo-states is too small to allow it to be observed using this method. Proteins *in vivo* can tolerate a wide range of environmental conditions, including high pressures in the cell membrane (several hundreds of atm) and bilayer tension caused by curvature frustration<sup>18</sup>. It is possible that the change induced in the bilayer by photoswitching between the cis and trans states is not significant enough to effect a change on the protein activity.

The stability of the reagents may have been a factor in the variation in the experimental results, but this was partly alleviated by re-extruding the liposomes and using fresh protein, assay mix, and DBG stock for every set of experiments. In addition, the condition of the liposomes was visually checked to ensure that there was no degradation during the experiments. The preparation of the DBG stock was complicated by the insolubility in water. Care was taken to ensure that all of the DBG for each stock solution was at least suspended in PIPES buffer prior to the experiment; however it is possible that the compound could have dropped out of solution while the experiments were running, thereby reducing the concentration of this reagent.

The azobenzene compound itself may have aggregated within the liposomes, which introduces another uncontrollable element to the experiments. The

appearance of the  $\pi$ - $\pi^*$  absorption band at  $\sim 320$  nm in the UV spectrum of DOPC/bis-Azo-PC liposomes has been attributed to a slight degree of H-aggregation<sup>9</sup>. The aggregation of the azobenzene compound may also contribute to the variation in the results.

Any of the factors described may have contributed to the variation in results. The reagent stability was partly alleviated by re-extruding the liposomes and re-synthesising the DBG stock for every set of experiments, but this introduces an unavoidable cost of time, and for DBG in particular, budget. The issue of possible aggregation of azobenzene compounds in DOPC liposomes may be solved by reducing the concentration; but a large decrease in concentration may render it impossible to analyse the samples using UV/vis spectroscopy.

## **Part 5. Conclusion**

UV/visible spectroscopy was used to analyse the spectra of three azobenzene-containing compounds: azobenzene compounds **1** and **2**, and bis-Azo-PC. A sample of azobenzene **2** produced  $\pi$ - $\pi^*$  and  $n$ - $\pi^*$  transitions of 350 nm and 440 nm, respectively, for the trans state isomers, and 345 nm and 440 nm for the cis state isomers. A repeat of the experiments on a sample of azobenzene **1** showed that the sample failed to photoisomerise under the same conditions, possibly due to tautomerism<sup>20</sup>. A sample of bis-Azo-PC produced  $\pi$ - $\pi^*$  and  $n$ - $\pi^*$  transitions of 350 nm and 438 nm, respectively, for the trans isomers, and 343 nm and 440 nm for the cis state isomers. The  $\pi$ - $\pi^*$  and  $n$ - $\pi^*$  transitions for these spectra are in agreement with those previously reported<sup>17</sup>.

When incorporated into DOPC liposomes, the  $\pi$ - $\pi^*$  transition was found to have changed to 320 nm, while the  $n$ - $\pi^*$  transition was no longer visible. Photoisomerisation between the trans and cis states also produced two isosbestic points, while only one was observed for the azobenzene compounds in isolation. The blue-shift of the  $\pi$ - $\pi^*$  transition may be attributed to a degree of H-aggregation of bis-Azo-PC in the DOPC bilayer<sup>9</sup>.

Enzyme assay experiments were then carried out on DOPC-only and DOPC/azobenzene liposomes. The enzyme assay experiment was successfully carried out using DOPC-only liposomes, and then repeated using DOPC/azobenzene **1** and DOPC/azobenzene **2** liposomes. The use of these azobenzene compounds inhibited the activity of the enzyme, possibly by competing for one of the reagents used in the assay.

The enzyme assay experiment was then carried out on DOPC/bis-Azo-PC liposomes. The azobenzene compound did not competitively inhibit the enzyme. However the investigation into the effect of azobenzene photoswitching on the enzyme activity could not be completed due to the fact that the subsequent change in activity was too small to be confidently attributed to influence on the protein by the change in bilayer properties.

## **Part 6. References**

1. Bieth, J.; Vratsanos, S. M.; Wassermann, N.; Erlanger, B. F., Photoregulation of biological activity by photochromic reagents, II. Inhibitors of acetylcholinesterase. *Proc. Natl. Acad. Sci.* **1969**, 64, (3), 1103 - 1106.
2. Kaufman, H.; Vratsanos, S. M.; Erlanger, B. F., Photoregulation of an enzymic process by means of a light-sensitive ligand. *Science* **1968**, 162, 1487 - 1489.
3. Balasubramanian, D.; Subramani, S.; Kumar, C., Modification of a model membrane structure by embedded photochrome. *Nature* **1975**, 254, (5497), 252-254.
4. Sandhu, S. S.; Yianni, Y. P.; Morgan, C. G.; Taylor, D. M.; Zaba, B., The formation and Langmuir-Blodgett deposition of monolayers of novel photochromic azobenzene-containing phospholipid molecules. *Biochim. Biophys. Acta* **1986**, 860, (2), 253-262.
5. Morgan, C. G.; Thomas, E. W.; Yianni, Y. P.; Sandhu, S. S., Incorporation of a novel photochromic phospholipid molecule into vesicles of dipalmitoylphosphatidylcholine. *Biochim. Biophys. Acta* **1985**, 820, (1), 107-114.

6. Bisby, R. H.; Mead, C.; Morgan, C. C., Wavelength-programmed solute release from photosensitive liposomes. *Biochem. Biophys. Res. Commun.* **2000**, 276, (1), 169-173.
7. Folgering, J. H. A.; Kuiper, J. M.; de Vries, A. H.; Engberts, J.; Poolman, B., Lipid-mediated light activation of a mechanosensitive channel of large conductance. *Langmuir* **2004**, 20, (17), 6985-6987.
8. Furman, I.; Geiger, H. C.; Whitten, D. G., Aggregation phenomena in Langmuir-Blodgett films of polar stilbene amphiphiles. *Langmuir* **1994**, 10, 837-843.
9. Kuiper, J. M.; Engberts, J. B. F. N., H-aggregation of azobenzene-substituted amphiphiles in vesicular membranes. *Langmuir* **2004**, 20, (4), 1152-1160.
10. Vinogradova, O.; Badola, P.; Czernski, L.; Sonnichsen, F. D.; Sanders, C. R., *Escherichia coli* diacylglycerol kinase: A case study in the application of solution NMR methods to an integral membrane protein. *Biophys. J.* **1997**, 72, (6), 2688-2701
11. Czernski, L.; Sanders, C. R., Functionality of a membrane protein in bicelles. *Anal. Biochem.* **2000**, 284, 327-333.
12. Loomis, C. R.; Walsh, J. P.; Bell, R. M., *sn*-1,2-Diacylglycerol kinase of *Escherichia coli*. Purification, reconstitution, and partial amino- and carboxyl-terminal analysis. *J. Biol. Chem.* **1985**, 260, 4091-4097.
13. Gorzelle, B. M.; Nagy, J. K.; Oxenoid, K.; Lonzer, W. L.; Cafiso, D. S.; Sanders, C. R., Reconstitutive refolding of diacylglycerol kinase, an integral membrane protein. *Biochem.* **1999**, 38, (49), 16373-16382.
14. Lau, F. W.; Nauli, S.; Zhou, Y.; Bowie, J. U., Changing single side-chains can greatly enhance the resistance of a membrane protein to irreversible inactivation. *J. Mol. Biol.* **1999**, 290, 559-564.
15. Zhou, Y.; Bowie, J. U., Building a thermostable membrane protein. *J. Biol. Chem.* **2000**, 275, (10), 6975-6979.
16. Smith, R. L.; O'Toole, J. F.; Maguire, M. E.; Sanders, C. R., Membrane topology of *Escherichia coli* diacylglycerol kinase. *J. Bacteriol.* **1994**, 176, (17), 5459-5465.
17. Song, X. D.; Perlstein, J.; Whitten, D. G., Supramolecular aggregates of azobenzene phospholipids and related compounds in bilayer assemblies and

other microheterogeneous media: Structure, properties, and photoreactivity. *J. Am. Chem. Soc.* **1997**, 119, (39), 9144-9159.

18. Lau, F. W.; Bowie, J. U., A method for assessing the stability of a membrane protein. *Biochem.* **1997**, 36, (19), 5884-5892.

19. Badola, P.; Sanders, C. R., *Escherichia coli* diacylglycerol kinase is an evolutionarily optimized membrane enzyme and catalyzes direct phosphoryl transfer *J. Biol. Chem.* **1997**, 272, 24176-24182.

20. Liu, X. M. Y., B.; Wang, Y. L.; Wang, J. Y., Photoisomerisable cholesterol derivatives as photo-trigger of liposomes: Effect of lipid polarity, temperature, incorporation ratio, and cholesterol. *Biochim. Biophys. Acta* **2005**, 1270, (1-2), 28-34.

21. Bezrukov, S. M., Functional consequences of lipid packing stress. *Curr. Op. Coll. Interface Sci.* **2000**, 5, 247-243.

## Chapter 3: Phase Behaviour

### Part 1. Introduction

*Analysis of Lipid Phase Behaviour* - The phase behaviour of lipids in model membranes has been extensively researched in an effort to predict the behaviour of the lipid species which comprise the plasma membrane. Issues of particular interest include the role of cholesterol and the formation of the  $l_o$  phase, as well as the function of membrane lipid heterogeneity<sup>1</sup>. Cell membranes are mimicked using a range of models, such as unilamellar and multilamellar vesicles of varying sizes, and lipid monolayers<sup>1</sup>. A variety of experimental techniques has been used to analyse lipid properties and phase behaviour in model membranes, including differential scanning calorimetry (DSC)<sup>2</sup>, Fourier transform infrared spectroscopy (FTIR)<sup>2</sup>, atomic force microscopy (AFM), wide- and small-angle x-ray scattering<sup>3-5</sup>, fluorescence microscopy<sup>5-7</sup>, fluorescence resonance energy transfer (FRET)<sup>5,8</sup>, and NMR spectroscopy<sup>9</sup>.

DPPC is a commonly used component of phospholipid mixtures due to its relatively low melting point and tendency to form the  $l_o$  phase in the presence of cholesterol or sphingomyelin. The phase behaviour of this lipid in a range of mixtures has been extensively reported<sup>7</sup>. Various methods have been used to produce phase diagrams of DPPC and deuterated DPPC bilayers containing varying amounts of cholesterol, including molecular acoustics techniques and DSC<sup>10,11</sup>; x-ray diffraction<sup>4</sup>; and <sup>2</sup>H-NMR<sup>12,13</sup>.

*Serotonin Receptor Agonists* – Serotonin (5-hydroxytryptamine, or 5-HT) (Figure 4.1) is a neurotransmitter with a variety of physiological roles, including the regulation of appetite, moods, sleeping patterns, and gastrointestinal function<sup>14</sup>.

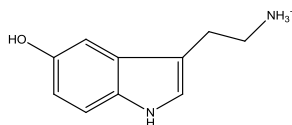
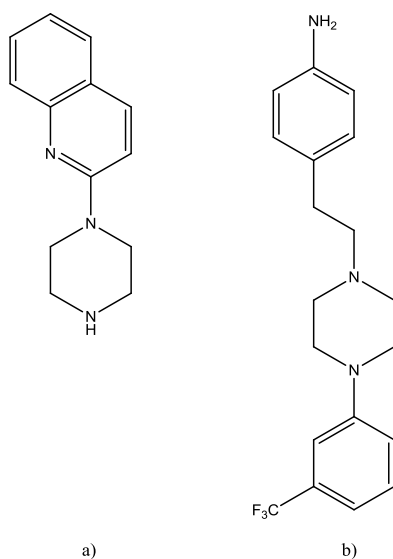


Figure 3.1. The structure of serotonin (5-hydroxytryptamine)<sup>15</sup>

The 5-HT receptors are G-coupled protein receptors with the sub-types 5-HT<sub>1-7</sub>, with the exception of 5-HT<sub>3</sub>, which is a ligand-gated ion channel (LGIC)<sup>16</sup>. Serotonin receptor agonists include many classes of drugs, such as antidepressants, antipsychotics, appetite suppressants and psychoactives<sup>17</sup>.

A study carried out by Lorch and Lopez analysed the locations and orientations of a range of 5-HT<sub>1A</sub> receptor ligands in DOPC/cholesterol bilayers using MAS-NOESY NMR<sup>18</sup>. The research analysed the agonists serotonin; LY-165,163; quipazine; 8-OH-DPAT; and buspirone. The study was expanded as part of the PhD research, focusing on the phase behaviour of DPPC/cholesterol/agonist bilayers.



*Figure 3.2. Structures of the 5-HT<sub>1A</sub> agonists a) quipazine, and b) LY-165,135*

Quipazine (Figure 3.2a) and LY-165,163 (Figure 3.2b) were selected from the group of agonist compounds due to the fact that they did not produce NMR resonances in the cholesterol region (up to 2.3 ppm). This allowed cholesterol/agonist cross-peaks to be observed when analysing d<sub>62</sub>-DPPC/cholesterol/agonist bilayers using MAS-NOESY NMR.

*Analysis of the Phase Behaviour of DPPC Samples Using  $^2\text{H}$ -NMR* - The phase behaviour of deuterated DPPC ( $d_{62}$ -DPPC) was analysed by Davis<sup>19</sup>. The main gel-to-fluid lamellar phase transition occurs at a temperature of 310 K, which is 4 K lower than the transition for protonated DPPC.

The phase behaviour of  $d_{62}$ -DPPC with varying concentrations of cholesterol (0 – 25 mol%) was analysed by Vist and Davis<sup>13</sup> and by Huang *et al*<sup>12</sup>. A phase diagram was generated for cholesterol concentrations from 0 – 30 mol%. At 20 mol%, the concentration used in this research, there is evidence of a mixed  $\text{I}_o + \text{I}_d$  phase from 310 K to 316 K, followed by the fluid lamellar phase.

*Characteristics of  $^2\text{H}$ -NMR Spectra of Lipid Bilayers* – Indications of phase behaviour in lipid bilayers such as DPPC/cholesterol samples can be obtained from the dePaked  $^2\text{H}$ -NMR spectra. DPPC spectra in the gel phase have broad shoulders, no well-defined central plateau, and no detail to the peaks of the plateau. As the temperature increases, and the sample enters the fluid lamellar phase, the edges of the plateau become sharp and well-defined, and the peaks in this region become resolvable. Figure 3.3 gives an example of the progression of the  $^2\text{H}$ -NMR spectra from the gel phase through to the fluid lamellar phase for a sample of  $d_{62}$ -DPPC<sup>13</sup>.

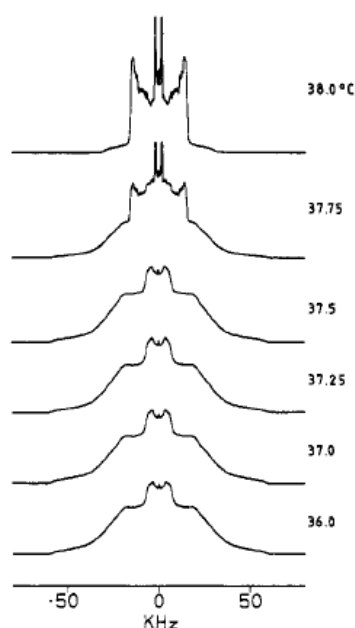


Figure 3.3.  $^2\text{H}$ -NMR spectra of  $d_{62}$ -DPPC showing the change in spectral characteristics as temperature increases, analysed by Vist and Davis<sup>13</sup>

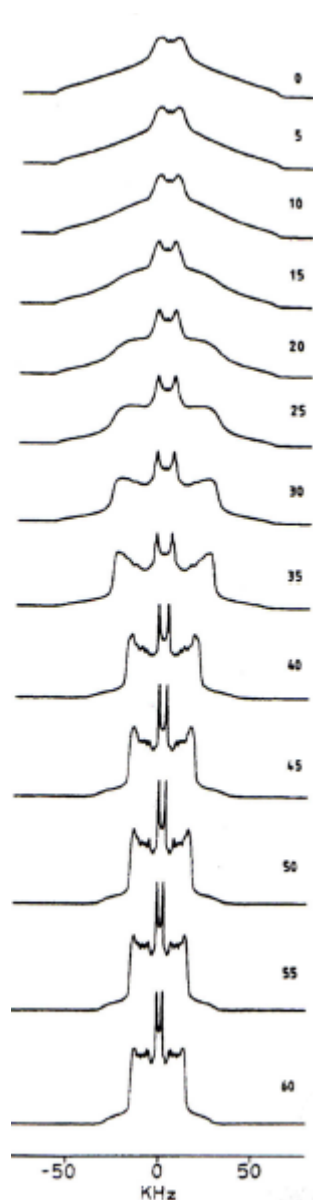


Figure 3.4.  $^2\text{H}$ -NMR spectra of  $d_{62}$ -DPPC with 15 mol% cholesterol showing the change in spectral characteristics as temperature increases, analysed by Vist and Davis<sup>13</sup>

There is a noticeable difference between the spectra for  $d_{62}$ -DPPC and those of  $d_{62}$ -DPPC/cholesterol at a concentration of 15 mol% (Figure 3.4). The gel phase spectra resemble those of  $d_{62}$ -DPPC until a temperature of 303 K. At this point, the shoulders of the spectrum become more sharply defined, which indicates a state of phase coexistence (gel +  $l_o$  phase). At 313 K the spectrum adopts the characteristics of the mixed  $l_d + l_o$  phase – sharply defined central peaks but rounded plateau edges. The spectral characteristics at 318 K indicate that the

sample is in the fluid lamellar phase, with no further phase coexistence. From this temperature onwards the spectra become narrower and increasingly well resolved due to increasing sample mobility<sup>13</sup>.

*Moments Analysis* – Phase behaviour can be analysed using moments analysis, a technique used to determine both the distribution of quadrupolar splittings ( $\Delta\nu_Q$ ) and the distribution of order parameters ( $S_{CD}$ ) in a <sup>2</sup>H NMR spectrum. Both of these distributions can indicate phases of lipid samples and show where phase transitions and phase coexistences occur. The first moment,  $M_1$ , is directly proportional to the average quadrupolar splitting ( $|\Delta\nu_Q|$ ) and the average order parameter ( $|S_{CD}|$ )<sup>19-25</sup>.

$$M_1 = \frac{4\pi}{\sqrt[3]{3}} \langle \delta_\nu \rangle \equiv \frac{4\pi}{\sqrt[3]{3}} \nu_Q \langle S_{CD} \rangle$$

*Equation 13*

The second moment,  $M_2$ , is directly proportional to the squares of the average quadrupolar splitting ( $|\Delta\nu_Q|^2$ ) and the average order parameter ( $|S_{CD}|^2$ )<sup>19-25</sup>.

$$M_2 = \frac{4\pi^2}{5} \langle (\delta_\nu)^2 \rangle \equiv \frac{4\pi^2}{5} \nu_Q^2 \langle S_{CD}^2 \rangle$$

*Equation 14*

The direct correlations between  $M_n$ , order parameter, and quadrupolar splitting, allows the moments to be used as a measure of increasing or decreasing order parameter and quadrupolar splitting. For example, a decrease in average order parameter, which may result from a gel-to-fluid lamellar phase transition, produces a decrease in  $M_1$ .

The first and second moments can then be used to generate the parameter  $\Delta_2$ , which is the relative mean square deviation (r.m.s.d.) of the distribution of quadrupolar splittings or order parameters<sup>19-25</sup>.

$$\Delta_2 = \frac{M_2}{1.35M_1^2} - 1$$

*Equation 15*

Small values of  $\Delta_2$  indicate small variations in the distribution of quadrupolar splittings, while a large  $\Delta_2$  value indicates larger variations. The highest value of  $\Delta_2$  is found at the phase transition point<sup>19-25</sup>.

*Central Terminal Methyl Splitting* – Central terminal methyl (CTM) splitting data provides an indication of the presence of the  $l_o$  phase, coexisting with either the gel or  $l_d$  phases. It arises due to the inequivalence of the terminal methyl groups of the phospholipid *sn1* and *sn2* acyl chains due to the physical properties of the bilayer in the  $l_o$  phase. It is not observed to occur in either the pure gel or fluid lamellar phases<sup>26, 27</sup>.

## **Part 2. Aims**

The aim of the experiment was to use  $^1\text{H}$  and  $^2\text{H}$  NMR spectroscopy to characterise the phase behaviour of liposomes containing DPPC, cholesterol and serotonin receptor agonists, which would then be further analysed using NOESY spectroscopy (as described in Chapter 4).

## **Part 3. Experimental**

*Materials* – 1,2-Dipalmitoyl-*sn*-glycero-3-phosphocholine (DPPC), chain-deuterated 1,2-dipalmitoyl-*sn*-glycero-3-phosphocholine ( $d_{62}$ -DPPC) and cholesterol were purchased from Avanti Polar Lipids (Alabaster, AL). All other chemicals including quipazine (Q) and LY-165, 135 (LY) were purchased from Sigma.

*Sample Preparation* – Samples of DPPC or DPPC-d<sub>62</sub>/cholesterol, DPPC or DPPC-d<sub>62</sub>/agonist, and DPPC or DPPC-d<sub>62</sub>/cholesterol/agonist were prepared at molar ratios of 8:2, 9:1 and 7:2:1 respectively. The typical amount of DPPC used in each experiment was approx. 80 mg. The lipids and agonist were co-dissolved in chloroform/methanol (1:1 v/v). The solvents were evaporated under vacuum, and the resulting lipid cake was suspended in 1 mL of doubly distilled water, frozen in liquid nitrogen, and then lyophilised overnight under high vacuum. The dry lipid mixtures were hydrated with ~ 200 µL of D<sub>2</sub>O for proton NMR and H<sub>2</sub>O for deuterium NMR. The mixtures were then transferred into 4mm MAS rotors.

*NMR Measurements* – All NMR experiments were carried out on a Bruker Avance II 500 MHz spectrometer using a 4mm MAS probe operating at a frequency of 500.1025 MHz (<sup>1</sup>H), and a wideline probe operating at a frequency of 76.773 MHz (<sup>2</sup>H). Experiments were carried out at an MAS speed of 10 kHz (<sup>1</sup>H), while deuterium experiments were carried out without spinning. <sup>1</sup>H NMR spectra were externally referenced to tetramethylsilane (TMS) at 0 ppm.

<sup>1</sup>H experiments were conducted with a typical  $\pi/2$  pulse length of 7 µs and a relaxation delay of 4 s. Proton decoupling was achieved using TPPM (30 kHz). <sup>2</sup>H experiments were conducted with a spectral width of 100 kHz, a recycle delay of 1 s, an echo delay of 30 µs, an acquisition time of 10 ms, 90° pulses of 5.5 µs, and between 2k and 4k scans. Measurements were taken at 1 K intervals between 273 K and 333 K (as determined by the thermocouple).

All of the NMR data were processed using TopSpin version 1.3 (Bruker Instruments, Karlsruhe, Germany). <sup>2</sup>H spectra were de-Paked and the spectral moments were calculated using NMR Depaker software<sup>28</sup>.

NMR experiments on the samples of d<sub>62</sub>-DPPC/LY and d<sub>62</sub>-DPPC/cholesterol/LY were carried out by C. Windle of the University of Hull. The results are reproduced here with permission.

#### Part 4. Results and Discussion

The assignments for the lipid, cholesterol and drug signals were allocated according to studies by Lopez and Lorch, Scheidt *et al.* and Soubias *et al.*<sup>18, 29, 30</sup>. The DPPC proton assignments are shown in Table 3.1, in order of increasing chemical shift (ppm).

| Carbon number  | Resonance/ppm |
|--|---------------|
| C16  | 0.9           |
| CH <sub>2</sub> (n)<br>The aliphatic lipid chain atoms | ~ 1.2         |
| C3   | 1.6           |
| C2   | 2.3           |
| γ, Gamma   | 3.3           |
| β, Beta  | 3.7           |
| G3   | 4.0           |
| Overlapped G1 and α, alpha resonances                  | 4.35          |
| G2   | 5.3           |

*Table 3.1. DPPC Proton Resonances*

The serotonin-receptor agonists' resonances (Q and LY) were also numbered in order of increasing chemical shift (ppm). These are shown in Tables 3.2 and 3.3.

| Carbon number | Q resonance/ppm |
|---------------|-----------------|
| Q1            | 3.45            |
| Q2            | 7.17            |
| Q3            | 7.33            |
| Q4            | 7.47            |
| Q5            | 7.60            |
| Q6            | 7.75            |
| Q7            | 7.97            |

*Table 3.2. Q proton resonances*

| <b>Carbon number</b> | <b>LY resonance/ppm</b> |
|----------------------|-------------------------|
| L1                   | 2.8                     |
| L2                   | 6.7                     |
| L3                   | 7.0                     |
| L4                   | 7.4                     |

*Table 3.3. LY proton resonances*

The cholesterol proton assignments are shown in Table 3.4, in order of increasing chemical shift (ppm).

| <b>Carbon number</b>       | <b>Resonance/ppm</b> |
|----------------------------|----------------------|
| C18 <sup>C</sup>           | 0.8                  |
| C26/27 <sup>C</sup>        | 0.9                  |
| C9/21/19 <sup>C</sup>      | 1.05                 |
| C14/17/24 <sup>C</sup>     | 1.20                 |
| C7/8/11/15/25 <sup>C</sup> | 1.50                 |
| C4 <sup>C</sup>            | 2.3                  |

*Table 3.4. Cholesterol proton resonances*

The use of a chain-deuterated phospholipid eliminates signals in the aliphatic region of the spectrum (0 ppm to 1.6 ppm), thereby ensuring that the previously hidden cholesterol aliphatic and methyl signals become visible. This enables the observation of cholesterol peaks which would otherwise be obscured by much more intense phospholipid peaks.

*Phase Behaviour* - The phase behaviour of all six samples was determined using data obtained from moments analysis, order parameters, visual analysis of the spectra, differential scanning calorimetry (DSC), and central terminal methyl (CTM) splitting data.

*Visual analysis* - The  $^2\text{H}$  NMR spectra of  $d_{62}$ -DPPC show characteristic gel phase spectra below the gel-to-fluid lamellar phase transition, as indicated by the lack of resolution (spectra at 308 K and 309 K, Figure 3.5). The fluid lamellar phase then appears at 310 K, as shown by the appearance of narrow splitting and well-resolved peaks. The resolution of the peaks improves with the increase of temperature.

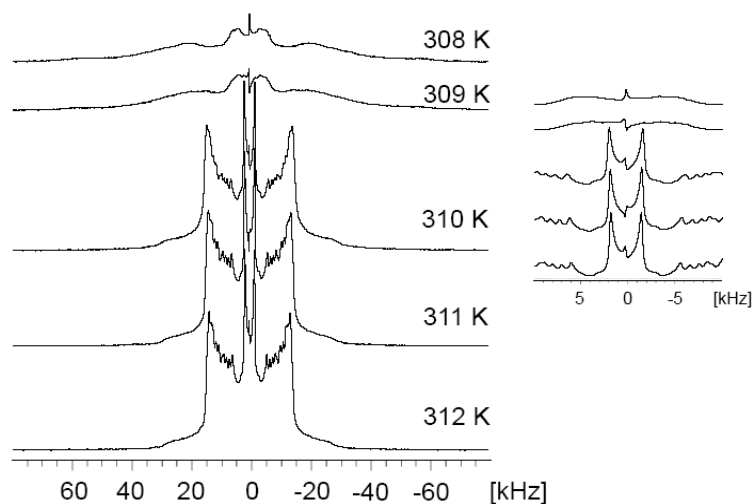


*Figure 3.5.  $^2\text{H}$  NMR spectra of  $d_{62}$ -DPPC at temperatures ranging from 308 K to 312 K at 1 K intervals, showing the gel-to-fluid lamellar phase transition. The inset displays an expansion of the middle of 20 kHz of each spectrum*

The  $^2\text{H}$  NMR spectra of  $d_{62}$ -DPPC/Q show the effect of Q on the  $d_{62}$ -DPPC bilayer (Figure 3.6). At 303 K the spectrum shows the emergence of shoulders and more resolved peaks which might indicate a separate phase between the gel and fluid lamellar phases, which is not evident from the  $M_1$  and  $\Delta_2$  data. This phase could be attributed to the ripple phase. It is possible that the elongated transition phase may be attributed to the  $P_\beta'$  phase; alternatively it could be an additional pre-transition phase. The spectra also show that the fluid lamellar phase transition occurs between 303 K and 308 K, as all of the spectra from this temperature onwards are in the fluid lamellar phase. This is corroborated by the data from the  $M_1$  and  $\Delta_2$  results.

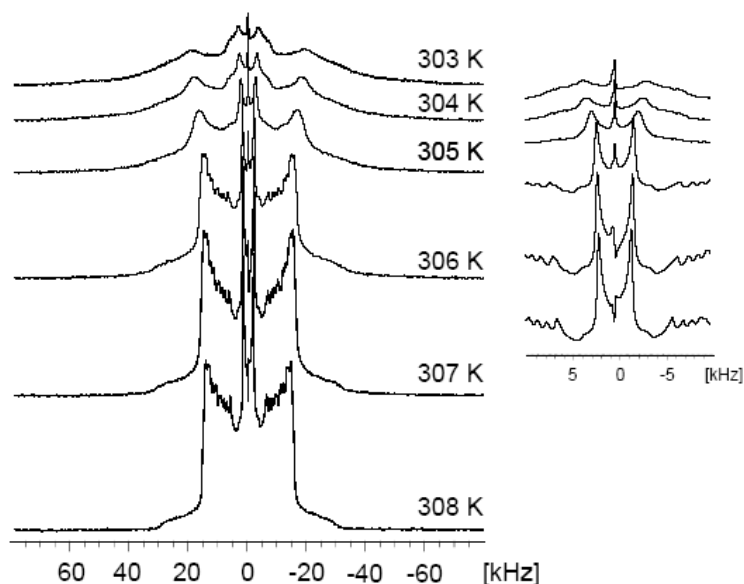


Figure 3.6.  $^2\text{H}$  NMR spectra of  $d_{62}\text{-DPPC/Q}$  at temperatures ranging from 303 K to 308 K at 1 K intervals, showing the gel-to-fluid lamellar phase transition. The inset displays an expansion of the middle of 20 kHz of each spectrum

The  $^2\text{H}$  NMR spectrum of the sample of  $d_{62}\text{-DPPC/cholesterol}$  show gel phase spectra at 283 K. At 293 K the appearance of prominent shoulders and evidence of splitting in the central terminal methyl peak suggests the emergence of a mixed [gel +  $l_o$ ] phase. At 313 K, when the sample is expected to be in the [ $l_d$  +  $l_o$ ] phase, the spectrum shows a wider distribution of splittings and an absence of central terminal methyl peak splitting, which indicates the presence of the fluid lamellar phase. Above 323 K the resolution of the spectrum increases, indicating that the system is in the fluid lamellar phase. These spectra are shown in Figure 3.7.

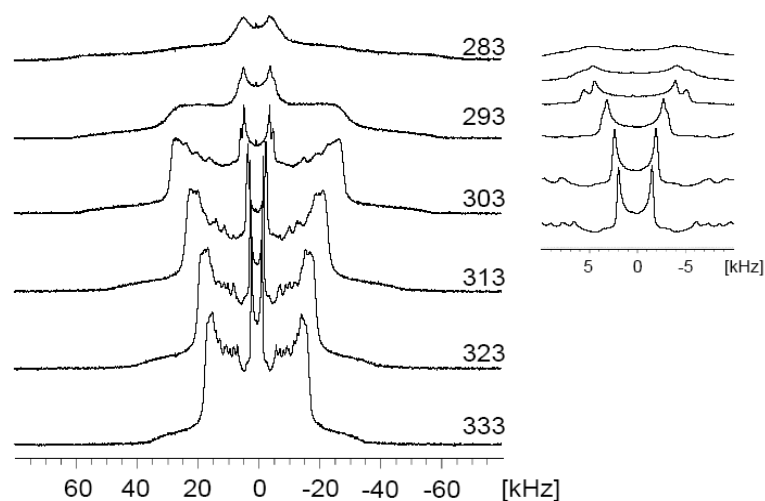


Figure 3.7.  $^2\text{H}$  NMR spectra of  $d_{62}$ -DPPC/cholesterol at temperatures ranging from 283 K to 333 K at 10 K intervals. The inset displays an expansion of the middle of 20 kHz of each spectrum

The  $^2\text{H}$  NMR spectrum of the sample of  $d_{62}$ -DPPC/cholesterol/Q shows gel phase spectra at 283 K, followed by the appearance of the [gel +  $l_o$ ] mixed phase at 293 K and 303 K. At 313 K an increased resolution indicates the appearance of the [ $l_d$  +  $l_o$ ] phase. From 323 K onwards the spectra are in the fluid lamellar phase. The spectra are shown in Figure 3.8.

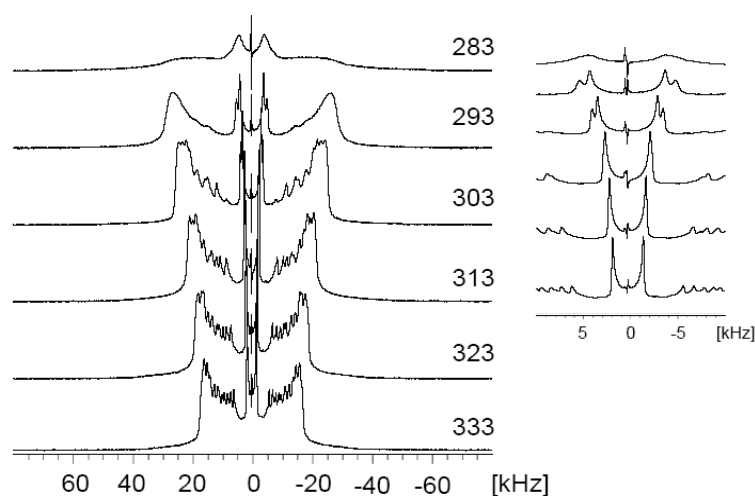
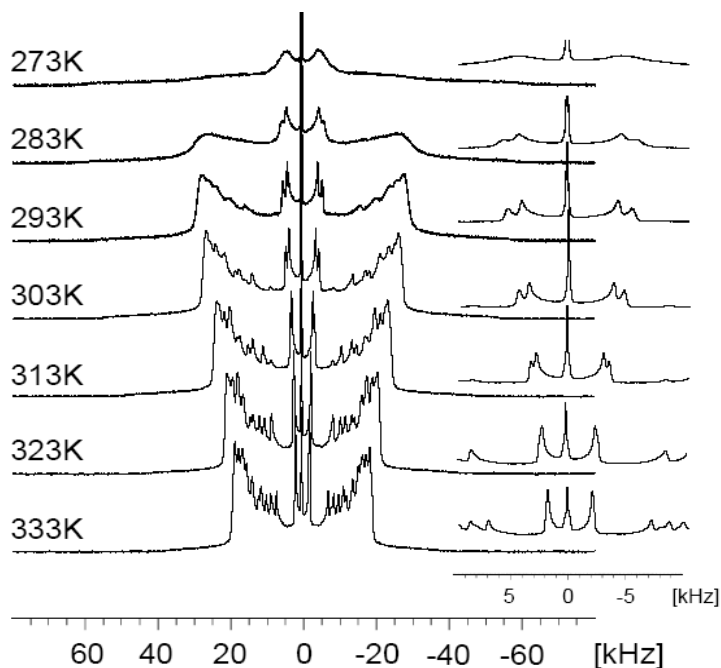


Figure 3.8.  $^2\text{H}$  NMR spectra of  $d_{62}$ -DPPC/cholesterol/Q at temperatures ranging from 283 K to 333 K at 10 K intervals. The inset displays an expansion of the middle of 20 kHz of each spectrum

The  $^2\text{H}$  NMR spectra of  $d_{62}$ -DPPC/cholesterol/LY show the presence of gel phase characteristics at 273 K, followed by the emergence of shoulders at 283 K, which indicates the existence of  $l_o$ -phase lipids (Figure 3.9). This corresponds with the presence of the  $l_o$  phase from 280 K to 325 K, as observed from the CTM splittings data.



*Figure 3.9.  $^2\text{H}$  NMR spectra of  $d_{62}$ -DPPC/cholesterol/LY at temperatures ranging from 273 K to 333 K in 10 K intervals. The inset displays an expansion of the middle of 20 kHz of each spectrum*

The  $^2\text{H}$  NMR spectra for the sample of  $d_{62}$ -DPPC/LY show the effect of LY on the bilayer (Figure 3.10). At 304 K and 305 K the spectrum shows the emergence of shoulders and more resolved peaks which might indicate a separate phase between the gel and fluid lamellar phases. The spectra show that the fluid lamellar phase transition occurs between 304 K and 309 K.

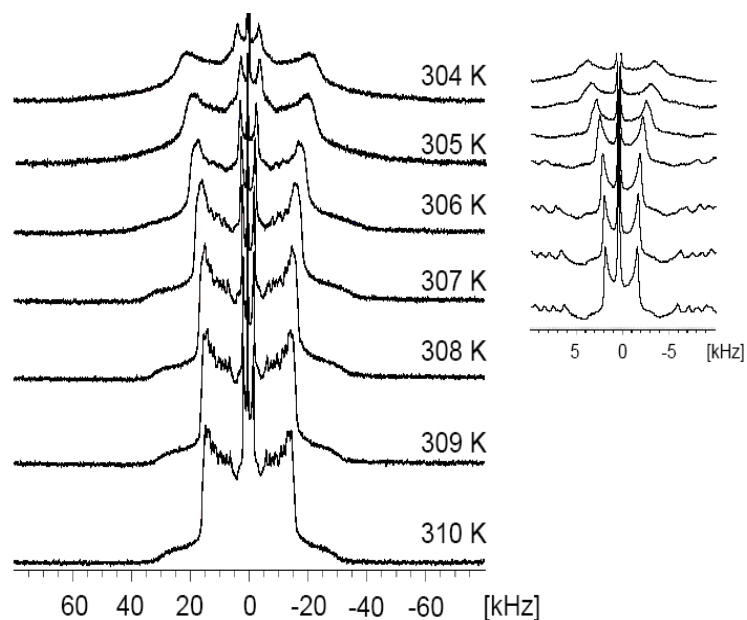
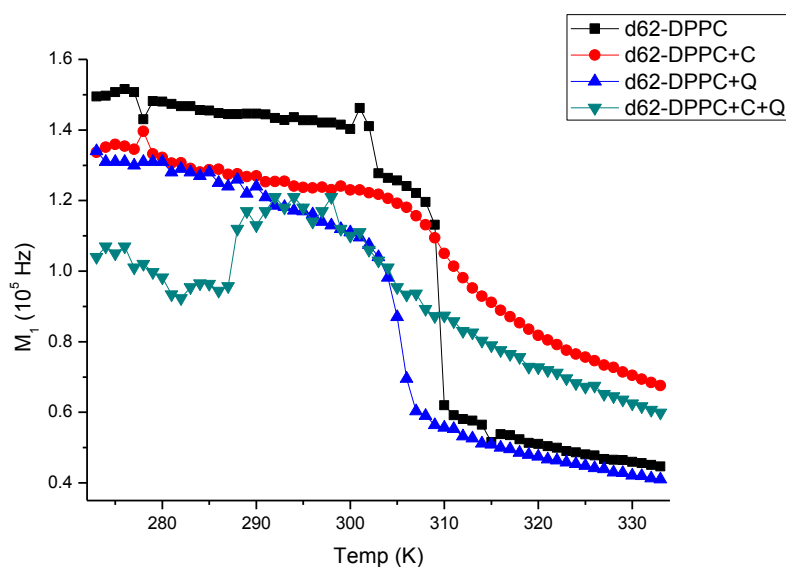


Figure 3.10.  $^2\text{H}$  NMR spectra of  $d_{62}$ -DPPC/LY at temperatures ranging from 304 K to 310 K at 1 K intervals, showing the gel-to-fluid lamellar phase transition. The inset displays an expansion of the middle of 20 kHz of each spectrum

$M_1$  data -  $M_1$  data obtained from deuterium NMR spectra of samples is shown in plots 3.1 (Q samples) and 3.2 (LY samples).



Plot 3.1 Comparison of  $M_1$  data for samples of  $d_{62}$ -DPPC (black squares),  $d_{62}$ -DPPC/Q (blue triangles),  $d_{62}$ -DPPC/cholesterol (red diamonds), and  $d_{62}$ -DPPC/cholesterol/Q (green triangles)

The main features of the plot of  $M_1$  for  $d_{62}$ -DPPC are the regions: 273 K to 300 K; 301 K to 309 K; and 310 K to 333 K. From 273 K to 300 K, a shallow negative slope indicates that the sample is in the gel ( $L_\beta$ ) phase. From 301 K to 303 K the negative gradient of the slope increases sharply, followed by another negative slope from 303 K to 309 K. The slope from 303 K to 309 K is attributed to the presence of another pre-fluid lamellar phase: the ripple ( $P_\beta'$ ) phase, in which the lipid molecules are tilted at an angle to the bilayer normal axis<sup>19, 31</sup>. The sharp decrease in gradient from 301 K to 303 K may be attributed to an additional sub-gel phase known as the tilted gel ( $L_\beta'$ ) phase, which has been shown to occur at  $\leq 301$  K; however, there is no further evidence from our studies to confidently assign this phase<sup>31, 32</sup>. The  $P_\beta'$  phase is then followed by the transition into the fluid lamellar ( $L_\alpha$ ) phase at 309/310 K. This is shown by a steep drop in  $M_1$  over a short, 1 K interval.

The  $M_1$  plot for the samples of  $d_{62}$ -DPPC only and  $d_{62}$ -DPPC/cholesterol match up well with those reported previously, although the  $M_1$  spectra reported for  $d_{62}$ -DPPC by Davis does not show the ripple phase as clearly as observed in Plot 3.1<sup>13, 19, 26</sup>. The smoothing effect observed on the addition of cholesterol also matches previous data<sup>13</sup>.

The addition of cholesterol to the  $d_{62}$ -DPPC bilayer produces some significant changes, most notably the disappearance of a steep gel-to-fluid lamellar phase transition. The plot of  $M_1$  shows a smooth curve which may be divided into three separate gradients, possibly delineating three phases or areas of phase coexistence. The areas of phase coexistence are found from 273 K to approximately 306 K; from approx. 306 K to approx. 318 K; and from approx. 318 K to 333 K. The phases were assigned according to previous phase diagrams of DPPC/20 mol% cholesterol, which gave the following phase areas: [gel +  $l_o$ ] phase coexistence from 303 K to 310 K; [ $l_d$  +  $l_o$ ] phase coexistence from 310 K to 316 K; and fluid lamellar phase from 316 K onwards<sup>13</sup>. The phases from the  $d_{62}$ -DPPC/cholesterol sample were therefore assigned as [gel +  $l_o$ ] phase coexistence, 273 K to approx. 306 K; [ $l_d$  +  $l_o$ ] phase coexistence from approx. 306 K to approx. 318 K; fluid lamellar phase from approx. 318 K to 333 K. The difference in transition temperatures may be due to the differences

between deuterated and protonated samples or due to the differences between methods of data analysis. From the  $M_1$  plot it is not possible to determine the temperature at which the [gel +  $l_o$ ] phase coexistence begins. The most important point to note is that the plot for this sample is dramatically different from the plots for  $d_{62}$ -DPPC and  $d_{62}$ -DPPC/Q, with regards to the steep gel-to-fluid lamellar phase transition observed for these samples. The addition of cholesterol leads to the phenomenon of phase coexistence, which removes the gel-to-fluid lamellar phase transition. Another important point to note is that  $M_1$  is lower in the gel/[gel +  $l_o$ ] phase than the values for the  $d_{62}$ -DPPC and  $d_{62}$ -DPPC/Q samples in this region, but highest overall in the fluid lamellar/[ $l_d$  +  $l_o$ ] phase.

The effect of cholesterol on a phospholipid bilayer has long been known to induce the appearance of the  $l_o$  phase, which has characteristics halfway between those of the gel phase and the  $l_d$ /fluid lamellar phase. Previous research has observed that the presence of cholesterol in liposomes of varying composition has removed the sharp gel-to-fluid phase transition, as seen in Plot 3.1<sup>13</sup>.

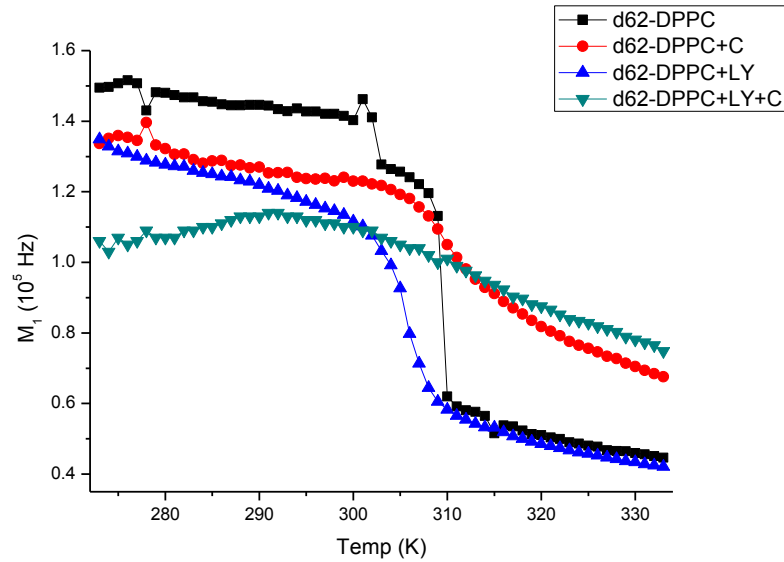
The addition of Q also results in some significant changes to the phase transition profile of  $d_{62}$ -DPPC. For the plot of  $M_1$  for  $d_{62}$ -DPPC/Q the main features are: 273 K to 303 K; 303 K to 307 K; and 307 K to 333 K. From 273 K to 303 K a shallow negative slope indicates that the sample is in the gel phase, which mirrors the phase transition profile of  $d_{62}$ -DPPC. Over the interval of 303 K to 307 K the sample undergoes a phase transition from the gel phase to the fluid lamellar phase, where it remains up to 333 K. There are several important points to note in comparison to the phase transition profile of  $d_{62}$ -DPPC alone. The first is that there is no evidence of the existence of the ripple phase, which is observed to occur in  $d_{62}$ -DPPC from 303 K to 309 K. The second is that the value of  $M_1$  is decreased in comparison to  $d_{62}$ -DPPC at the sub-fluid lamellar temperatures (from 273 K to 307 K). The values become similar in the fluid lamellar phase. The third important point to note is that the gel-to-fluid lamellar phase transition takes place over a wider temperature interval than for  $d_{62}$ -DPPC alone. In addition, the phase transition is complete at a lower temperature (307 K) for this sample than for  $d_{62}$ -DPPC (310 K). In the case of  $d_{62}$ -DPPC/Q it takes place over a range of 3 K, compared to 1 K for  $d_{62}$ -DPPC. From these three points it

can be theorised that the presence of Q has a disruptive effect on the  $d_{62}$ -DPPC bilayer. The relatively low value of  $M_1$  in the sub-fluid lamellar phases indicates that the bilayer has a lower distribution of both order parameters and quadrupolar splittings in this region than  $d_{62}$ -DPPC alone, which reflects greater disorder and fluidity. The presence of Q therefore has the effect of disrupting the rigidity of a gel-phase  $d_{62}$ -DPPC bilayer, possibly by intercalating with the phospholipid molecules. This also explains the lowering of the gel-to-fluid lamellar phase transition. The apparent disappearance of the ripple phase from the spectra of samples containing Q may be due to the presence of Q molecules in the bilayer preventing the lipids from adopting a tilted conformation.

The plot of  $M_1$  for  $d_{62}$ -DPPC/cholesterol/Q has a very different profile to those of the other samples. The main regions of interest are: 273 K to 278 K; 278 K to 288 K; 288 K to 298 K; 298 K to approx. 312 K; and approx. 312 K to 333 K. The assignment of phases relies on the assignments previously made for  $d_{62}$ -DPPC/Q and  $d_{62}$ -DPPC/cholesterol. The assignments obtained for  $d_{62}$ -DPPC/cholesterol showed that there is an undefined mixture of the gel and [gel +  $l_o$ ] phases until approx. 310 K, followed by the appearance of the [ $l_d$  +  $l_o$ ] phase coexistence from 310 K until 316 K, and the fluid lamellar phase from this temperature onwards. The  $d_{62}$ -DPPC/Q data showed that the presence of Q lowered the gel-to-fluid lamellar phase transition temperature by approx. 3 K. These data indicate that the region from 298 K to 312 K may be attributed to the [ $l_d$  +  $l_o$ ] mixed phase, followed by the fluid lamellar phase from 312 K onwards. Although the phases from 298 K onwards may be fairly confidently assigned, the phase behaviour of the sample below this temperature requires the addition of more data from different methods due to the unexpectedly low  $M_1$  values present in these regions.

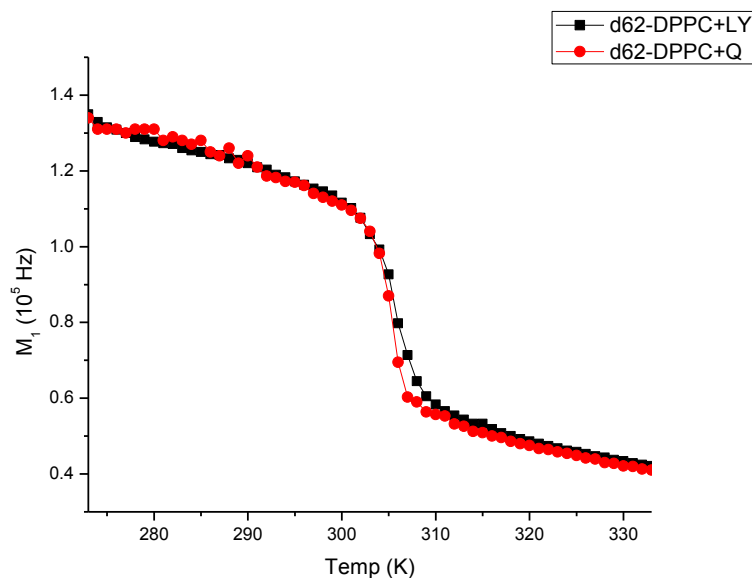
In comparison to the  $M_1$  plot of  $d_{62}$ -DPPC/cholesterol, it is clear that the addition of Q once again has a significant effect on the phase behaviour of the sample. The plots differ significantly from 273 K to 287 K with the appearance of the region of relatively low  $M_1$  values, and also differ in the region from 300 K to 305 K, with the disappearance of the 'hump' observed in the  $d_{62}$ -DPPC/cholesterol spectrum. Overall the  $M_1$  values are lower in the presence of

Q. Although the region from 273 K to 287 K could be assigned to an additional sub-gel phase, this is counter-intuitive to the high  $M_1$  values (and hence high order parameters) expected at these low temperatures. It has also not been observed to occur in any other system. The regions of the spectrum are assigned as: 273 K to 287 K, gel phase; 287 K to 298 K, [gel +  $l_o$ ] phase; 298 K to approx. 310 K, [ $l_d$  +  $l_o$ ] phase; and from approx. 310 K onwards, fluid lamellar phase.



*Plot 3.2 Comparison of  $M_1$  data for samples of  $d_{62}$ -DPPC (black squares),  $d_{62}$ -DPPC/LY (blue triangles),  $d_{62}$ -DPPC/cholesterol (red stars), and  $d_{62}$ -DPPC/cholesterol/LY (green triangles)*

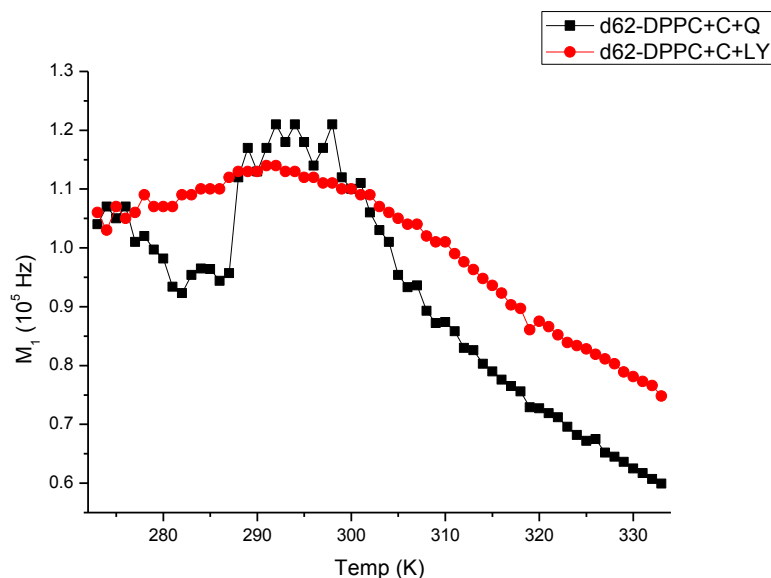
The main features of the plot of  $M_1$  for  $d_{62}$ -DPPC/LY are: 273 K to 303 K; 303 K to 309 K; and 309 K to 333 K. From 273 K to 303 K a shallow negative slope indicates that the sample is in the gel phase. Over the interval of 303 K to 309 K the sample undergoes a phase transition from the gel phase to the fluid lamellar phase, where it remains up to 333 K.



*Plot 3.3 Comparison of  $M_1$  data for samples of  $d_{62}$ -DPPC/Q (black squares) and  $d_{62}$ -DPPC/LY (red diamonds)*

A comparison of the  $M_1$  plots for  $d_{62}$ -DPPC/Q and  $d_{62}$ -DPPC/LY shows very little difference between the data; the only difference occurs during the gel-to-fluid lamellar phase transition, which takes place over a slightly longer temperature interval for LY than for Q (303 K to 309 K, rather than to 307 K). This result indicates that the presence of LY has a similar effect to the presence of Q on the bilayer; both drugs disrupt the bilayer and lower the gel-to-fluid lamellar phase transition temperature.

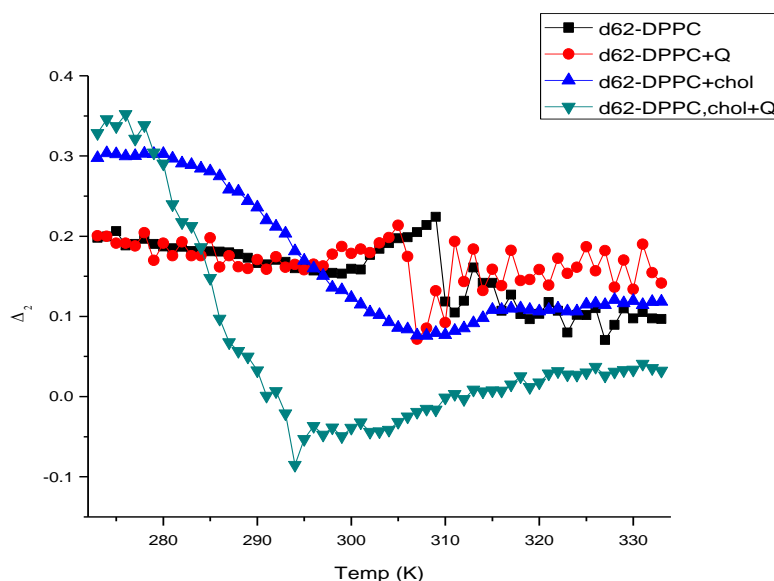
The main features of the plot of  $M_1$  for  $d_{62}$ -DPPC/cholesterol/LY are: 273 K to 292 K; 293 K to 305 K; and 306 K to 333 K. As for the previous plots of  $d_{62}$ -DPPC/cholesterol and  $d_{62}$ -DPPC/cholesterol/Q, it is divided up into three approximate areas with different gradients. The region from 293 K to 305 K is assigned to the  $[l_d + l_o]$  mixed phase, with the fluid lamellar phase from 306 K to 333 K. The  $[gel + l_o]$  phase may also be assigned to the region from 273 K to 293 K, although it is not possible to tell from this data where the gel phase coexistence with  $l_o$ -phase begins.



*Plot 3.4 Comparison of  $M_1$  data for samples of  $d_{62}$ -DPPC/cholesterol/Q (black squares) and  $d_{62}$ -DPPC/cholesterol/LY (red circles)*

The main difference between the plots for  $d_{62}$ -DPPC/cholesterol/Q and for  $d_{62}$ -DPPC/cholesterol/LY is the absence of the problematic region of low  $M_1$  values in a region normally associated with high  $M_1$  values (correlating to high order and parameter and quadrupolar splittings distributions), although the plot does show an increase in  $M_1$  from lower to higher temperatures before peaking. Since high order parameters and large splittings are expected for lower temperatures, producing high  $M_1$  values, it is possible that an experimental error has resulted in low  $M_1$  values at low temperatures.

$\Delta_2$  data -  $\Delta_2$  data obtained from deuterium NMR spectra of samples is shown in plots 3.5 (Q samples) and 3.6 (LY samples).



*Plot 3.5 Comparison of  $\Delta_2$  data for samples of  $d_{62}$ -DPPC (black squares),  $d_{62}$ -DPPC/Q (red circles),  $d_{62}$ -DPPC/cholesterol (blue triangles), and  $d_{62}$ -DPPC/cholesterol/Q (green triangles)*

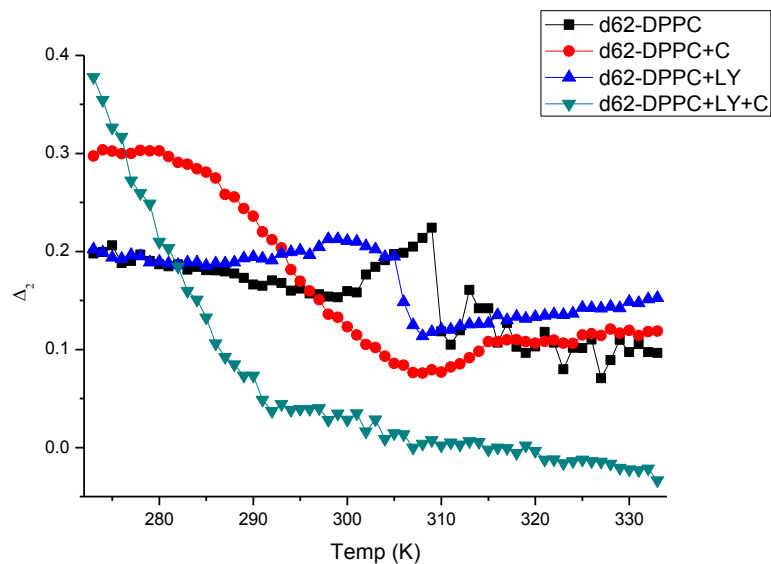
The main features of the plot of  $\Delta_2$  for the sample of  $d_{62}$ -DPPC are: a negative slope from 273 K to 302 K; a positive slope followed by a peak maximum at 309 K; and a steep drop from 309 K to 310 K, followed by a negative slope until 333 K. The maximum coincides with the gel-to-fluid lamellar phase transition temperature at 309 K, as shown in the  $M_1$  data. The data shows three clear phases: gel phase from 273 K to 302 K;  $P_{\beta}'$  phase from 303 K to 309 K; and finally the fluid lamellar phase from 310 K to 333 K. This correlates with the phase transitions assigned from the  $M_1$  plot for this sample.

The plot of  $\Delta_2$  for the sample of  $d_{62}$ -DPPC/Q comprises: a flat region extending from 273 K to 305 K; a peak maximum occurring at 305 K, which drops to a minimum at 307 K; and a flat region from 307 K to 333 K.  $\Delta_2$  is at a maximum at the point of phase coexistence (305 K). The  $\Delta_2$  profile resembles that of the  $d_{62}$ -DPPC system, although it is less clear.

In the  $\Delta_2$  plot of the sample of d<sub>62</sub>-DPPC/cholesterol there is no characteristic peak maximum followed by a trough as observed with the  $\Delta_2$  plot of d<sub>62</sub>-DPPC. The lowest point of the plot occurs at approx. 308 K, and from that point the slope increases positively until 315 K then takes the form of a plateau until 333 K. Phase transition data obtained from the plot of M<sub>1</sub> for this sample showed that the sample was in the fluid lamellar phase from approx. 316 K. The area of low  $\Delta_2$  plus a positive gradient, from 306 K to 315 K, corresponds to the region of [l<sub>d</sub> + l<sub>o</sub>] phase coexistence. The onset of the fluid lamellar phase corresponds with the appearance of the second plateau. Although this plot is not as clear, it is possible to see the same pattern as observed for the sample of d<sub>62</sub>-DPPC; the plot goes through a minimum point (at approx. 308 K) before rising to a higher point (at 315 K) and levelling off. The lack of the peak maximum (observed to occur at 309 K for d<sub>62</sub>-DPPC and immediately followed by a steep drop to a minimum point) may reflect the lack of a clear phase transition from the [l<sub>d</sub> + l<sub>o</sub>] phase coexistence to the fluid lamellar phase, which is also observed in the M<sub>1</sub> plot.

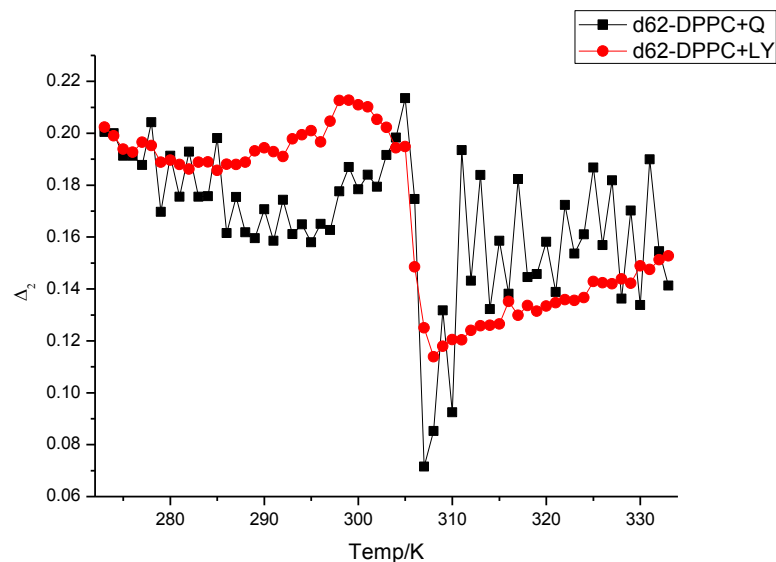
The plot of  $\Delta_2$  for the sample of d<sub>62</sub>-DPPC/cholesterol/Q does not appear to produce much useful information on the phase behaviour of the mixture. The only significant feature of the plot is a minimum at 304 K, which coincides with the middle of the temperature range at which the [l<sub>d</sub> + l<sub>o</sub>] phase is observed to occur in the M<sub>1</sub> plot (298 K to 312 K). It is not possible to derive any information from any other part of the plot.

The general shapes and features of the  $\Delta_2$  plot obtained for the sample of d<sub>62</sub>-DPPC agrees with previously published plots, although there is less variation between the values at different temperatures<sup>19</sup>. The general shape of the  $\Delta_2$  plot of d<sub>62</sub>-DPPC/cholesterol also matches a previously published plot by Davis *et al.*, although the concentration of cholesterol is higher (25 % vs. 20 %)<sup>32</sup>.



*Plot 3.6 Comparison of  $\Delta_2$  data for samples of  $d_{62}$ -DPPC (black squares),  $d_{62}$ -DPPC/LY (blue triangles),  $d_{62}$ -DPPC/cholesterol (red stars), and  $d_{62}$ -DPPC/cholesterol/LY (green triangles)*

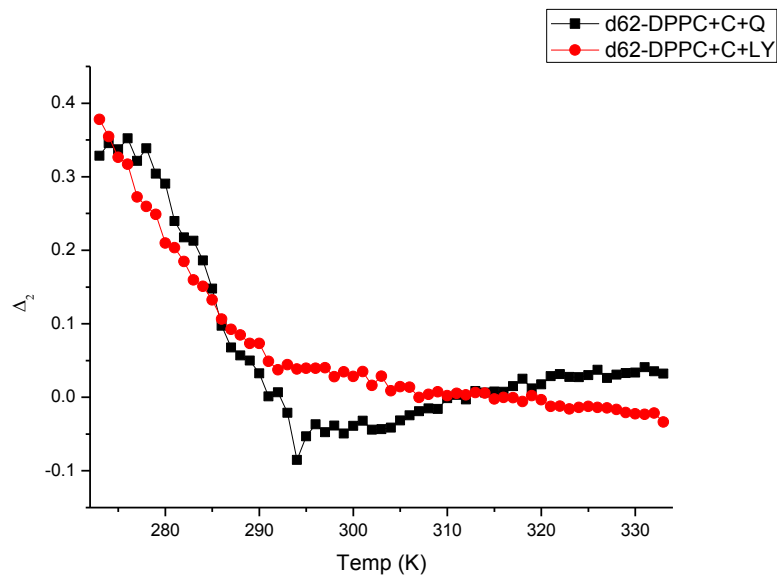
The plot of  $\Delta_2$  for the sample of  $d_{62}$ -DPPC/LY shows some similarities to that of the  $d_{62}$ -DPPC/Q, but is much clearer. The main features are a peak maximum at 298 K, followed by a negative slope leading to a point (at 305 K) followed immediately by a steep drop to a minimum point (308 K). The steep drop takes place over an interval of 3 K.



*Plot 3.7 Comparison of  $\Delta_2$  data for samples of  $d_{62}$ -DPPC/Q (black squares) and  $d_{62}$ -DPPC/LY (red circles)*

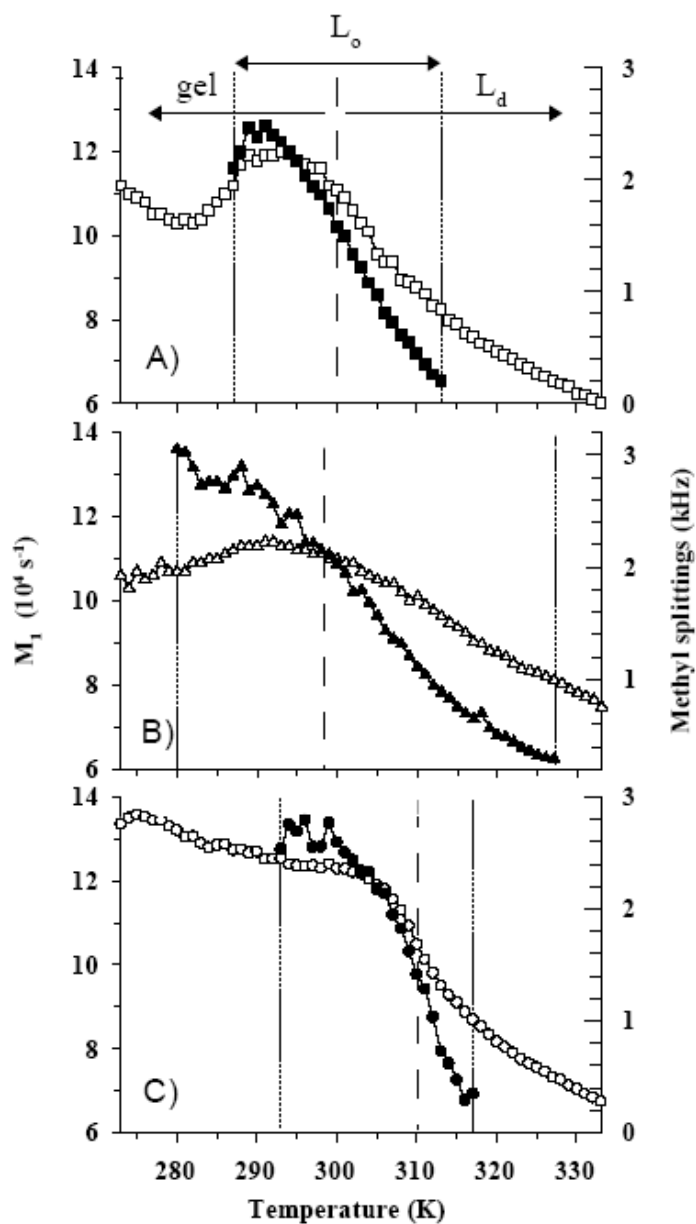
Analysis of the  $M_1$  data showed that the gel-to-fluid lamellar phase transition took place from 303 K to 309 K, followed by the fluid lamellar phase from 309 K onwards. The results found for  $\Delta_2$  (305 K to 308 K) follow these results closely. However the maximum point at 298 K occurs when the sample is in the gel phase, which may indicate the presence of a sub-gel phase previously unseen in the  $M_1$  data.

The plot of  $\Delta_2$  for the sample of  $d_{62}$ -DPPC/cholesterol/LY closely resembles that of the plot for  $d_{62}$ -DPPC/cholesterol/Q, and also gives no clear information about the phase behaviour of the sample. However it does succeed in showing that the plot obtained for the sample of  $d_{62}$ -DPPC/cholesterol/Q was not an anomaly, and that both mixtures containing  $d_{62}$ -DPPC, cholesterol, and drug have the same effect on the calculation and subsequent plotting of  $\Delta_2$  values.



*Plot 3.8 Comparison of  $\Delta_2$  data for samples of  $d_{62}$ -DPPC/cholesterol/Q (black squares) and  $d_{62}$ -DPPC/cholesterol/LY (red stars)*

*Central terminal methyl splitting data* - Central terminal methyl (CTM) splitting data for the samples containing cholesterol is shown in Plot 3.9 in comparison with the corresponding  $M_1$  data.



Plot 3.9 Central terminal methyl splitting data (right-hand axis, closed symbols) and  $M_1$  data (left-hand axis, open symbols for samples of  $d_{62}$ -DPPC/cholesterol/Q (A),  $d_{62}$ -DPPC/cholesterol/LY (B), and  $d_{62}$ -DPPC/cholesterol (C). The phase transition boundaries are also denoted for  $l_o$  (between the dotted lines) and gel/ $l_d$  (between the dashed lines)

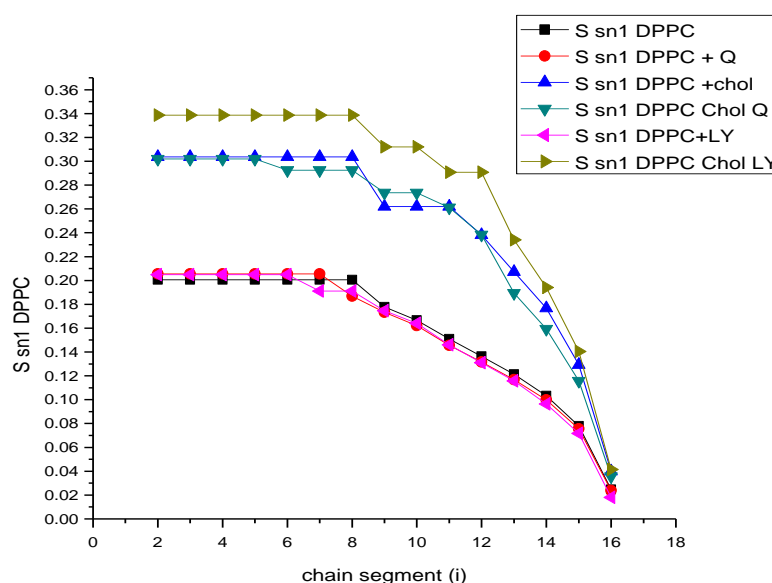
The central terminal methyl (CTM) splitting peak data for the sample of  $d_{62}$ -DPPC/cholesterol shows that the splitting appears at a temperature of 293 K and disappears at a temperature of 317 K, which indicates that the  $l_o$  phase emerges at 293 K (and possibly lower, as it becomes more difficult to analyse the data for

splittings as temperature and resolution decrease), and that the sample is in the fluid lamellar phase from 317 K onwards. This correlates closely to the phase transition temperatures obtained from the  $M_1$  data, which found that the sample was in the fluid lamellar phase from 318 K onwards. It also provides a temperature for the emergence of the mixed [gel +  $l_o$ ] at 293 K, which was not obtained from the  $M_1$  data.

The CTM splitting peak data for the sample of  $d_{62}$ -DPPC/cholesterol/Q shows that the splitting appears at a temperature of 287 K and disappears at a temperature of 313 K. Interestingly 287 K, the temperature at the start of the [gel +  $l_o$ ] phase coexistence, is also the temperature at which the region of low  $M_1$  transitions into the next region of higher  $M_1$  (plot 3.9). This indicates that the low- $M_1$  region may be attributed to the gel phase. The end temperature of 313 K also correlates closely with the start of the fluid lamellar phase indicated by the  $M_1$  results (312 K). This temperature is lower than the start of the fluid lamellar phase found for the sample of  $d_{62}$ -DPPC/cholesterol (318 K), which agrees with the theory that the presence of Q lowers the temperature of the start of the fluid lamellar phase.

The CTM splitting peak data for the sample of  $d_{62}$ -DPPC/cholesterol/LY shows that splitting appears at a temperature of 280 K and disappears at a temperature of 327 K, which indicates a much wider  $l_o$  phase range than observed for the sample containing Q.

Order parameter data - Order parameter data for all samples is shown in Plot 3.10.



Plot 3.10 Comparison of order parameter data for samples of  $d_{62}$ -DPPC (black squares),  $d_{62}$ -DPPC/Q (red diamonds),  $d_{62}$ -DPPC/cholesterol (blue triangles),  $d_{62}$ -DPPC/cholesterol/Q (green triangles),  $d_{62}$ -DPPC/LY (pink triangles), and  $d_{62}$ -DPPC/cholesterol/LY (mustard triangles), all at 323 K

The order parameter profile for the sample of  $d_{62}$ -DPPC shows the profile expected of a lipid in the fluid lamellar phase. The lowest order is found at the end of the sn-1 chain, C16. Order parameter then increases towards the centre of the chain, reaching a maximum value at C8, before levelling off between C8 and C2. The order parameter profile for the sample of  $d_{62}$ -DPPC/Q is almost identical to that of  $d_{62}$ -DPPC, indicating that in the fluid lamellar phase, the presence of Q does not have much of an effect on the dynamics of the bilayer.

The order parameter profiles for the samples of  $d_{62}$ -DPPC/cholesterol and  $d_{62}$ -DPPC/cholesterol/Q are also almost identical, confirming that the presence of Q does not have much of an effect when the samples are in the fluid lamellar phase. The order parameter profiles for the cholesterol-containing samples display increased order parameter values relative to the samples without cholesterol, which is due to the increased rigidity of lipid bilayers containing intercalated

cholesterol molecules. The order parameter profile for the sample of  $d_{62}$ -DPPC/LY is almost identical to its Q-containing counterpart. The profile for the sample of  $d_{62}$ -DPPC/cholesterol/LY is more notable in that it displays the highest order overall, indicating that the presence of LY together with cholesterol has a significant effect on the order of the bilayer.

*DSC data* - The DSC scan for the sample of  $d_{62}$ -DPPC has two significant peaks, one at 304.3 K and one at 311.8 K (Figure 3.11). These correspond to the onset of the ripple phase, at 303 K, and the fluid lamellar phase, at 310 K, as calculated from the  $M_1$  and  $\Delta_2$  data.

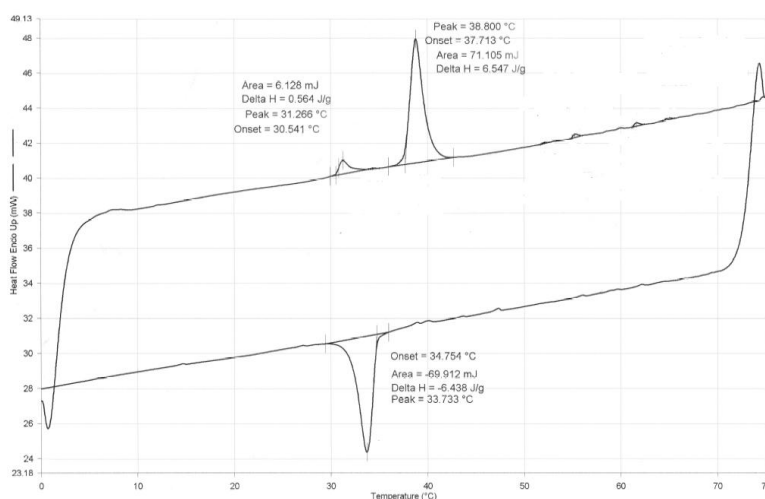


*Figure 3.11. DSC scan of a sample of  $d_{62}$ -DPPC, showing the ripple phase (304.4 K) and fluid lamellar phase (310 K) peaks*

The scan for the sample of  $d_{62}$ -DPPC + Q shows a significant difference from that of the sample of  $d_{62}$ -DPPC. The two separate peaks denoting the ripple and fluid lamellar phase transitions are replaced by a single elongated peak at 307.6 K, with an onset of 302 K. This peak corresponds to the start of the elongated transition phase at 303 K, and the start of the fluid lamellar phase at 307 K. The difference between the scans of  $d_{62}$ -DPPC and  $d_{62}$ -DPPC + Q indicates that the ripple phase does not appear in the Q-containing sample. The scan is shown in Figure 3.12.

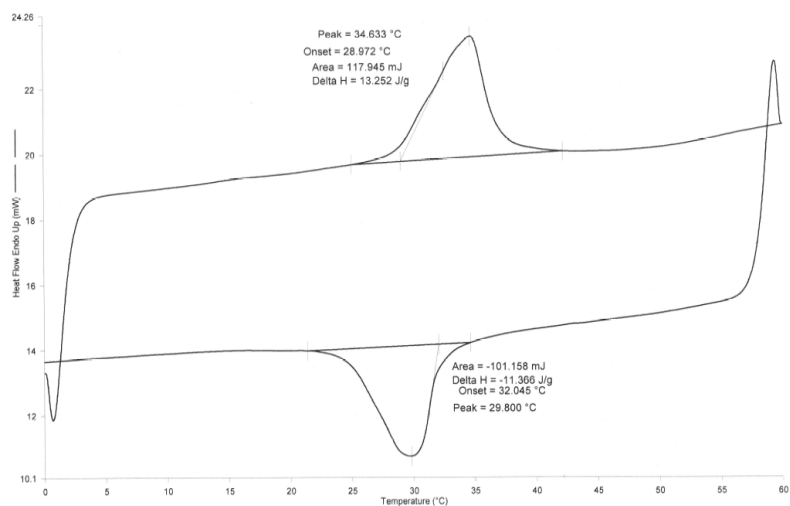


Figure 3.12. DSC scan of a sample of  $d_{62}$ -DPPC/Q, showing a wide peak at 307.6 K with an onset of 302 K

The scan for the sample of  $d_{62}$ -DPPC + Chol also shows a single peak, with an onset of 306.3 K, corresponding to the start of the  $[l_d + l_o]$  phase; a peak centre at 310.6 K, corresponding to the centre of the  $[l_d + l_o]$  phase; and the end of the peak at approx. 320 K, which corresponds to the end of the  $[l_d + l_o]$  and the beginning of the fluid lamellar phase. The scan for this sample is shown in Figure 3.13.

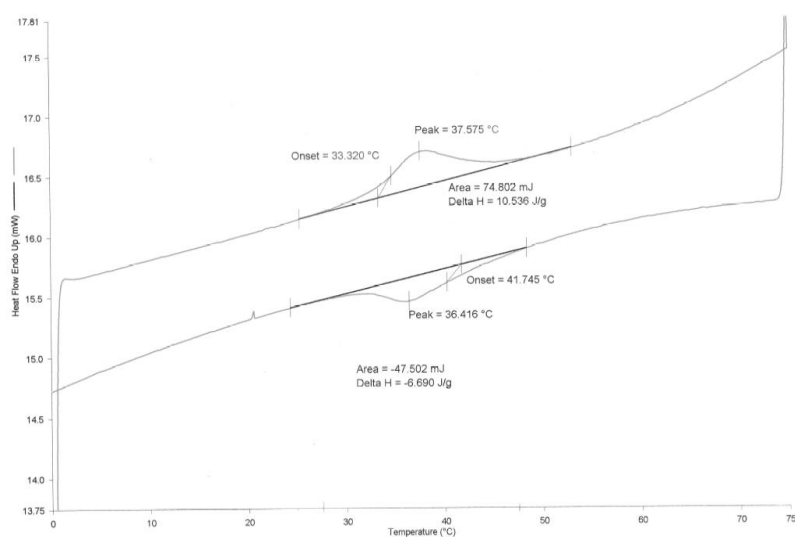
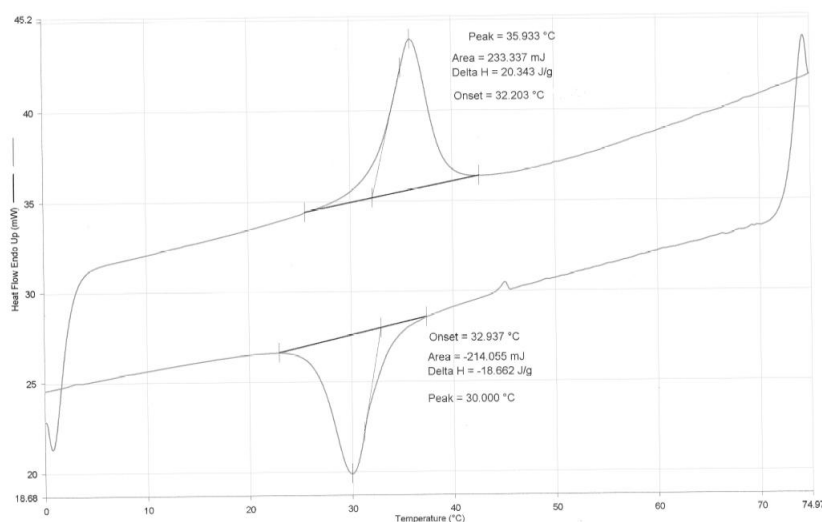


Figure 3.13. DSC scan of a sample of  $d_{62}$ -DPPC/cholesterol, showing a wide peak at 310.6 K with an onset of 306.3 K

The scan for the sample of  $d_{62}$ -DPPC + LY shows a single peak with an onset of 305.2 K and a peak centre at 308.9 K (Figure 3.14). These temperatures correspond to the start of the elongated transition phase (303 K), and the start of the fluid lamellar phase at 309 K.



*Figure 3.14. DSC scan of a sample of  $d_{62}$ -DPPC/LY, showing a peak at 308.9 K with an onset of 305.32 K*

## Part 5. Conclusion

The data obtained for the sample of  $d_{62}$ -DPPC indicates that it is in the gel phase until 303 K. From 303 K to 309 K it is believed to be in the ripple phase, and from 310 K onwards it adopts the fluid lamellar phase. The phase transition temperatures are consistent for all datasets, with minor variations found in the case of  $\Delta_2$ , which may be due to the difficulty of visually analysing the data. The order parameter data is consistent with the assumption that the sample should be in the fluid lamellar phase at 323 K. Visual analysis of the spectra also agrees with the results, with the gel phase observed up to a temperature of 298 K, followed by the ripple phase from 303 K to 308 K, and the fluid lamellar phase from 313 K onwards. Previously reported phase diagrams for DPPC give a ripple phase-to-fluid lamellar phase transition temperature of 315 K; ripple phase from 306 K to 315 K; and the gel phase below 306 K, in the case of protonated DPPC, and temperatures of 313 K for the start of the fluid lamellar phase, 301 K

for the start of the ripple phase, and gel phase below 301 K for deuterated samples<sup>4, 12, 19</sup>.

The addition of 20 mol% cholesterol is expected to induce the formation of the liquid-ordered phase, and this is supported by the data generated for the sample of  $d_{62}$ -DPPC/cholesterol. The  $M_1$  data showed three gradual phase transitions, assigned to the [gel +  $l_o$ ] phase (273 K to 306 K), [ $l_o$  +  $l_d$ ] phase (306 K to 318 K), and fluid lamellar phase (318 K to 333 K). These transition temperatures are only approximate due to the lack of clear-cut phase transitions in the presence of cholesterol. The  $\Delta_2$  data also shows evidence of possible phases, although it is not as clear to see as for the sample of  $d_{62}$ -DPPC.

Although the  $M_1$  and  $\Delta_2$  data cannot be used to ascertain the start of the [gel +  $l_o$ ] phase, the CTM splitting data gives a temperature of 293 K for the start of this phase, ending at 317 K. Since the temperature of the start of the fluid lamellar phase is so similar to the temperature found using the  $M_1$  data (318 K), it can be assumed that this is a good estimate of the start of the [gel +  $l_o$ ] phase. However, since the resolution of the CTM splitting decreases with temperature, it may be possible that the start temperature of this phase is lower than stated. Visual analysis of the spectra shows the emergence of shoulders characteristic of the mixed [gel +  $l_o$ ] phase at 288 K, and indicated that the fluid lamellar phase starts at 318 K. The DSC results cannot be used to clarify the start temperature of the [gel +  $l_o$ ] phase, as the peak only shows the start of the [ $l_d$  +  $l_o$ ] and fluid lamellar phases. The exact transition temperatures of the phases in this sample may be clarified in further work by using additional techniques such as X-ray scattering, which measures bilayer thickness, to provide further evidence.

The addition of Q to the  $d_{62}$ -DPPC bilayer has more of a profound effect than expected. The  $M_1$  data shows that the presence of Q both elongates the gel-to-fluid lamellar phase transition and lowers the start temperature of this transition, as well as removing the ripple phase. The gel-to-fluid lamellar phase transition begins at a temperature approx. 6 K lower than that of  $d_{62}$ -DPPC's ripple phase-to-fluid lamellar phase transition (303 K versus 309 K), and takes place over a range of 4 K (instead of over 1 K). There is also no evidence of the formation of

an  $l_o$  phase, which might be induced by the phase separation of the Q molecules. The  $\Delta_2$  data is very unclear, but a pattern can be discerned which follows the characteristic plot of trough-peak-trough. The order parameter data for this sample, and for the sample containing LY, shows that the addition of agonist does not have much of an effect on the profile of  $d_{62}$ -DPPC only, indicating that the overall order parameter in the fluid lamellar phase does not change significantly in the presence of agonist. Data derived from visual analysis and DSC confirm the gel-to-fluid lamellar phase transition temperatures as described.

The addition of LY to the bilayer also has a significant effect on the phase behaviour. The  $M_1$  data shows that the gel-to-fluid lamellar phase transition starts at 303 K (the same temperature as Q), but takes place over a range of 6 K. Interestingly, further research carried out by Windle, Buchoux and Lorch (unpublished data) suggests  $l_o$ -phase formation at a temperature of 306 K in this sample, as shown by CTM splitting data. This may suggest phase separation of the LY molecules, possibly due to the relative locations and orientations of these molecules (as discussed in Chapter 4). The widened gel-to-fluid lamellar phase transition, from 303 K to 309 K, may be mirrored by the main features of the  $\Delta_2$  data, which show a negative slope from 305 K to 308 K.

For both agonists, the addition of cholesterol mirrors the typical profile for a sample of DPPC/cholesterol at higher temperatures, but departs from this behaviour at lower temperatures. In the case of the  $M_1$  data, both agonists display an increase in  $M_1$  before the start of  $l_o$  phase onset (which occurs at 287 K for Q and 280 K for LY, according to CTM splitting data). The region of low  $M_1$  for Q lasts from 273 K to 277 K; from 277 K to 278 K there is significant increase in the value of  $M_1$ , which corresponds exactly to the start of the mixed [gel +  $l_o$ ] phase. The change in  $M_1$  for LY is less dramatic but still significant. It is possible that there is an additional sub-gel phase which accounts for the region of low  $M_1$  at these low temperatures, although lipid phases at these temperatures are expected to produce higher  $M_1$  values due to increased order. The results from the CTM splittings data show a significant increase in the temperature range of the  $l_o$  phase for LY in comparison to Q; the range has expanded from 286 K to 310 K (Q), to 280 K to 325 K (LY). This suggests that LY has a much

greater effect on the bilayer than Q, possibly due to its orientation in the bilayer. The order parameter data shows a much higher order overall for the sample of d<sub>62</sub>-DPPC/cholesterol/LY than for any of the other samples; the sample is expected to be in a mixed l<sub>o</sub> phase at 323 K, which accounts for the increased order.

In conclusion, the addition of agonists to d<sub>62</sub>-DPPC bilayers with and without cholesterol has marked effects on the physical properties of the bilayer. The addition of Q, a relatively small molecule which orients parallel to the bilayer normal, thereby minimising disruption, shifts the start of the gel-to-fluid lamellar phase transition lower by 6 K, widens the temperature range over which the transition takes place, and removes evidence of the pre-transition ripple phase. The addition of a larger agonist molecule, LY, which orients perpendicular to the bilayer, also lowers the phase transition temperature and widens it by a greater amount. LY also removes the ripple phase and possibly induces the presence of the l<sub>o</sub> phase in the absence of cholesterol. In the presence of cholesterol, unidentified sub-gel phases are observed at low temperatures. The sample of cholesterol with LY also has a much larger l<sub>o</sub> phase range when compared to samples containing cholesterol alone and cholesterol with Q. These results show that the addition of molecules such as agonists or other drugs may have significant, unpredictable effects on a lipid bilayer.

## Part 6. References

1. Bagatolli, L. A.; Kumar, P. B. S., Phase behavior of multicomponent membranes: Experimental and computational techniques. *Soft Matter* **2009**, *5*, 3234-3248.
2. Fidorra, M.; Duelund, L.; Leidy, C.; Simonsen, A. C.; Bagatolli, L. A., Absence of fluid-ordered/fluid-disordered phase coexistence in ceramide/POPC mixtures containing cholesterol. *Biophys. J.* **2006**, *90*, (12), 4437-4451.
3. Mills, T. T.; Tristram-Nagle, S.; Heberle, F. A.; Morales, N. F.; Zhao, J.; Wu, J.; Toombes, G. E. S.; Nagle, J. F.; Feigenson, G., Liquid-liquid domains in bilayers detected by wide angle x-ray scattering. *Biophys. J.* **2008**, *95*, (2), 682-690.

4. Karmakar, S.; Raghunathan, V. A.; Mayor, S., Phase behaviour of dipalmitoyl phosphatidylcholine (DPPC)-cholesterol membranes. *J. Phys.: Condens. Matter* **2005**, *17*, S1177-S1182.
5. Zhao, J.; Wu, J.; Heberle, F. A.; Mills, T. T.; Klawitter, P.; Huang, G.; Costanza, G.; Feigenson, G., Phase studies of model biomembranes: Complex behavior of DSPC/DOPC/cholesterol. *Biochim. Biophys. Acta* **2007**, *1768*, 2764-2776.
6. Dietrich, C.; Bagatolli, L. A.; Volovyk, Z. N.; Thompson, N. L.; Levi, M.; Jacobson, K.; Gratton, E., Lipid rafts reconstituted in model membranes. *Biophys. J.* **2001**, *80*, 1417-1428.
7. Veatch, S.; Keller, S. L., Seeing spots: Complex phase behavior in simple membranes. *Biochim. Biophys. Acta* **2005**, *1746*, 172-185.
8. Heberle, F. A.; Buboltz, J. T.; Stringer, D.; Feigenson, G., Fluorescence methods to detect phase boundaries in lipid bilayer mixtures. *Biochim. Biophys. Acta* **2005**, *1746*, 186-192.
9. Polozov, I. V.; Gawrisch, K., Characterization of the liquid-ordered state by proton MAS NMR. *Biophys. J.* **2006**, *90*, (6), 2051-2061.
10. Krivanek, R.; Okoro, L.; Winter, R., Effect of cholesterol and ergosterol on the compressibility and volume fluctuations of phospholipid-sterol bilayers in the critical point region: A molecular acoustic and calorimetric study. *Biophys. J.* **2008**, *94*, (9), 3538-3548.
11. McMullen, T. P. W.; McElhaney, R. N., New aspects of the interaction of cholesterol with dipalmitoylphosphatidylcholine bilayers as revealed by high-sensitivity differential scanning calorimetry. *Biochim. Biophys. Acta* **1995**, *1234*, 90-98.
12. Huang, T.-H.; Lee, C. W. B.; Das Gupta, S. K.; Blume, A.; Griffin, R. G., A  $^{13}\text{C}$  and  $^2\text{H}$  nuclear magnetic resonance study of phosphatidylcholine/cholesterol interactions: Characterization of liquid-gel phases. *Biochem.* **1993**, *32*, 13277-13287.
13. Vist, M. R.; Davis, J. H., Phase equilibria of cholesterol/dipalmitoylphosphatidylcholine mixtures:  $^2\text{H}$  nuclear magnetic resonance and differential scanning calorimetry. *Biochem.* **1990**, *29*, (2), 451-464.

14. Berger, M.; Gray, J. A.; Roth, B. L., The expanded biology of serotonin. *Ann. Rev. Med.*, **2009**, 60, 355-366.
15. Alberts, B.; Bray, D.; Lewis, J., Raff, M., Roberts, K.; Watson, J. D., In *Molecular Biology of the Cell*, 2 ed.; Garland Publishing, Inc.: New York, 1989; p 1093
16. Pytliak, M.; Vargová, V.; Mechírová, V., Felšöci, M., Serotonin receptors - From molecular biology to clinical applications. *Physiol. Res.* **2011**, 60, 15-25
17. Nichols, D. E.; Nichols, C. D., Serotonin receptors. *Chem. Rev.* **2008**, 108, 1614-1641
18. Lopez, J. J.; Lorch, M., Location and orientation of serotonin receptor 1a agonists in model and complex lipid membranes. *J. Biol. Chem.* **2008**, 283, (12), 7813-7822.
19. Davis, J. H., Deuterium magnetic resonance study of the gel and liquid crystalline phases of dipalmitoyl phosphatidylcholine. *Biophys. J.* **1979**, 27, 339-358.
20. Bartels, T.; Lankalapalli, R. S.; Bittman, R.; Beyer, K.; Brown, M. F., Raftlike mixtures of sphingomyelin and cholesterol investigated by solid-state  $^2\text{H}$  NMR spectroscopy. *J. Am. Chem. Soc.* **2008**, 130, 14521-14532.
21. Davis, J. H.; Clare, D. M.; Hodges, R. S.; Bloom, M., Interaction of a synthetic amphiphilic polypeptide and lipids in a bilayer structure. *Biochem.* **1983**, 22, (23), 5298-5305.
22. Lafleur, M.; Cullis, P. R.; Fine, B.; Bloom, M., Comparison of the orientational order of lipid chains in the  $L_a$  and  $H_{II}$  phases. *Biochem.* **1990**, 29, (36), 8325-8333.
23. Otten, D.; Loebbecke, L.; Beyer, K., Stages of the bilayer-micelle transition in the system phosphatidylcholine- $\text{C}_{12}\text{E}_8$  as studied by deuterium- and phosphorus-NMR, light scattering, and calorimetry. *Biophys. J.* **1995**, 68, 584-597.
24. Paddy, M. R.; Dahlquist, F. W.; Davis, J. H.; Bloom, M., Dynamical and temperature-dependent effects of lipid-protein interactions. Application of deuterium nuclear magnetic resonance and electron paramagnetic resonance spectroscopy to the same reconstitutions of cytochrome *c* oxidase. *Biochem.* **1981**, 20, 3152-3162.

25. Shaikh, S. R.; Cherezov, V.; Caffrey, M.; Stillwell, W.; Wassall, S. R., Interaction of cholesterol with a docosahexaenoic acid-containing phosphatidylethanolamine: Trigger for microdomain/raft formation? *Biochem.* **2003**, 42, 12028-12037.
26. Reinl, H.; Brumm, T.; Bayerl, T. M., Changes of the physical properties of the liquid-ordered phase with temperature in binary mixtures of DPPC with cholesterol. *Biophys. J.* **1992**, 61, 1025-1035.
27. Sankaram, M. B.; Thompson, T. E., Modulation of phospholipid acyl chain order by cholesterol. A solid-state  $^2\text{H}$  nuclear magnetic resonance study. *Biochem.* **1990**, 29, (47), 10676-10684.
28. Buchoux, S. *NMR-Depaker 1.0 RC1*.
29. Scheidt, H. A.; Huster, D.; Gawrisch, K., Diffusion of cholesterol and its precursors in lipid membranes studied by  $^1\text{H}$  PFG MAS NMR. *Biophys. J.* **2005**, 89, 2504-2512.
30. Soubias, O.; Jolibois, F.; Reat, V.; Milon, A., Understanding sterol-membrane interactions, part II: Complete  $^1\text{H}$  and  $^{13}\text{C}$  assignments by solid-state NMR spectroscopy and determination of the hydrogen-bonding partners of cholesterol in a lipid bilayer. *Chem. Eur. J.* **2004**, 10, 6005-6014.
31. Jones, J. W.; Lue, L.; Saiani, A.; Tiddy, G. J. T., Density measurements through the gel and lamellar phase transitions of di-tetradecanoyl- and di-hexadecanoyl-phosphatidylcholines: Observation of slow relaxation processes and mechanisms of phase transitions. *Liq. Cryst.* **2005**, 32, (11-12), 1465-1481.
32. Davis, J. H.; Clair, J. J.; Juhasz, J., Phase equilibria in DOPC/DPPC- $\text{d}_{62}$ /cholesterol mixtures. *Biophys. J.* **2009**, 96, (2), 521-539.

## **Chapter 4: Analysis of Drug Localisation and Orientation in a Model Membrane by NMR Spectroscopic Methods**

### **Part 1. Introduction**

The interactions of a foreign molecule, such as ethanol or pharmacological drugs, with the cell membrane depend on their molecular structures and chemical properties. The interactions with the membrane vary; some drugs interact with protein receptors on the surface of the cell, initiating a cascade of events within the cell's interior such as enzyme activation, enzyme inhibition, or protein synthesis; some diffuse through the cell membrane in order to interact directly with biological macromolecules inside the cell; and some interact with the cell membrane itself, altering properties such as membrane composition and curvature<sup>1</sup>. Drug design and synthesis is a costly and time-intensive process, but it may be partly facilitated by studying the effects of existing drugs on the membrane. The interactions of a variety of drugs with the cell membrane have been studied; a comprehensive list of such studies has been compiled by Lucio *et al*<sup>1</sup>.

A variety of methods have been used to investigate the drug/membrane interaction, including water/octanol partitioning, fluorescence experiments, DSC and X-ray scattering<sup>1</sup>. However the technique of most relevance to this research is NMR spectroscopy; in particular, solid-state NMR, which is well-suited to the analysis of model membranes<sup>1</sup>.

Kuroda *et al.* used deuterium NMR to analyse the orientations and locations of the anaesthetic drugs benzocaine and butamben, using lipid suspensions of mixed compositions, and discovered that the locations of the drugs changed in the presence of cholesterol<sup>2</sup>. Gaede and Gawrisch used pulsed field gradient (PFG) MAS-NMR to investigate the diffusion rate of ibuprofen in unilamellar liposomes<sup>3</sup>. A variety of studies have used the technique of generating cross-relaxation rates from NOESY experiments to indicate the probability of contact between lipid and drug molecules, thereby showing the location and orientation of drug molecules relative to the lipid bilayer. Cross-relaxation rate experiments

have been used to determine the locations and orientations of ethanol, flavonoids, tryptophan, multi-drug transporter substrate molecules (including antibiotics such as ampicillin and penicillin G), and serotonin receptor agonist drugs<sup>4-9</sup>. Holte and Gawrisch showed that ethanol locates in the interfacial region of the bilayer<sup>4</sup>, which was also found to occur for various flavonoid molecules<sup>6</sup> and tryptophan<sup>7</sup>. The interfacial region was also found to interact strongly with the aromatic moieties of various multi-drug transporter substrates<sup>8</sup>. Scheidt and Huster carried out a comprehensive review of the research into the interactions of various small-molecule species with phospholipid bilayers using NOESY cross-relaxation rates, which also includes interactions between peptides and fluorescent dyes with the bilayer<sup>10</sup>. The studies carried out showed that the various compounds analysed tended to locate mostly in the interface region of the bilayer due to their chemical properties. The interfacial region allows contact with both the apolar (the top of the acyl chains) and polar (the charged headgroup) regions, and allows the formation of hydrogen bonds due to the presence of the carbonyl oxygen atoms in the glycerol group. This allows a variety of compounds with different chemical compositions to adopt positions in this part of the bilayer.

Eisensamer *et al.* found that the serotonin receptor protein co-localised with certain serotonin receptor agonist drugs in low buoyant density (LBD) fractions of cell membranes<sup>11</sup>. This is the fraction closely associated with cholesterol-enriched lipid domains, thus implying that both the serotonin receptor protein and their agonist drugs are co-localised within lipid domains. It has been suggested that the co-localisation of receptor proteins with agonist drugs may facilitate or enhance signal transduction by decreasing the distance between drug and receptor, and increasing the probability of the drug coming into contact with the membrane-based receptor protein<sup>12</sup>.

The study carried out by Lorch and Lopez used MAS NOESY cross-relaxation rates and induced chemical shifts to analyse the locations of serotonin-receptor agonist drugs in relation to a DOPC or brain lipids bilayer, where the brain lipids contained various phospholipids together with cholesterol<sup>9</sup>. Induced chemical shift data showed that the serotonin-receptor agonist drugs interacted with

cholesterol more strongly than with phospholipids, which agrees with the hypothesis that certain drugs co-localise together with their receptors inside cholesterol-enriched lipid domains<sup>9</sup>.

## **Part 2. Aims**

The aim of this research is to expand on the results found by Lorch and Lopez<sup>9</sup> for the serotonin-agonist receptor drugs, quipazine (Q) and LY-163,165 (LY), using three-component model membranes containing a chain-deuterated phospholipid, cholesterol, and drug, and provide further evidence for the hypothesis that certain drugs co-localise with their receptor proteins in cholesterol-enriched lipid domains. The use of chain-deuterated phospholipids enables the appearance and analysis of drug-cholesterol cross-peaks in the NOESY spectrum, which would otherwise be masked by the aliphatic phospholipid resonances.

## **Part 3. Experimental**

*Materials* – 1,2-Dipalmitoyl-*sn*-glycero-3-phosphocholine (DPPC), chain-deuterated 1,2-dipalmitoyl-*sn*-glycero-3-phosphocholine (d<sub>62</sub>-DPPC) and cholesterol were purchased from Avanti Polar Lipids (Alabaster, AL). All other chemicals including Q and LY were purchased from Sigma.

*Sample Preparation* – Samples of DPPC or DPPC-d<sub>62</sub>/cholesterol, DPPC or DPPC-d<sub>62</sub>/agonist, and DPPC or DPPC-d<sub>62</sub>/cholesterol/agonist were prepared at molar ratios of 8:2, 9:1 and 7:2:1, respectively, as described in Chapter 3.

*NMR Measurements* – All NMR experiments were carried out on a Bruker Avance II 500 MHz spectrometer using a 4 mm MAS probe operating at a frequency of 500.1025 MHz (<sup>1</sup>H). Experiments were carried out at an MAS speed of 10 kHz (<sup>1</sup>H). <sup>1</sup>H NMR spectra were externally referenced to tetramethylsilane (TMS) at 0 ppm.

$^1\text{H}$  experiments were conducted with a typical  $\pi/2$  pulse length of 7  $\mu\text{s}$  and a relaxation delay of 4 s. 2D NOESY experiments had 256 or 512 increments and up to 64 scans per increment, with mixing times between 10 ms and 1000 ms. Experiments were conducted at 298 K, 308 K and 316 K (temperature established by a thermocouple in the probehead). The sample temperature was adjusted according to the effects of sample heating by MAS spinning, which heats the sample by 1.8 K at 10 kHz spinning.

All of the NMR data was processed using TopSpin version 1.3 (Bruker Instruments, Karlsruhe, Germany). NOESY peak volumes were obtained by peak fitting and integration using CARRA<sup>13</sup>.

*NOESY Cross-Relaxation Rates and Location Probability Determination* - The NOESY cross-relaxation rates were obtained at a range of mixing times and at three temperatures: 298 K, 308 K, 316 K. The full matrix analysis approach was used to calculate cross-relaxation rates of cross-peaks using data obtained from the NOESY spectrum<sup>14</sup>. The experimentally measured NOESY peak volumes, represented by the matrix,  $A$ , at the mixing time  $t_m$ , and the cross-relaxation rates,  $R$ , are linked by the following matrix equation (Equation 13):

$$A(t_m) = A(0) \cdot \exp(-Rt_m)$$

*Equation 13*

The relaxation rate matrix,  $R$ , is calculated by rewriting equation 13:

$$R = -\frac{X(\ln D)X^{-1}}{t_m}$$

*Equation 14*

In equation 14,  $X$  is the matrix of eigenvectors, and  $D$  is the diagonal matrix of eigenvalues of the normalised peak volume matrix,  $a(t_m)$  (where  $a(t_m) = A(t_m)$ )

$[(A(0)^{-1})]$ . The relaxation rates, contained in  $R$ , were taken as indicators of the relative location probabilities, and are plotted to give a location profile of the agonists, at atomic resolution. All calculations were carried out using Python 2.5, specifically with the modules ‘pylab’ and ‘scipy’<sup>15-17</sup>. The calculated cross-relaxation rates were plotted against carbon number for each measured drug resonance.

#### Part 4. Results and Discussion

*NMR Assignments* – Figure 4.1 shows the proton spectra of the samples of DPPC (A),  $d_{62}$ -DPPC/cholesterol (B),  $d_{62}$ -DPPC/cholesterol/LY (C) and  $d_{62}$ -DPPC/cholesterol/Q (D) at 300 K and 318 K. The spectra show the assignments of DPPC (peaks a to j), cholesterol (peaks k to p), LY (peaks 1 and 2 in spectrum C at 300 K), and Q (peaks 1 and 2 in spectrum D at 318 K).

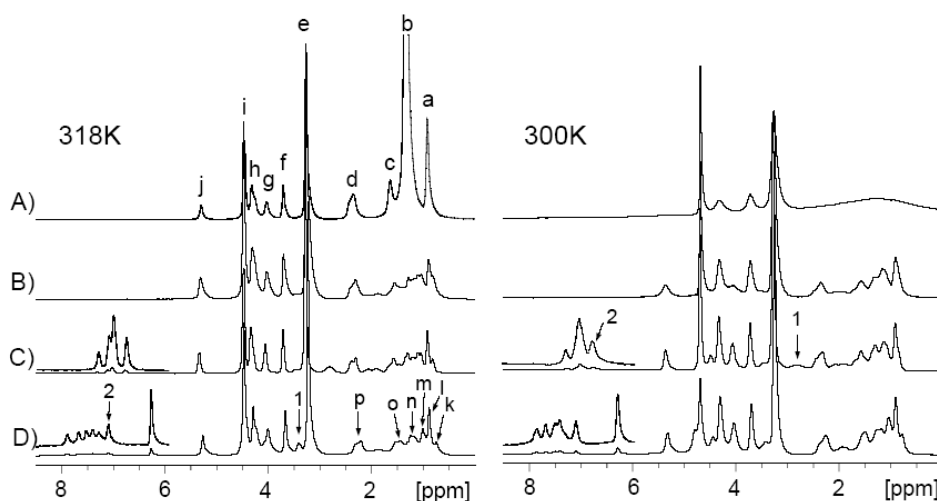


*Figure 4.1. Proton spectra at temperatures of 300 K and 318 K for samples of DPPC (A),  $d_{62}$ -DPPC/cholesterol (B),  $d_{62}$ -DPPC/cholesterol/LY (C) and  $d_{62}$ -DPPC/cholesterol/Q (D). Spectrum (A) denotes the DPPC peaks with letters a – j, as described in Table 4.1. Spectra (C) and (D) denote the LY and Q peaks with the numbers 1 and 2; spectrum (D) denotes the cholesterol peaks with letters k – p, as described in Table 4.4*

The assignments for the lipid, cholesterol and drug signals were allocated according to studies by Lopez and Lorch, Scheidt *et al.* and Soubias *et al.*<sup>9, 10, 18</sup>. The DPPC proton assignments are shown in Table 4.1, in order of increasing chemical shift (ppm).

| Carbon number  | Resonance/ppm |
|--|---------------|
| C16  | 0.9           |
| CH <sub>2</sub> (n)<br>The aliphatic lipid chain atoms | ~ 1.2         |
| C3   | 1.6           |
| C2   | 2.3           |
| γ, Gamma   | 3.3           |
| β, Beta  | 3.7           |
| G3   | 4.0           |
| Overlapped G1 and α, alpha resonances                  | 4.35          |
| G2   | 5.3           |

Table 4.1. DPPC Proton Resonances

Figure 4.2 shows an annotated molecule of DPPC, displaying the parts of the lipid referred to by carbon number in Table 4.1.

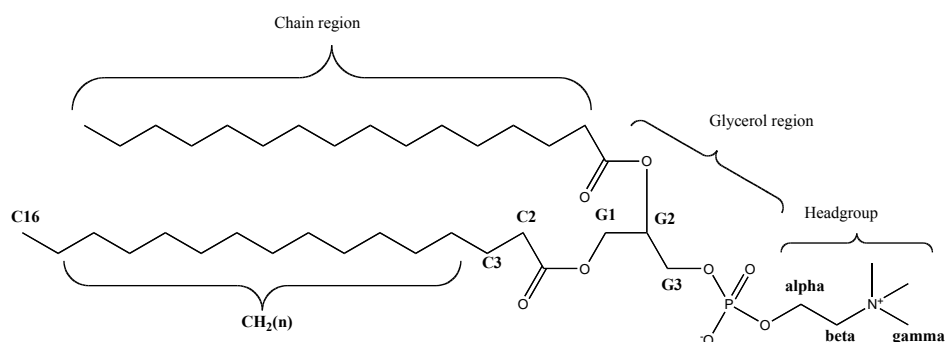


Figure 4.2. Annotated DPPC molecule indicating the positions of the labelled resonances

The serotonin-receptor agonists' resonances (Q and LY) were also numbered in order of increasing chemical shift (ppm). These are shown in Tables 4.2 and 4.3.

| Carbon number | Q resonance/ppm |
|---------------|-----------------|
| Q1            | 3.45            |
| Q2            | 7.17            |
| Q3            | 7.33            |
| Q4            | 7.47            |
| Q5            | 7.60            |
| Q6            | 7.75            |
| Q7            | 7.97            |

*Table 4.2. Q proton resonances*

Figure 4.3 shows the annotated structure of Q, showing the positions of resonances **1** and **2**.

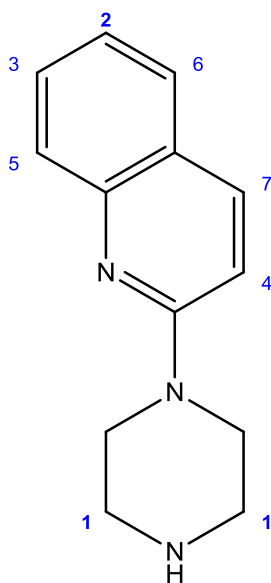


*Figure 4.3. Annotated quipazine molecule indicating the positions of resonances 1 and 2*

| Carbon number | LY resonance/ppm |
|---------------|------------------|
| L1            | 2.8              |
| L2            | 6.7              |
| L3            | 7.0              |
| L4            | 7.4              |

Table 4.3. LY proton resonances

Figure 4.4 shows the structure of LY. The labelled molecules correspond to signals **1** and **2** shown in the proton spectrum of  $d_{62}$ -DPPC/cholesterol/LY.

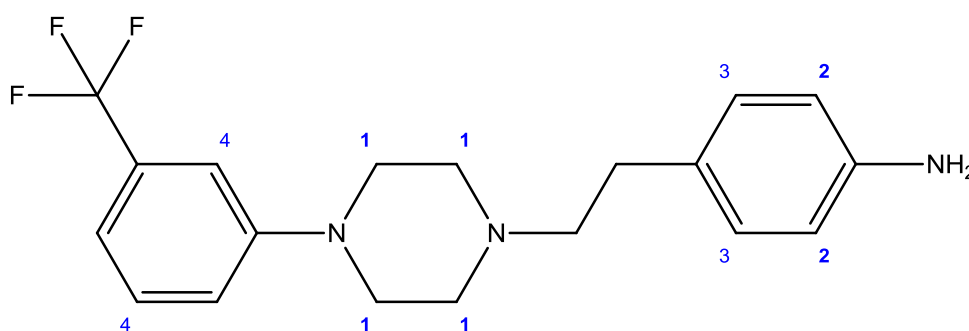


Figure 4.4. Annotated LY molecule indicating the positions of resonances **1** and **2**

The cholesterol proton assignments are shown in Table 4.4, in order of increasing chemical shift (ppm).

| Carbon number              | Resonance/ppm |
|----------------------------|---------------|
| C18 <sup>C</sup>           | 0.8           |
| C26/27 <sup>C</sup>        | 0.9           |
| C9/21/19 <sup>C</sup>      | 1.05          |
| C14/17/24 <sup>C</sup>     | 1.20          |
| C7/8/11/15/25 <sup>C</sup> | 1.50          |
| C4 <sup>C</sup>            | 2.3           |

Table 4.4. Cholesterol proton resonances

Figure 4.5 shows an annotated molecule of cholesterol, displaying the parts of the lipid referred to by carbon number in Table 4.4.

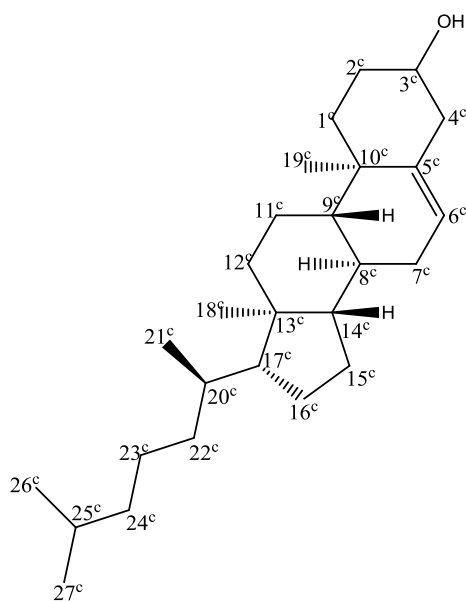


*Figure 4.5. Annotated cholesterol molecule indicating the positions of the labelled resonances*

The use of a chain-deuterated phospholipid eliminates signals in the aliphatic region of the spectrum (0 ppm to 1.6 ppm), thereby ensuring that the previously hidden cholesterol aliphatic and methyl signals become visible. This enables the observation of cholesterol/agonist cross-peaks which would otherwise be obscured by much more intense phospholipid/agonist cross-peaks.

A typical NOESY spectrum of the sample of d<sub>62</sub>-DPPC/cholesterol/LY is shown in Figure 4.6, showing the cross-peaks arising between the lipid, cholesterol and agonist resonances. The cross-peak intensity gives an indication of the proximity of two peaks. The calculated cross-peak rates were used to generate plots of location probability versus lipid number for each drug resonance.

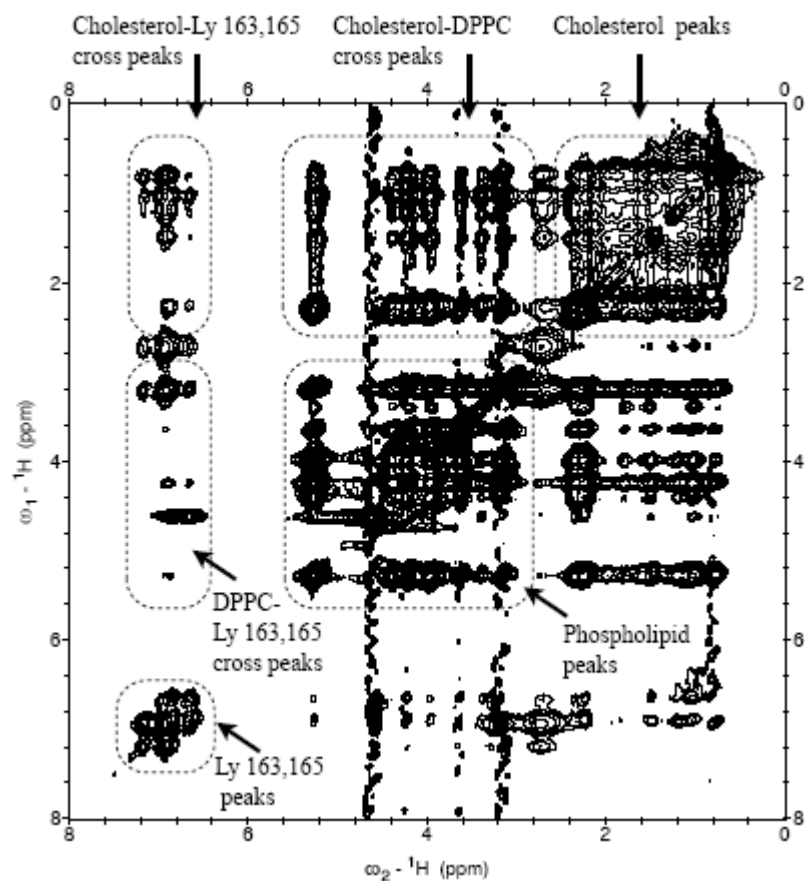


Fig. 4.6. MAS-NOESY spectrum of  $d_{62}$ -DPPC/cholesterol/LY at a temperature of 300 K and a mixing time of 200 ms. The spectrum shows the positions of the cholesterol (0 to 2.5 ppm), lipid (3 to 6 ppm) and agonist peaks (2.8 ppm and 6.5 to 7.5 ppm) along the diagonal. The cholesterol/agonist and lipid/agonist cross-peaks are also indicated

*NOESY Location Probabilities for the DPPC/Agonist Samples* – NOESY experiments were carried out on samples of DPPC/Q and DPPC/LY at a temperature of 310 K, at mixing times of 10, 100, 200, and 400 ms. At this temperature both samples are in the fluid lamellar phase, as indicated by the results discussed in Chapter 3. The cross-relaxation rates calculated for these samples are displayed in Figure 4.7.

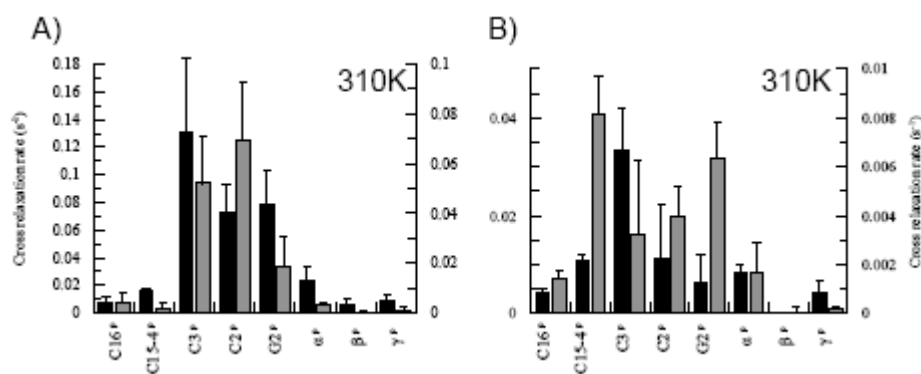


Fig. 4.7. Cross-relaxation rates for the samples of DPPC/LY (A) and DPPC/Q (B). The black bars (left axes) represent position 1 of each agonist, while the grey bars (right axes) represent position 2, as indicated in figures 3.3 and 3.4 (Experimental section, Chapter 3). The cross-relaxation rates are the mean of the results from three mixing times. The error bars represent the standard deviation

The results for the sample of DPPC/LY show that there is very little interaction between the agonist and the carbon atoms in the headgroup ( $\gamma$ ,  $\beta$  and  $\alpha$  resonances) and chain terminus (C16) regions. The strongest interactions occur between the agonist and the carbon atoms in the interfacial region (C3, C2 and G2 resonances). The interactions between the carbon atoms in the headgroup and chain terminus regions and the agonist at position 1 are stronger overall than for position 2. The strongest interaction for position 1 occurs at C3, with weaker interactions for C2, G2 and  $\alpha$ . The strongest interaction for position 2 occurs at C2, with weaker interactions for C3 and G2.

The results for the sample of DPPC/Q show a distinct difference from those of DPPC/LY, with interactions occurring between a greater number of lipid resonances. There is very little interaction between the agonist and the carbon atoms in the headgroup ( $\beta$  and  $\gamma$  resonances). The strongest interactions occur between the agonist and the carbon atoms in the chain (C15-4 resonances) and interfacial (C3, C2 and G2 resonances) regions, with weaker interactions occurring in the chain terminus (C16) region and for the  $\alpha$  resonance. The interactions between the lipid and the agonist at position 2 are stronger overall

than for position 1, except in the headgroup region ( $\gamma$  and  $\alpha$  resonances) and for C3.

The results for the sample of DPPC/LY indicate that the agonist is oriented perpendicular to the bilayer normal axis, in the interfacial region of the bilayer. The interactions between the lipid and the agonist at positions 1 and 2 are similar in intensity and occur at the same resonances. An approximate location and orientation of the agonist with respect to the lipid is displayed in Figure 4.8.

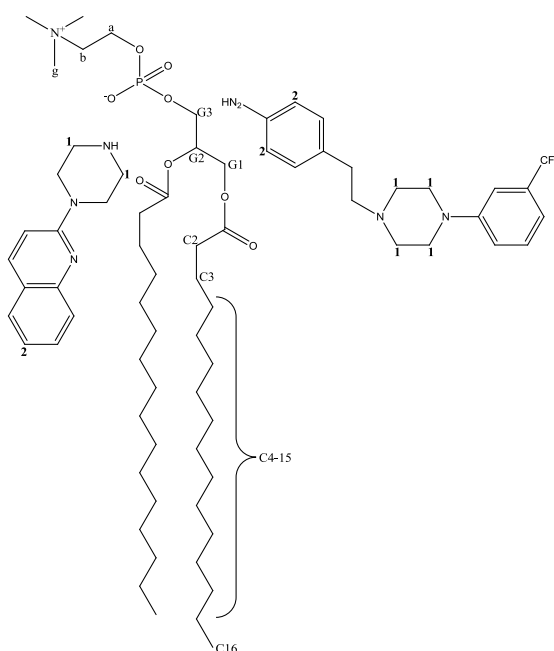


*Fig. 4.8. The relative locations and orientations of LY and Q with respect to DPPC at 310 K. LY is oriented perpendicular to the lipid, and located in the interfacial region of the bilayer. Q is oriented parallel to the lipid, and located in the interfacial region and at the start of the headgroup and chain regions*

The results for the sample of Q indicate that the agonist is located parallel to the bilayer normal axis, in the interfacial region of the bilayer. The differences between the interactions at position 1 and position 2 with the lipid indicate that the terminal benzene ring (position 2) is positioned towards the chain region of the lipid, while the piperazine ring (position 1) is positioned towards the headgroup region.

The increased amount of interactions between the agonist and the lipid in the case of Q may indicate that this molecule experiences greater movement within the bilayer than LY, which is concentrated in the interfacial region with very little interaction in either the chain or headgroup regions. In contrast, Q has recorded interactions at the extremes of the lipid molecule (the lipid termini (C16 and  $\gamma$  resonances)).

*NOESY Location Probabilities for the  $d_{62}$ -DPPC/cholesterol/agonist Samples* – NOESY experiments were carried out on samples of  $d_{62}$ -DPPC/cholesterol/Q and  $d_{62}$ -DPPC/cholesterol/LY at temperatures of 300 K, at mixing times of 10, 200, 300 and 400 ms, and 318 K, at mixing times of 20, 400, 500, and 600 ms. The mixing times are increased at higher temperatures to account for an decrease in correlation times<sup>4</sup>. At 300 K the sample of  $d_{62}$ -DPPC/cholesterol/Q is in the mixed [gel +  $l_o$ ] phase, while the sample of  $d_{62}$ -DPPC/cholesterol/LY is in the mixed [ $l_d$  +  $l_o$ ] phase. At 318 K the sample containing Q is in the fluid lamellar phase, although the sample containing LY is still in the mixed [ $l_d$  +  $l_o$ ] phase. The sample of  $d_{62}$ -DPPC/cholesterol/LY could not be measured in the fluid lamellar phase as the increase in temperature (the pure fluid lamellar phase does not start until 327 K) would produce correlation times too short to be practically analysed; however the amount of  $l_d$  phase lipid will be significantly greater at the higher temperature. The phases are identified in Chapter 3. The cross-relaxation rates calculated for these samples are displayed in Figure 4.9.

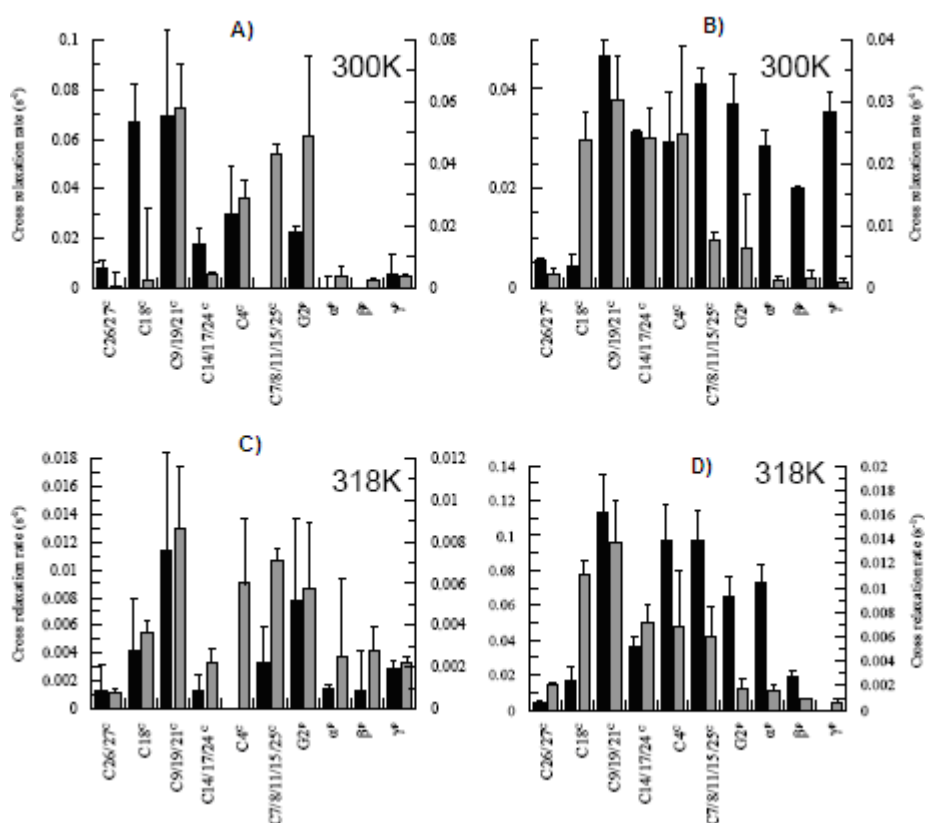
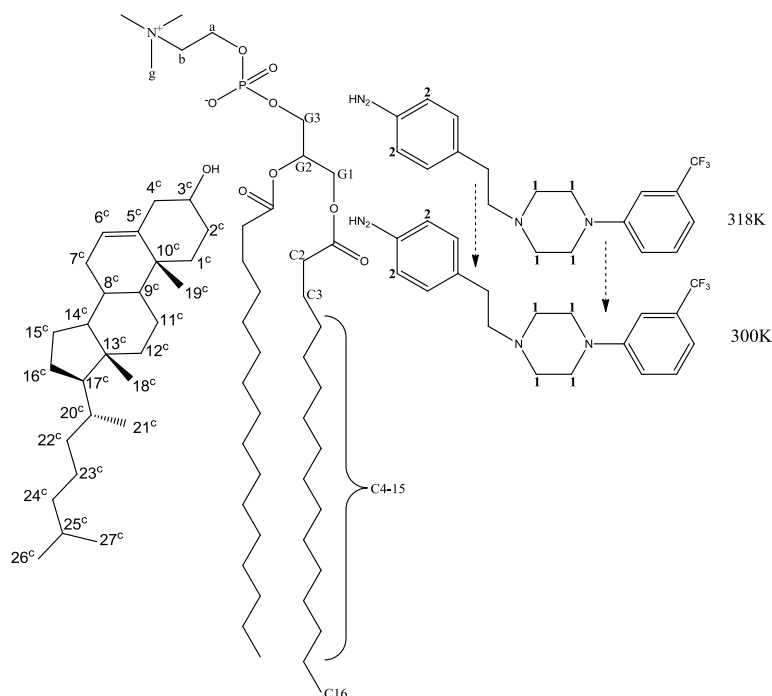


Fig. 4.9. Cross-relaxation rates for the samples of  $d_{62}$ -DPPC/cholesterol/LY at 300 K (A) and at 318 K (C), and  $d_{62}$ -DPPC/cholesterol/Q at 300 K (B) and at 318 K (D). The black bars (left axes) represent position 1 of each agonist, while the grey bars (right axes) represent position 2. The cross-relaxation rates are the mean of the results from three mixing times. The error bars represent the standard deviation

The results for  $d_{62}$ -DPPC/cholesterol/LY at 300 K show that for position 1, the strongest interactions occur at the C18<sup>C</sup> and C9/19/21<sup>C</sup> cholesterol resonances, with weaker interactions found for the C14/17/24<sup>C</sup> and C4<sup>C</sup> resonances. These cholesterol resonances are all located in the main sterol body of the molecule. Cholesterol has been found to orient parallel to the bilayer normal axis, with the hydroxyl chain terminus located in the interfacial region of the bilayer and the terminal aliphatic methyl groups (C26/27<sup>C</sup>) located towards the end of the chain region (Figure 4.10)<sup>9</sup>.



*Fig. 4.10. The relative locations and orientations of LY and cholesterol with respect to DPPC at 318 K and 300 K. The presence of cholesterol in the  $l_o$  phase at 300 K pushes the agonist deeper into the bilayer. Cholesterol is oriented parallel to the bilayer normal axis, with the hydroxyl terminus located in the interfacial region and the terminal aliphatic methyl terminus located in the chain region*

There are significant differences between the lipid and cholesterol interactions for position 1 and position 2. For position 2, the strongest interactions occur at the C9/19/21<sup>C</sup>, C7/8/11/15/25<sup>C</sup>, and G2 resonances, with weaker interactions occurring at the C4<sup>C</sup> positions. The weakest interactions for positions 1 and 2 occur in the headgroup region of the lipid, while the weakest interactions for position 2 occur at the C18<sup>C</sup> and C14/17/24<sup>C</sup> resonances.

These results indicate that the LY molecule is oriented perpendicular to the sterol body of the cholesterol molecule, with both located in the interfacial region of the bilayer. At a temperature of 300 K, both parts of the LY molecule interact strongly with the main sterol body of the cholesterol molecule. At this temperature the sample is in the mixed [ $l_d + l_o$ ] phase. The strong interactions of

LY with cholesterol suggest that the agonist molecule is present in the cholesterol-rich  $l_o$  domains which proliferate in this mixed phase system.

The profile of cross-relaxation rate interactions changes when the temperature is increased to 318 K (and the phase changes to the fluid lamellar phase). There are now significant interactions between LY at position 1 and the lipid which were not present at 300 K. The interactions with the lipid headgroup ( $\alpha$ ,  $\beta$  and  $\gamma$  resonances) and with G2 are strengthened, while the interactions with the main sterol body of the cholesterol molecule are weaker. This pattern of stronger interactions with the lipid headgroup and interfacial region is also observed for position 2, although the interactions with the cholesterol molecule remain relatively strong. The strengths of the interactions with the lipid molecule have increased, which suggests that at lower temperatures the agonist is pushed deeper into the bilayer, towards the chain terminus and away from the headgroup, by the presence of cholesterol.

The results for  $d_{62}$ -DPPC/Chol/Q at 300 K show a markedly different cross-relaxation rate profile when compared to those for the samples containing LY. For position 1, strong interactions occur at all cholesterol and lipid resonances apart from the  $C_{26/27}^C$  and  $C_{18}^C$  resonances. For position 2, the strongest interactions occur for the main sterol body of the cholesterol molecule ( $C_{18}^C$ ,  $C_{9/19/21}^C$ ,  $C_{14/17/24}^C$  and  $C_4^C$  resonances), with weaker interactions occurring for the  $C_{7/8/11/15/25}^C$  and G2 resonances. The weakest interactions occur at the lipid headgroup and cholesterol aliphatic chain terminus regions. These results indicate that the Q molecule is in contact with almost all parts of the cholesterol and lipid molecules, in contrast to the results for LY at this temperature. This indicates that Q has retained its orientation with respect to the bilayer in the presence of cholesterol. The relative orientations and locations of cholesterol, lipid and agonist are shown in Figure 4.11.

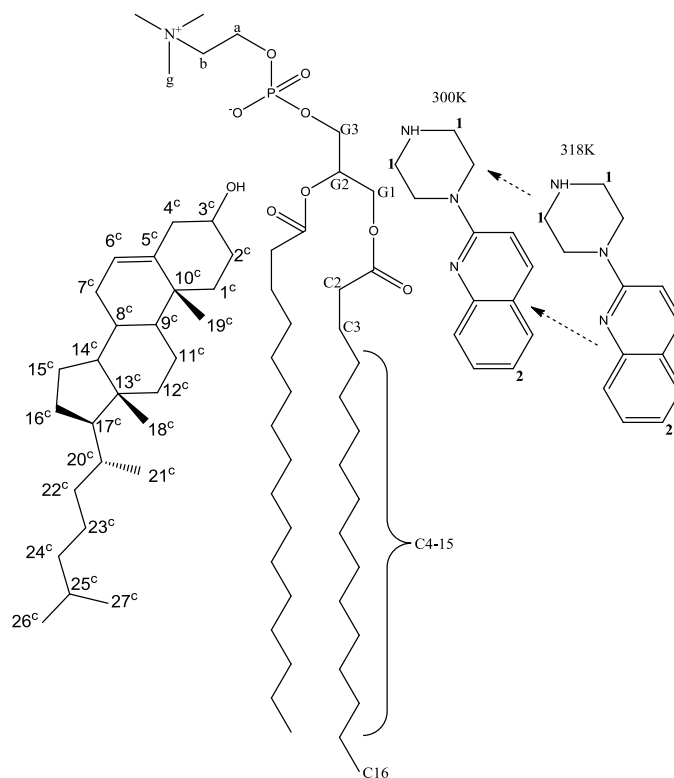


*Fig. 4.11. The relative locations and orientations of Q and cholesterol with respect to DPPC at 300 K and 318 K. The presence of cholesterol in the  $l_o$  phase at 300 K pushes the agonist closer towards the surface of the bilayer. Cholesterol is oriented parallel to the bilayer normal axis, with the hydroxyl terminus located in the interfacial region and the terminal aliphatic methyl terminus located in the chain region*

At 318 K the sample containing Q is in the fluid lamellar phase, according to the results from Chapter 3. The cross-relaxation rate profile at this temperature is similar to that of 300 K, but with markedly reduced interactions between the agonist and the lipid headgroup. The pattern of interactions between the agonist and the cholesterol molecule remains similar. This suggests that the presence of the cholesterol-enriched  $l_o$  phase, which is present at 300 K but not at 318 K, may have the effect of pushing the quipazine molecule towards the surface of the bilayer, causing increased amounts of agonist/headgroup interaction at the lower temperature.

The addition of cholesterol has a significant effect on the samples of d<sub>62</sub>-DPPC/cholesterol/agonist. In the case of Q, the most significant difference is observed at 318 K, with the decreased strength of interactions of the agonist with the lipid headgroup (in comparison to the sample of DPPC/Q at 310 K). Although at these temperatures both samples are in the fluid lamellar phase, the interactions with the headgroup lipids are enhanced by the presence of cholesterol, which may indicate that the cholesterol has altered the location of Q with respect to the lipid molecule. It is difficult to make similar comparisons in the case of LY, however, because the phase of the sample of DPPC/LY at 310 K exists in the fluid lamellar phase, while the sample of d<sub>62</sub>-DPPC/cholesterol/LY exists in the mixed [l<sub>d</sub> + l<sub>o</sub>] phase at both temperatures.

*The Effect of Agonist Molecules on the Bilayer* – The results suggest that Q and LY, despite differing only slightly in terms of molecular structure and size, have significantly different effects on the bilayer, both in the presence and absence of cholesterol. Q orients parallel to the bilayer normal axis, in the interfacial region, while LY adopts an orientation perpendicular to the bilayer in the same region. The reason for this orientation is unknown, as it would appear from the linear structure of the molecule that it is particularly well-suited to adopting a parallel orientation. It is possible that the perpendicular orientation has a disruptive effect on the bilayer; the results from the phase behaviour of the DPPC/LY sample, in which the transition temperature is lowered by several degrees in comparison with the Q sample, may point to a disruptive influence on the bilayer.

The presence of cholesterol, in the form of cholesterol-enriched microdomains, appears to have contrasting effects on the relative positions of the agonists. Q is pushed further towards the phospholipid headgroup, as shown by increasing interactions with the headgroup resonances coupled with decreasing interactions with the cholesterol aliphatic methyl terminus, while conversely LY is pushed further towards the centre of the bilayer. Both agonist molecules are associated with lipid microdomains when the sample is in a mixed l<sub>o</sub> phase.

## Part 5. Conclusions

MAS-NOESY experiments were carried out on samples of DPPC containing agonist molecules (Q and LY), and on samples of deuterated DPPC containing cholesterol and agonist. Cross-relaxation rate calculations were carried out using the full-mixing time approach to produce plots of cross-peak intensity between each lipid and/or cholesterol resonance and the agonist. The results for the samples of DPPC/agonist provided orientations and positions of agonist with respect to the bilayer; Q was found to orient parallel to the bilayer normal axis, in the interfacial region, while LY was found to adopt a perpendicular orientation with respect to the bilayer normal, also in the interfacial region. These results correspond to the research carried out by Lopez and Lorch on samples of DOPC/agonist<sup>9</sup>.

The results for the samples of deuterated DPPC/cholesterol/agonist showed that Q and LY interacted with the cholesterol in slightly different ways. At 300 K, in the mixed [gel + l<sub>o</sub>] phase, Q interacted strongly with all parts of the cholesterol molecule with the exception of C26/27<sup>C</sup>, and also showed significant interactions with the phospholipid headgroup. When the temperature was increased to 318 K, and the phase changed from [gel + l<sub>o</sub>] to fluid lamellar, the pattern of the interactions changed; the strong interactions with the phospholipid headgroup were greatly decreased, indicating that Q had moved away from the headgroup as temperature increased. The opposite effect is noted for LY; the results showed weak agonist/headgroup interactions at 300 K, which then increased in intensity as the temperature increased to 318 K. This indicates that LY is pushed deeper into the bilayer, towards the phospholipid C16 chain terminus, when the temperature decreases. The plots of cross-relaxation rates for LY show different profiles at the two temperatures, although the sample of d<sub>62</sub>-DPPC/cholesterol/LY is ostensibly in the same mixed [l<sub>d</sub> + l<sub>o</sub>] phase at these temperatures (the results from Chapter 3 indicate that the onset of the fluid lamellar phase takes place at 325 K for this sample); this may be due to the fact that the proportion of l<sub>o</sub> phase lipids at the higher temperature may be reduced as the sample approaches the phase transition.

The cholesterol/agonist cross-relaxation rates for both agonist drugs show that both agonists partition into  $l_o$ -phase domains, a hypothesis which is supported by the research cited in the introduction. Eisensamer *et al.* reported the co-localisation of the serotonin receptor protein with serotonin receptor agonist drugs in LBD fractions. The results from this research indicate the partitioning of two serotonin receptor agonist drugs into cholesterol-rich domains. The advantage of this partitioning activity is the sequestration of a protein with its substrate in close proximity, which enhances the activity of the protein.

The results also show that two drugs with only slightly different molecular structures, compositions and sizes (Q has a molecular mass of 213, while LY has a molecular mass of 349), and with similar linear structures, can adopt completely different orientations in the bilayer. This shows the importance of the analysis of drug/membrane interactions, as drugs which are expected to have a similar mode of action may have differing levels of interaction with the cell membrane. It would be interesting to expand this research to include further examples of serotonin receptor agonist drugs, as explored by Lopez and Lorch<sup>9</sup>. It would also be interesting to observe the behaviour of LY in the fluid lamellar phase, but practical difficulties prevent this.

## Part 6. References

1. Lucio, M.; Lima, J. L. F. C.; Reis, S., Drug-Membrane Interactions: Significance for Medicinal Chemistry. *Curr. Med. Chem.* **2010**, 17, (17), 1795-1809.
2. Kuroda, Y.; Nasu, H.; Fujiwara, Y.; Nakagawa, T., Orientations and locations of local anesthetics benzocaine and butamben in phospholipid membranes as studied by  $^2\text{H}$  NMR spectroscopy. *J. Membrane Biol.* **2000**, 177, 117-128.
3. Gaede, H. C.; Gawrisch, K., Lateral diffusion rates of lipid, water, and a hydrophobic drug in a multilamellar liposome. *Biophys. J.* **2003**, 85, 1734-1740.
4. Holte, L. L.; Gawrisch, K., Determining ethanol distribution in phospholipid multilayers with MAS-NOESY spectra. *Biochem.* **1997**, 36, 4669-4674.

5. Feller, S. E.; Brown, C. A.; Nizza, D. T.; Gawrisch, K., Nuclear Overhauser enhancement spectroscopy cross-relaxation rates and ethanol distribution across membranes. *Biophys. J.* **2002**, 82, 1396-1404.
6. Scheidt, H. A.; Pampel, A.; Nissler, L.; Gebhardt, R.; Huster, D., Investigation of the membrane localization and distribution of flavonoids by high-resolution magic angle spinning NMR spectroscopy. *Biochim. Biophys. Acta* **2004**, 1663, 97-107.
7. Yau, W.-M.; Wimley, W. C.; Gawrisch, K.; White, S. H., The preference of tryptophan for membrane interfaces. *Biochem.* **1998**, 37, 14713-14718.
8. Siarheyeva, A.; Lopez, J. J.; Glaubitz, C., Localization of multidrug transporter substrates within model membranes. *Biochem.* **2006**, 45, (19), 6203-6211.
9. Lopez, J. J.; Lorch, M., Location and orientation of serotonin receptor 1a agonists in model and complex lipid membranes. *J. Biol. Chem.* **2008**, 283, (12), 7813-7822.
10. Scheidt, H. A.; Huster, D., The interaction of small molecules with phospholipid membranes studied by <sup>1</sup>H NOESY NMR under magic-angle spinning. *Acta Pharmacol. Sin.* **2008**, 29, (1), 35-49.
11. Eisensamer, B.; Uhr, M.; Meyr, S.; Gimpl, G.; Deiml, T.; Rammes, G.; Lambert, J. J.; Zieglansberger, W.; Holsboer, F.; Rupprecht, R., Antidepressants and antipsychotic drugs colocalize with 5-HT<sub>3</sub> receptors in raft-like domains. *J. Neurosci.* **2005**, 25, (44), 10198-10206.
12. Allen, J. A.; Halverson-Tamboli, R. A.; Rasenick, M. M., Lipid raft microdomains and neurotransmitter signalling. *Nat. Rev.: Neurosci.* **2007**, 8, (2), 128-140.
13. Keller, R. *The Computer Aided Resonance Assignment Tutorial*, Cantina Verlag 2004.
14. Huster, D.; Arnold, K.; Gawrisch, K., Investigation of lipid organization in biological membranes by two-dimensional nuclear Overhauser enhancement spectroscopy. *J. Phys. Chem. B* **1999**, 103, (1), 243-251.
15. <http://www.python.org>.
16. <http://matplotlib.sourceforge.net/>.
17. Jones, E.; Oliphant, T.; Peterson, P., SciPy: Open Source Scientific Tools for Python. **2002**

18. Soubias, O.; Jolibois, F.; Reat, V.; Milon, A., Understanding sterol-membrane interactions, part II: Complete  $^1\text{H}$  and  $^{13}\text{C}$  assignments by solid-state NMR spectroscopy and determination of the hydrogen-bonding partners of cholesterol in a lipid bilayer. *Chem. Eur. J.* **2004**, 10, 6005-6014.

## Chapter 5: Use of an Enzyme Substrate to Investigate Bilayer Dynamics

### Part 1. Introduction

*Dipolar Recoupling On-Axis with Scaling and Shape Preservation (DROSS)* – The DROSS technique was first developed by Gross *et al.* to obtain order parameter measurements in lipid bilayers from  $^{13}\text{C}$ - $^1\text{H}$  dipolar couplings<sup>1</sup>. Order parameters for lipid samples were previously obtained from  $^2\text{H}$ -NMR measurements, but this technique requires the synthesis of expensive deuterated lipid compounds. The development of DROSS enabled the measurement of lipid order parameters of from natural abundance  $^{13}\text{C}$  signals<sup>1</sup>. A typical DROSS projected spectrum is shown in Figure 5.1.

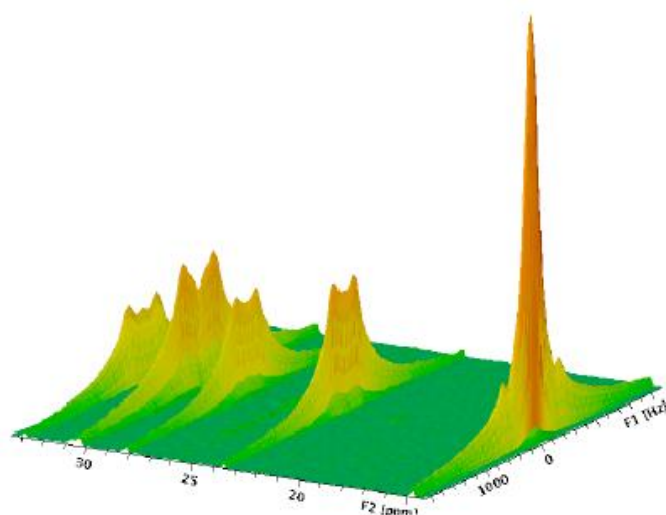


*Figure 5.1. 2D projected DROSS spectrum of a phospholipid compound, showing the  $^{13}\text{C}$ - $^1\text{H}$  dipolar couplings. The  $^{13}\text{C}$  spectrum is shown along the F2 axis (ppm);  $^1\text{H}$ - $^1\text{H}$  couplings are shown along the F1 axis (Hz). The width of the  $^1\text{H}$ - $^1\text{H}$  coupling can be used to generate order parameters, using Equation 15 (Experimental section)*

DROSS has been used to study lipid bilayers<sup>1</sup> and phase behaviour in mixed phospholipid/cholesterol systems<sup>2</sup>.

*Fluorescence Emission Spectroscopy of Lipid Bilayers* – Fluorescence emission spectroscopy of lipid bilayers may be carried out using a fluorophore-labelled lipid analogue as a probe, with the advantage that these lipid analogues align themselves with the bulk of the lipid bilayer at the correct location and orientation, and do not cause too much perturbation of the bilayer, although there is an unavoidable perturbation due to the bulky size of the pyrene moiety. Depending on where the fluorophore is positioned, they may also report on different regions of the bilayer<sup>3</sup>. Examples of widely-used fluorophore labels for lipid analogues are the dipyrenylated phospholipids, such as 1,2-bis-(1-pyrenedecanoyl)-*sn*-glycero-3-phosphocholine (Figure 5.2).

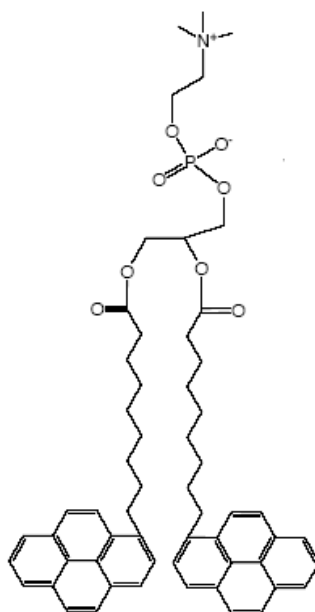


*Figure 5.2. Chemical structure of 1,2-bis-(1-pyrenedecanoyl)-sn-glycero-3-phosphocholine (dipyPC)*

The pyrene moieties have certain physical properties which make them particularly suited to their use as fluorescence probes in lipid bilayers. They have a tendency to form monomers, dimers and excimers inside the bilayer. The formation of excimers depends on the close proximity ( $< 3.5 \text{ \AA}$ ) of an excited monomer to a ground-state monomer. If the pyrene moieties also adopt the correct orientation (face-to-face), then the excimer will form<sup>4</sup>. The probability of excimer formation depends on the lateral pressure in the acyl region of the

bilayer, if the concentration of the fluorescence probe is sufficiently low to prevent intermolecular correlations. Therefore the ratio of excimers to monomers can be used as a measure of lateral pressure in the bilayer. A typical fluorescence emission spectrum for a dipyrenyl lipid analogue in a DOPC bilayer is shown in Figure 5.3.

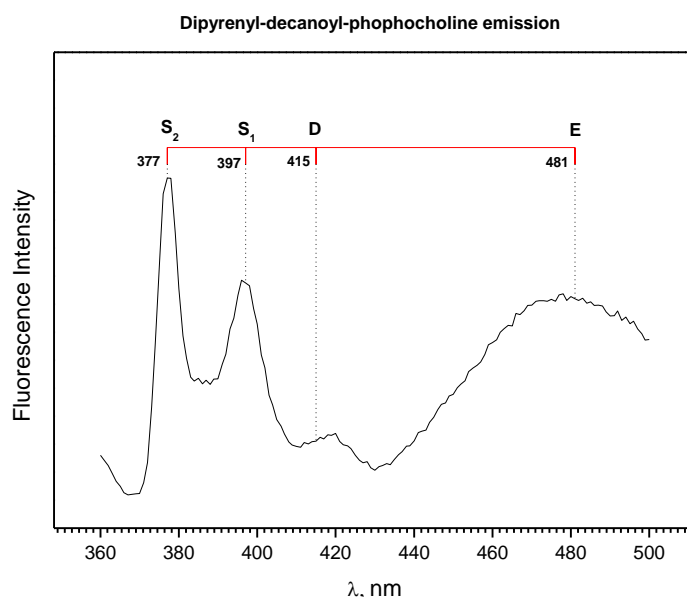


*Figure 5.3. Typical fluorescence emission spectrum for a dipyrenyl lipid analogue in a DOPC bilayer, excited at 347 nm. S<sub>2,1</sub> show monomer excitation at 377 nm and 397 nm, respectively; D shows dimer excitation at 415 nm; and E shows excimer excitation at 481 nm*

Pyrene-containing lipid analogues have previously been used to study lateral diffusion of bilayer lipids, curvature stress, and lipid dynamics<sup>3-5</sup>.

## **Part 2. Aims**

The aim of the experiment was to analyse the effect of changes in bilayer composition on the physical properties of the bilayer. The enzyme-catalysed conversion of the lipid di-octanoyl-*sn*-glycerol (DOG) to phosphatidic acid (PA) was utilised by measuring the effect of this conversion on the order parameter of a DOPC bilayer. In theory, the conversion of DOG to PA in a DOPC bilayer is

expected to increase the order parameter and the lateral tension within the bilayer, relative to the values in the presence of DOG, which is due to the structural and physical differences between the lipid molecules.

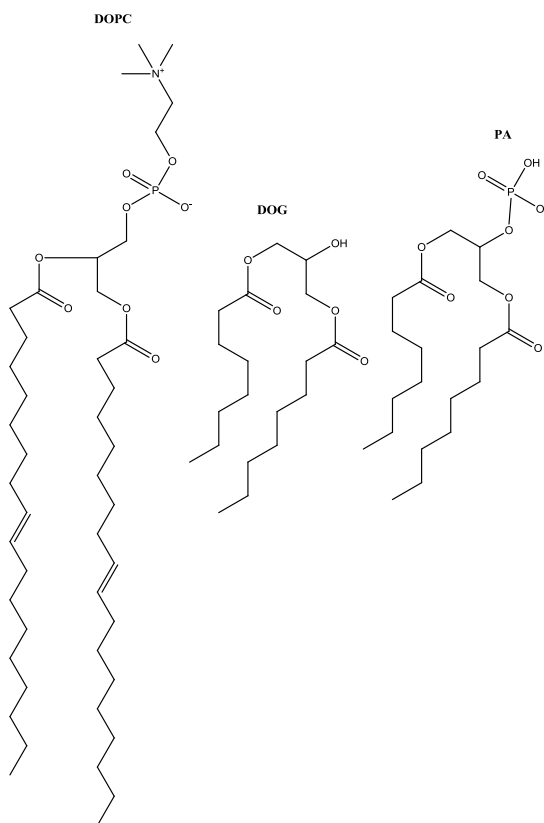


*Figure 5.4. The positions of DOG and PA relative to DOPC in a bilayer. The interactions of DOG with the bilayer change from occurring mainly in the interface and tail regions to the head, interface and tail regions with the addition of a phosphate headgroup*

DOG and PA are expected to interact with the bilayer in different ways, as shown in Figure 5.4. The addition of the phosphate headgroup increases the volume of space in the bilayer occupied by the lipid. PA is a cone-shaped lipid (as pictured in Figure 1.7d, Chapter 1), which increases the tension in the bilayer relative to the tension experienced in the presence of a cylindrical lipid (DOG). The increase in bilayer tension is expected to produce higher order parameters and a higher ratio of excimer to monomer formation.

### Part 3. Experimental

*Materials* – 1,2-Dioctanoyl-*sn*-glycerol and 1,2-dioleoyl-*sn*-glycero-3-phosphocholine (DOPC) and PA were purchased from Avanti Polar Lipids (Alabaster, AL). All other chemicals including adenosine triphosphate (ATP) were purchased from Sigma. DGK and PIPES buffer were synthesised as described in Chapter 2.

*Sample Preparation* – Samples of DOPC/DOG, DOPC/DOG/DGK, and DOPC/PA were prepared at concentrations of 20 mol% DOG or PA, with or without DGK. The typical amount of DOPC used in each experiment was approximately 80 mg. The lipids were co-dissolved in chloroform/methanol (1:1 v/v). The solvents were evaporated under vacuum, and the resulting lipid cake was suspended in 8.4 mL PIPES buffer (pH 6.8), resulting in a lipid concentration of approximately 10 mg mL<sup>-1</sup>. The suspension was extruded to produce 0.2 µm multilamellar liposomes. DGK was added from a stock solution to a molar ratio of 1:2000. 100 mM ATP was then added from a stock solution, and the liposomes were left to equilibrate before the ATP was removed by dialysing against distilled, deionised water containing charcoal. The distilled, deionised water was exchanged for fresh water in 500 mL amounts for four hours before leaving overnight. Samples were also synthesised without the addition of ATP in order to provide a comparison of order parameters.

*NMR Measurements* – All NMR experiments were carried out on a Bruker Avance II 500 MHz spectrometer using a 4-mm MAS probe operating at a frequency of 500.1025 MHz (<sup>1</sup>H) and 125.7546 (<sup>13</sup>C). Experiments were carried out at 7 kHz sample spinning.

<sup>1</sup>H experiments were conducted with a typical  $\pi/2$  pulse length of 7 µs and a relaxation delay of 2 s. <sup>13</sup>C experiments were conducted with a typical  $\pi/2$  pulse length of 3.7 µs. Proton decoupling was achieved using TPPM. <sup>31</sup>P experiments were typically carried out with 32 (spinning) or 1 k (static) scans, with a  $\pi/2$  pulse length of 4.59 µs. Lipid order parameters were determined by measuring <sup>1</sup>H-<sup>13</sup>C dipolar couplings using two-dimensional recoupling on-axis with scaling

and shape preservation (DROSS) experiments<sup>1</sup>. DROSS measurements were typically carried out with 96 increments and 512 scans per increment, with a recycle delay of 2 s. The <sup>1</sup>H-<sup>13</sup>C dipolar couplings were taken directly from the spectrum and converted to segmental order parameters using the method described by Warschawski and Devaux<sup>6</sup>.

All of the NMR data were processed using TopSpin version 1.3 (Bruker Instruments, Karlsruhe, Germany).

*Fluorescence Emission Spectroscopy* – All fluorescence emission experiments were carried out by Natalia Goehring and Oscar Ces at the Department of Chemistry, Imperial College London. The results are replicated here with permission.

#### **Part 4. Results and Discussion**

*DROSS Results* – DROSS experiments were carried out on samples containing: DOPC/DOG; DOPC/DOG/DGK; DOPC/DOG/DGK/ATP; and DOPC/PA. DOG and PA were present at 20%, and ATP was removed prior to NMR, as described in the Experimental section. Slices through the DROSS spectra display the <sup>13</sup>C-<sup>1</sup>H splittings for each sample (Figure 5.5).

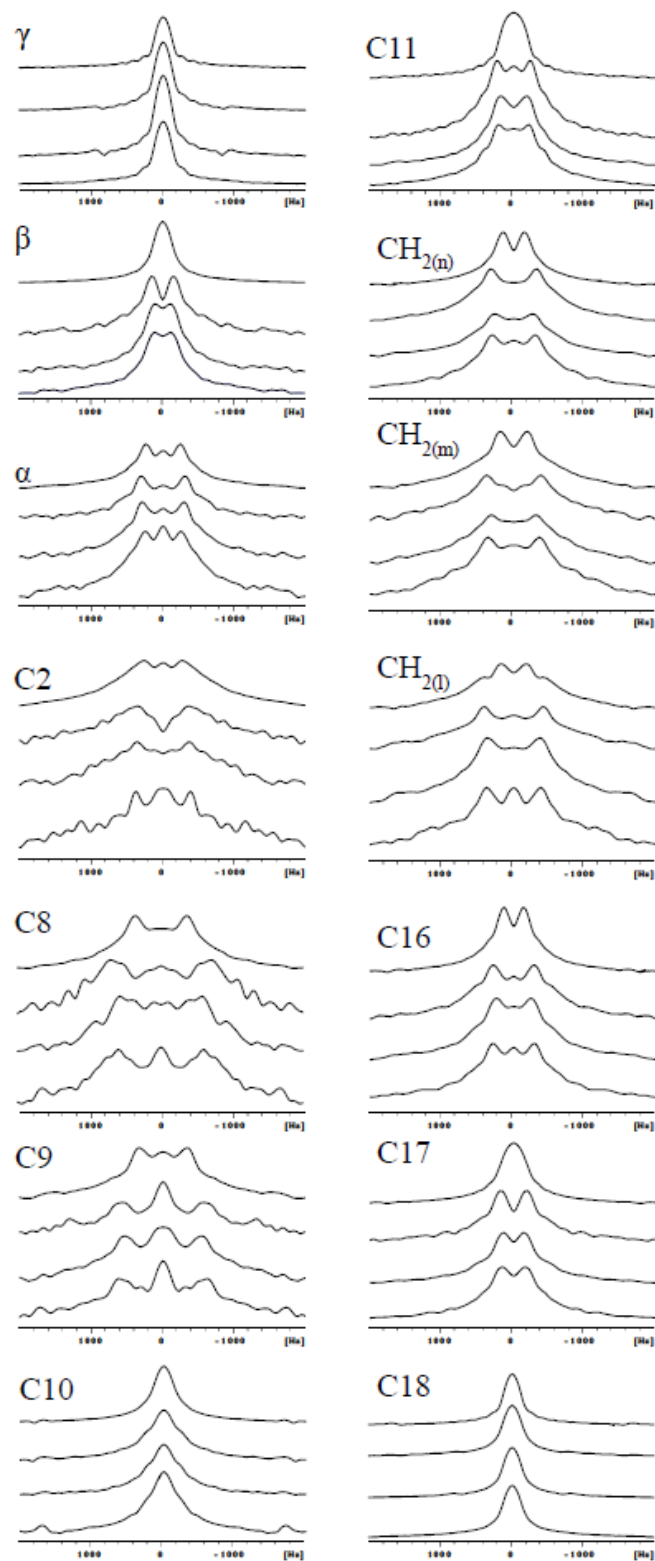


Figure 5.5.  $^{13}\text{C}$ - $^1\text{H}$  splittings for each sample at each DOPC resonance: DOPC/PA (the top splitting, 1); DOPC/DOG/DGK (second from the top, 2); DOPC/DOG (third from the top, 3); and DOPC/DOG/DGK/ATP (the lowest splitting, 4)

Order parameters were calculated from the measured  $^{13}\text{C}$ - $^1\text{H}$  splittings using Equation 15<sup>1</sup>:

$$S_{CH} = \frac{(W_{CH} \div \chi)}{20200} \text{ MHz}$$

*Equation 15. Equation for the calculation of order parameter using DROSS, where  $S_{CH}$  is the  $^{13}\text{C}$ - $^1\text{H}$  order parameter,  $W_{CH}$  is the width of the  $^{13}\text{C}$ - $^1\text{H}$  dipolar splitting, and  $\chi$  is the scaling factor (equal to 0.393). The  $W_{CH}$  term is divided by 20200 MHz in the case of methylene protons, and 20800 MHz in the case of vinylic protons<sup>2</sup>*

The order parameters were then plotted against carbon number for DOPC. The numbered parts of the DOPC molecule are shown in Figure 5.6.

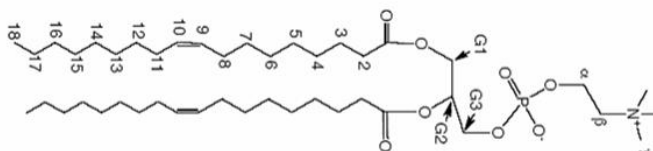
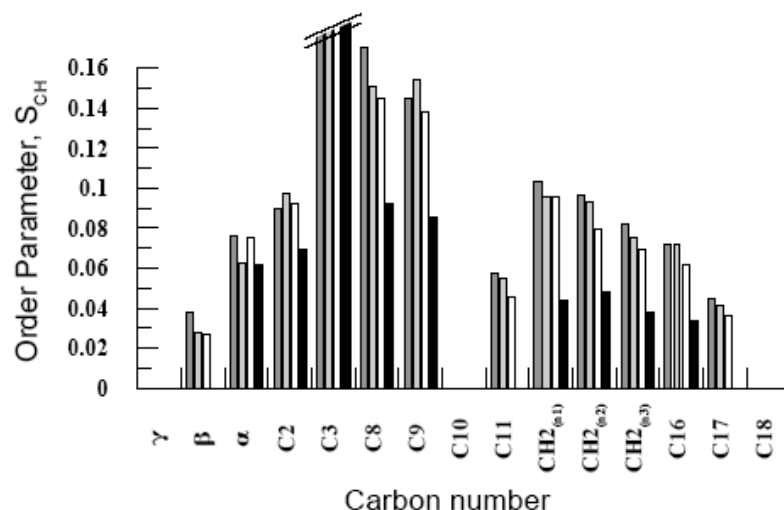


*Figure 5.6. DOPC displaying the carbon numbers representing parts of the molecule. Numbers 1 – 18 represent the carbon atoms of the alkyl chain; G1 – 3 represent the glycerol carbon atoms; and  $\alpha$ ,  $\beta$  and  $\gamma$  represent the headgroup molecules*

The plot of order parameters per carbon number for the four samples is shown in Plot 5.1.



*Plot 5.1. Plot of order parameter for each carbon moiety of DOPC, represented by carbon number. Samples of DOPC/DOG/DGK (dark grey), DOPC/DOG (light grey), DOPC/DOG/DGK/ATP (white), and DOPC/PA (black) are shown*

The sample of DOPC/DOG/DGK shows the highest order parameters overall, with the greatest difference between order parameter values for this sample and the other samples occurring at the  $\alpha$ ,  $\beta$  and C8 carbon atoms. For the alkyl chain carbons, the order parameter values for this sample are equal to or only slightly higher than the values for the other samples. Order parameter values are lower in comparison to the other samples at the C2 and C9 positions.

The order parameter values for the sample of DOPC/DOG are expected to closely mirror those of the sample of DOPC/DOG/DGK, due to the fact that the only difference between the two samples is a relatively low concentration of DGK. However the order parameters only mirror those of DOPC/DOG/DGK in the alkyl chain region, where they are equal to or only slightly lower than the results for the DGK-containing sample. The results are significantly lower than for the DGK-containing sample for the  $\beta$ ,  $\alpha$  and C8 positions, and slightly higher than for the C2 and C9 positions. This suggests that the presence of DGK may have an ordering effect on the headgroup region of the DOPC bilayer.

The order parameter values for the sample of DOPC/DOG/DGK/ATP closely match those of the sample of DOPC/DOG. The values are equal or slightly

lower for DOPC/DOG/DGK/ATP than for DOPC/DOG in the alkyl chain region, suggesting that the order in this region is similar for both samples. The values are also similar in the  $\beta$ , C2 and C8 positions, but vary more in the  $\alpha$  and C9 positions. The order parameter value for the  $\alpha$ -carbon is almost as high as for the sample of DOPC/DOG/DGK. This observation, coupled with the relatively high C2 value, may mean that there is a slight ordering effect in the interfacial region of the bilayer.

The sample of DOPC/DOG/DGK/ATP contains PA catalysed from DOG by DGK in the presence of ATP, and so would be expected to closely match the order parameter values found for the sample of DOPC/PA, as the only difference between the two samples is the presence of DGK; this has already been shown to have a small effect on order parameter, particularly in the headgroup region, from comparison of the results for the samples of DOPC/DOG/DGK and DOPC/DOG. The effect from the presence of ATP can be ignored as ATP is removed by dialysis prior to the NMR experiment. However the order parameter profile for the sample of DOPC/PA shows significantly lower order parameter values overall compared to the three samples previously analysed. For the C17, C11 and  $\beta$  carbon atoms, the splittings are no longer visible for measurement. These results show that there is a significant difference between the behaviour of DOPC bilayers doped with PA and those in which PA is synthesised from the enzyme-catalysed turn-over of DOG.

*<sup>31</sup>P-NMR Results* – <sup>31</sup>P-NMR experiments were carried out on samples containing: DOPC/DOG/DGK; DOPC/PA; and DOPC/DOG/DGK/ATP. DOG and PA were present at 20%, and ATP was removed prior to NMR, as described in the experimental section. The <sup>31</sup>P spectra, obtained at a spinning speed of 5 kHz, are shown in Figure 5.7.

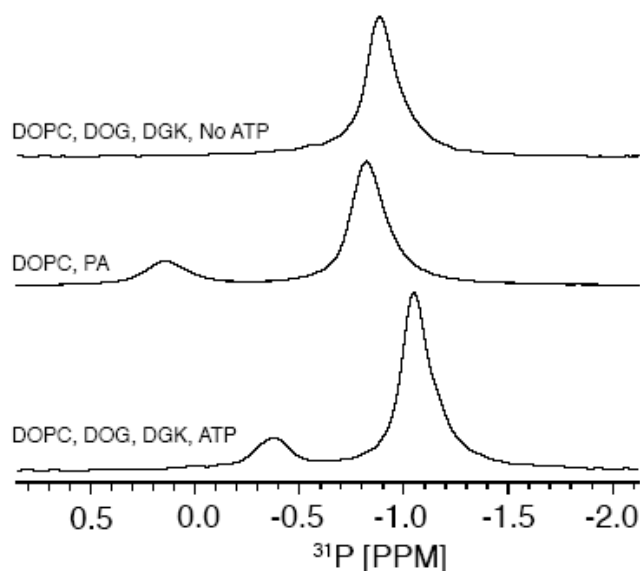


Figure 5.7.  $^{31}\text{P}$ -NMR spectra (5 kHz spinning speed) of samples of DOPC/DOG/DGK, DOPC/PA, and DOPC/DOG/DGK/ATP

The  $^{31}\text{P}$  spectrum of DOPC/DOG/DGK displays a single peak, assigned to the DOPC phosphate headgroup. The spectrum of DOPC/PA shows two peaks; one corresponding to the DOPC phosphate headgroup, and the other to the PA phosphate headgroup. The spectrum of DOPC/DOG/DGK/ATP also shows two peaks; one corresponding to the DOPC phosphate headgroup, and the other to the phosphate headgroup from the enzyme-catalysed PA. The intensity of this peak is roughly equal to 20% of the intensity of the DOPC phosphate headgroup peak, which suggests that all of the DOG has been converted to PA by the action of the enzyme. The peaks corresponding to the PA phosphate headgroup from the sample of DOPC/PA and from the sample of DOPC/DOG/DGK/ATP have different chemical shift values, which indicates that the two types of PA are in different chemical environments.

*Fluorescence Results* – Fluorescence emission spectra were obtained for samples of: DOPC/DOG  $\pm$  DGK; DOPC/PA  $\pm$  DGK; DOPC/DOG/ATP  $\pm$  DGK; and DOPC/PA/ATP  $\pm$  DGK. Ratios of excimer formation (E) over monomer formation ( $S^2$ ) were obtained from the emission spectrum for each sample. The E/ $S^2$  ratio gives an indication of the lateral stress in the bilayer in the acyl chain region. The E/ $S^2$  ratio for each sample is shown in Figure 5.8.

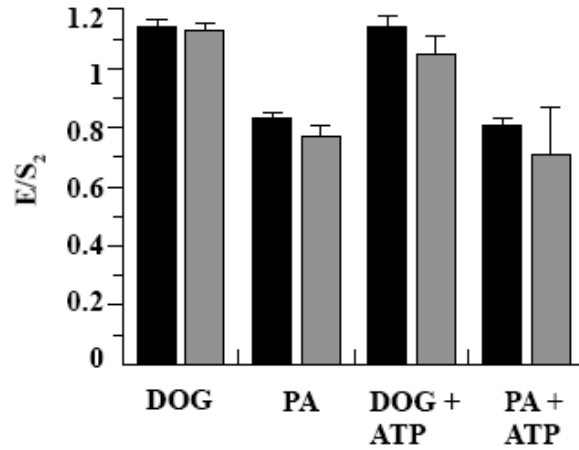


Figure 5.8. Plot of  $E/S^2$  ratio for each sample: DOPC/DOG  $\pm$  DGK; DOPC/PA  $\pm$  DGK; DOPC/DOG/ATP  $\pm$  DGK; and DOPC/PA/ATP  $\pm$  DGK, where the black bars represent the DGK-containing samples and the grey bars represent the samples containing no DGK

The highest  $E/S^2$  ratios are found for both DOPC/DOG  $\pm$  DGK samples, which matches the observation that the highest order parameters were found for these samples. The  $E/S^2$  ratios for these samples are identical. The next highest  $E/S^2$  ratio is found for the sample of DOPC/DOG/ATP/DGK, with a slight decrease observed for the sample of DOPC/DOG/ATP. The  $E/S^2$  ratios for the samples containing DOG, and notably for the sample containing PA catalysed from DOG by DGK, are higher overall than the  $E/S^2$  ratios for the samples containing PA.

These results suggest that lateral bilayer pressure is highest for the DOG samples containing DGK, which correlates with the relatively high acyl chain region order parameters observed for these samples. Lateral bilayer pressure is slightly higher for the sample of DOPC/DOG/ATP plus DGK than for the non-DGK sample, but there is no difference for the DGK and non-DGK samples of DOPC/DOG. The bilayer pressure is significantly decreased for both the DOPC/PA and DOPC/PA/ATP samples, with and without DGK, which is also observed in the order parameter results for these samples.

*Differences Between Doped and Enzyme-Catalysed PA in DOPC Bilayers* – The results from the DROSS and fluorescence emission spectroscopy experiments display an interesting difference between the behaviour of a DOPC bilayer when

PA is co-dissolved with DOPC during liposome formation, and when PA is synthesised from the catalysis of DOG by DGK. The results show that the order parameters and lateral bilayer pressures of the samples containing co-dissolved PA are significantly higher than those of the samples containing turned-over PA, and that the presence of turned-over PA does not significantly change the behaviour or physical properties of the lipid bilayer.

The relatively low bilayer tension associated with the presence of co-dissolved PA is due to the phosphate headgroup allowing the molecules to intercalate efficiently with neighbouring phospholipids. The absence of the phosphate headgroup (as in DOG) prevents efficient intercalation with DOPC, thereby increasing the order parameter and lateral pressure. It was expected that the enzyme-catalysed synthesis of PA from DOG would reduce the order parameter and lateral pressure of the sample to the same degree as for co-dissolved PA, but this was not observed to happen; in fact, there was a very slight decrease in these parameters. The removal of ATP and ADP prior to making the measurements ensures that the samples containing co-dissolved PA and turned-over PA were identical. <sup>31</sup>P-NMR results also showed that all of the DOG had been converted to PA; hence, there was no remaining DOG to affect the order parameter and lateral pressure measurements. Therefore the differences between the sets of results must be due to differences between the behaviour of co-dissolved and turned-over PA.

It is assumed that co-dissolving PA with DOPC results in an even distribution of PA throughout the main DOPC bulk. The difference between order parameter and lateral pressure for the two types of PA may be due to an uneven distribution of turned-over PA compared to co-dissolved PA. Each trimer of DGK is surrounded by an annulus of 25 to 50 lipids. The concentration of the protein in these samples is 1:2000 for DOPC, and 1:400 for PA. Two rings of lipid molecules around the protein could account for approximately 300 PA molecules. The sequestration of PA in the vicinity of DGK could account for the relatively small decrease in order parameter and lateral pressure in the bilayer, as the enzyme-catalysed PA does not intercalate with DOPC. PA molecules, which contain a negatively-charged phosphate headgroup, may be attracted to positive

amino acid residues - this effect would also result in sequestration of PA away from the DOPC bulk. However, analysis of the topology of DGK suggests that there are few charged amino acid residues present in the lipid bilayer<sup>7</sup>.

## **Part 5. Conclusion**

DROSS-NMR and fluorescence emission spectroscopy experiments were carried out on DOPC bilayers containing DOG, PA, and DGK in order to investigate the difference in lipid behaviour and physical properties between co-dissolved PA, which was mixed with DOPC before liposome formation, and enzyme-catalysed PA, which was synthesised from the catalysis of DOG in the presence of ATP. The experiments measured order parameters and bilayer lateral pressures, respectively. DOPC bilayers containing DOG and turned-over PA were found to have higher order parameters and lateral pressures overall when compared to those containing co-dissolved PA. There was only a small difference between the order parameters and lateral pressures of the DOPC/DOG bilayers and the DOPC/turned-over PA bilayers.

The explanation for the observed differences may lie in the different distributions of co-dissolved PA and turned-over PA in a DOPC bilayer. Co-dissolved PA is expected to have an even distribution throughout the bilayer, and is expected to intercalate efficiently with DOPC molecules, thereby producing low bilayer tensions. The higher bilayer tensions observed for turned-over PA may result from sequestration of PA in the lipid annulus of DGK. This experiment has shown that the behaviour and physical properties of a lipid component in a model membrane formed by co-dissolving two or more lipids may differ considerably from the behaviour of the same lipid when produced *in vitro* through enzyme catalysis.

## **Part 6. References**

1. Gross, J. D.; Warschawski, D. E.; Griffin, R. G., Dipolar recoupling in MAS NMR: A probe for segmental order in lipid bilayers. *J. Am. Chem. Soc.* **1997**, 119, (4), 796-802.

2. Warschawski, D. E.; Devaux, P. F.,  $^1\text{H}$ - $^{13}\text{C}$  polarization transfer in membranes: A tool for probing lipid dynamics and the effect of cholesterol. *J. Magn. Reson.* **2005**, 177, 166-171.
3. Somerharju, P., Pyrene-labeled lipids as tools in membrane biophysics and cell biology. *Chem. Phys. Lipids* **2002**, 116, 57-74.
4. Templer, R. H.; Castle, S. J.; Curran, A. R.; Rumbles, G.; Klug, D. R., Sensing isothermal changes in the lateral pressure in model membranes using dipyranyl phosphatidylcholine. *Faraday Discuss.* **1998**, 111, 41-53.
5. Cheng, K. H.; Somerharju, P., Effects of unsaturation and curvature on the transverse distribution of intramolecular dynamics of dipyranyl lipids. *Biophys. J.* **1996**, 70, 2287-2298.
6. Warschawski, D. E.; Devaux, P. F., Order parameters of unsaturated phospholipids in membranes and the effect of cholesterol: a  $^1\text{H}$ - $^{13}\text{C}$  solid-state NMR study at natural abundance. *Eur. Biophys. J. Biophys. Lett.* **2005**, 34, (8), 987-996.
7. Oxenoid, K.; Kim, H. K.; Jacob, J.; Sönnichsen, F. D.; Sanders, C. R., NMR assignments for a helical 40 kDa membrane protein. *J. Am. Chem. Soc.* **2004**, 126, 5048-5049

## Conclusion

The aim of the research was to assess the use of enzymes, isomerisable lipid analogues, and small molecules to modulate the structure and dynamics of lipid bilayers. The effects of the bilayer modulation were measured using various NMR spectroscopic methods, DSC, fluorescence emission spectroscopy, and enzyme assay experiments. Overall the research showed that the effect of small molecules and enzyme-catalysed substrates on the structure and properties of the bilayer may be unexpected.

The analysis of phase behaviour of  $d_{62}$ -DPPC bilayers containing cholesterol and serotonin-receptor agonist drugs showed that the presence of a relatively small molecule in a bilayer may cause a significant change to the phase behaviour by lowering phase transition temperatures, elongating phase transition boundaries, and removing sub-fluid lamellar phases such as the ripple phase. NOESY cross-relaxation rates also showed that small molecules may adopt an unexpected orientation in the bilayer; LY was found to lie perpendicular to the bilayer normal, although it has a relatively linear structure, while Q was found to adopt an orientation parallel to the bilayer. The NOESY results also showed that drug/cholesterol interactions cause the drug to change position as the temperature in the bilayer increases. LY was found to move towards the headgroup region of the bilayer as the temperature increased, while Q moved towards the centre of the bilayer. These results show that small molecules *in vivo* such as these serotonin-receptor agonists may adopt unpredictable positions in the membrane and may affect the membrane's physical properties.

The analysis of bilayer tension and order parameter for samples containing enzyme-catalysed PA and co-dissolved PA also produced unexpected results. Bilayer tension was found to be much higher for enzyme-catalysed PA than for co-dissolved PA, which may be due to sequestration of the PA in the protein's lipid annulus.

A photoisomerisable azobenzene lipid analogue was synthesised for inclusion into DOPC liposomes containing DGK, but the enzyme activity assay for each

photochemical state was not sufficiently different to enable the effect of photoswitching on enzyme activity to be confidently assessed. However the azobenzene lipid analogue was characterised and was shown to produce a relatively small amount of aggregation in the liposome.